STOCHASTIC ANALYSIS OF SPATIAL VARIABILITY IN TWO-DIMENSIONAL GROUNDWATER FLOW WITH IMPLICATIONS FOR OBSERVATION-WELL-NETWORK DESIGN

by

Stephen A. Mizell

Submitted in Partial Fulfillment of
the Requirements for the Degree of
Doctor of Philosophy

NEW MEXICO INSTITUTE OF MINING AND TECHNOLOGY
Socorro, New Mexico

November 1980

ABSTRACT

Variability and continuity of aquifer materials in groundwater systems have historically been ignored in analyses which use discrete sampling of parameters to represent the entire flow system. This paper applies recently proposed methods of stochastic and spectral analysis to investigate effects of spatial variability on two-dimensional groundwater flow.

The spectral equation describing two-dimensional flow is developed using Fourier-Stieltjes representation for statistically homogeneous fluctuations of the stochastic processes (hydraulic head and log-transmissivity). Selecting a convenient form for the spectral and covariance functions of log-transmissivity allows determination of head variance and covariance. Hydraulic head variance is shown to be highly dependent on the variance and spatial correlation structure of the log-transmissivity process, and head variance is significantly reduced as a result of multi-dimensional flow. The head covariance function indicates that head fluctuations are correlated over greater distances than are log-transmissivity fluctuations.

Relationships between variance of estimated parameters and size of observation-well networks are developed using the head covariance function resulting from analysis of groundwater flow. These relationships allow determination of the anticipated variance in a parameter estimate for a specific network or determination of network size required to produce an acceptable variance in the parameter estimate.

ACKNOWLEDGEMENTS

The author wishes to thank his dissertation advisory committee, Drs. L. W. Gelhar, A. L. Gutjahr, J. R. MacMillan, and R. A. Freeze, for their interest in this project. Helpful comments were provided by all committee members during preparation of this paper. Special appreciation is extended to Dr. Gelhar for suggesting the stochastic approach and contributing immeasurably to an understanding of the technique. Dr. Gutjahr's assistance with the more complicated mathematics was an essential factor leading to completion of critical initial tasks.

Two years of financial support by the U. S. Geological Survey, Water Resources Division, is gratefully acknowledged. During the period of this support, Dr. R. L. Cooley acted as the author's contact with the Survey, providing invaluable assistance in dealing with the bureaucratic process as well as offering considerable encouragement.

Joan Pendleton edited the manuscript, offering many valuable suggestions. Also helpful were discussions of research with fellow graduate students Rich Naff, Chris Duffy, and Jim Yeh.

The constant encouragement and financial support provided by Nancy Mizell is greatly appreciated. Ben Mizell offered continual respite from the tedium of study. John and Betty Mizell and Earle and Nan Hunt provided additional encouragement and contributed financially throughout this period of study.

The author wishes to express his deep appreciation to the Creator of all things for the basic talents and abilities endowed him, making successful completion of this project possible.

TABLE OF CONTENTS

	Page
ABSTRACT	ii
ACKNOWLEDGEMENTS	iii
LIST OF FIGURES AND TABLES	vi
LIST OF SYMBOLS	viii
INTRODUCTION	1
Statement of Problem	1
Statement of Objectives	2
Literature Review	3
Procedure	8
ANALYSIS OF STEADY FLOW	13
Spectral-Equation Derivation	13
ln T Spectral and Covariance Functions	18
Head Variance and Covariance Functions	25
Cross-Covariance Functions	33
Interpretation of Covariance Functions	37
Limitations	38
Summary	39
ANALYSIS OF TRANSIENT FLOW	41
Spectral-Equation Development	41
Head Variance and Covariance Functions	46
Comparison of Transient and Steady Analyses	48
Summary	51
APPLICATIONS TO NETWORK DESIGN	53
Variance in Estimated Gradient Magnitude	54

Page

Error in Estimated Gradient Direction. 61

Variance in Estimated ln T 67

Summary. 75

CONCLUSIONS AND RECOMMENDATIONS 76

REFERENCES. 78

APPENDIX I: DERIVATION OF THE COVARIANCE FUNCTION ASSOCIATED WITH SPECTRUM A 83

APPENDIX II: DERIVATION OF THE COVARIANCE FUNCTION ASSOCIATED WITH SPECTRUM B. 89

APPENDIX III: DERIVATION OF THE HEAD COVARIANCE FUNCTION ASSUMING INPUT SPECTRUM A. 94

APPENDIX IV: DERIVATION OF THE HEAD COVARIANCE FUNCTION ASSUMING INPUT SPECTRUM B 100

APPENDIX V: DERIVATION OF THE CROSS-COVARIANCE FUNCTION BETWEEN HEAD AND ln T ASSUMING INPUT SPECTRUM A. 103

APPENDIX VI: DERIVATION OF THE CROSS-COVARIANCE FUNCTION BETWEEN HEAD AND ln T ASSUMING INPUT SPECTRUM B . 106

APPENDIX VII: DERIVATION OF THE HEAD COVARIANCE FUNCTION IN THE TRANSIENT ANALYSIS ASSUMING INPUT SPECTRUM B 109

APPENDIX VIII: GRADIENT-MAGNITUDE ESTIMATION 113

APPENDIX IX: GRADIENT-DIRECTION ESTIMATION 116

APPENDIX X: ln T ESTIMATING EQUATION 118

APPENDIX XI: FLOW PARAMETERS OF THE SAN ACACIA IRRIGATION AND DRAINAGE SYSTEM 120

LIST OF FIGURES AND TABLES

Figure		Page
2.1	Comparison of Potential Two-Dimensional Ln T Spectra with the Three-Dimensional Ln K Spectrum Assumed by Bakr et al. (1978).	21
2.2	Comparison of Potential Two-Dimensional Ln T Correlation Functions with the Three-Dimensional Correlation Function Assumed by Bakr et al. (1978)	23
2.3	Comparison of Steady Head Variances for 1- and 2-Dimensional Phreatic Flow and 1-, 2-, and 3-Dimensional Confined Flow	28
2.4	Ln T and Head Correlation Functions Assuming Input Spectrum A.	29
2.5	Ln T and Head Correlation Functions Assuming Input Spectrum B.	30
2.6	Three-Dimensional Ln K and Head Correlation Functions (from Bakr et al., 1978).	31
2.7	Dimensionless Cross-Covariance Function Between Ln T and Head Assuming Input Spectrum A.	35
2.8	Dimensionless Cross-Covariance Function Between Ln T and Head Assuming Input Spectrum B.	36
3.1	Contributions to Transient Head Correlation Function from Terms Reflecting the Mean-Gradient and Mean-Transient Parameters.	49
3.2	Transient Head Correlation Function Evaluated for Several values of Ω at $\chi = 0.0$.	50

Figure Page

4.1 Three-Point Observation-Well Network for Estimating Gradient Magnitude and Direction. 58

4.2 Normalized Variance of Estimated Gradient Magnitude . . . 60

4.3 Normalized Mean Square Error of Estimated Gradient Direction 66

4.4 Normalized Variance of Estimated Ln T Assuming $\Omega = 1$ and a Typical Range of Measurement-Error Values 72

4.5 Normalized Variance of Estimated Ln T Illustrating Effects of various values of Ω with zero Measurement-Error. . . 74

XI.1 Map of the Field Study Area at San Acacia, New Mexico Showing Five-Point Well Network and Water-Level Controls During Winter 1977-1978 (from Wierenga, et al., 1979) 121

XI.2 Plots of Stallman Data ($\Sigma\phi$ vs $\frac{\Delta\bar{\phi}}{\Delta t}$) for (A) Winter and (B) Summer Flow Regimes 124

XI.3 Average Water Level Hydrograph of Five-Point Network San Acacia, New Mexico. 125

Table

4.1 Polar Coordinates of Separation Vectors Required in Determination of Variance of Estimated Ln T 70

XI.1 Weekly Water-Level Data Collected from the Five-Point Network, February 1977-April 1978 with $\bar{\phi}$, $\Sigma\phi$, $\frac{\Delta\bar{\phi}}{\Delta t}$ . . . 129

XI.2 Mean Gradient Magnitude and Direction as Estimated from Weekly Water-Level Data of the 1977-1978 Winter Season. 132

XI.3 Summary of Parameter Values used in the Illustrative Network-Design Calculations 133

LIST OF SYMBOLS

Symbol	Definition
$\vec{a}_i$	vector coefficient of observation point i in three-point plane equation
dZ_f	complex Fourier amplitude of ln T fluctuations
dZ_h	complex Fourier amplitude of head fluctuations
E(X)	expected value or ensemble average of random process X
F	= E(ln T): mean value of ln T process
f	= ln T - F: fluctuation of ln T process
H	= E(ϕ): mean value of head process
h	= ϕ - H: fluctuation of head process
J_1	mean-gradient magnitude
$\hat{J}$	estimated gradient
k	wave-number space vector, with coordinates k_1, k_2
K_0	modified Bessel function, second kind, 0 order
K_1	modified Bessel function, second kind, 1st order
L	network scale; length of principal network side
ln T	natural logarithm of transmissivity
R	covariance function
R_W	ln T covariance function for Whittle input spectrum
R_A	ln T covariance function for modified Whittle type A input spectrum
R_B	ln T covariance function for modified Whittle type B input spectrum
R_h	head covariance function
R_{Ah}	head covariance function assuming ln T spectrum A

Symbol	Definition
R_{Bh}	head covariance function assuming ln T spectrum B
R_{Ahf}	head and ln T cross-covariance function assuming ln T spectrum A
R_{Bhf}	head and ln T cross-covariance function assuming ln T spectrum B
S	storage coefficient
T	transmissivity
T_ℓ	= exp[E(ln T)]: transmissivity associated with mean of ln T
t	time coordinate
x_i	x coordinate of well i
x, y	cartesian coordinates
γ	angle of network rotation with respect to mean groundwater flow
ε	error in measurement of water level
θ	angle between estimated and true gradient direction
λ	integral scale of ln T process
λ_e	effective integral scale; lag distance at which ln T correlation function is e^{-1}
ξ	separation vector between observation points
ξ_1, ξ_2	cartesian coordinates of separation vector
ξ	magnitude component of separation vector in polar coordinates
ρ	$= R/\sigma^2$: correlation function
$\Sigma\phi$	sum of observed heads in Stallman (1956) procedure to estimate transmissivity

Symbol	Definition
ΣH	sum of mean heads in Stallman (1956) procedure to estimate transmissivity
σ	standard deviation
σ^2	variance
σ_{Ah}^2	head variance assuming input spectrum A
σ_{Bh}^2	head variance assuming input spectrum B
σ_f^2	theoretical variance of ln T
$\sigma_{\hat{f}}^2$	variance of estimated ln T
σ_J^2	variance of estimated gradient magnitude
σ_ε^2	variance of measurement error
σ_h^2	variance of head
Φ	spectrum of random process
Φ_A	modified Whittle input spectrum A
Φ_B	modified Whittle input spectrum B
Φ_W	Whittle (1954) input spectrum
Φ_f	ln T spectrum
Φ_h	head spectrum
Φ_{hf}	ln T and head cross-spectrum
ϕ_i	observed head at well i
χ	angular component of separation vector in polar coordinates
ψ	angle between principal network side and strike of head surface
Ω	weighting function for sum of terms in transient head correlation function

INTRODUCTION

Statement of Problem

Casual observation of geologic formations will reveal a great diversity of geologic material. A closer look will convince the observer that even those geologic units which appear to be uniform exhibit considerable variation in both horizontal and vertical directions. In sedimentary formations, which form the most common aquifer units, variation of geologic materials is seen among the same physical properties (e.g., grain size, grain orientation) that are basic factors in determining hydrologic properties of aquifers. The interested person will, after consideration of active geologic processes, realize that processes which contribute to development of sedimentary rock units are constantly changing in intensity and location and so produce geologic formations whose physical and hydrologic properties vary within a spatial continuum.

Equations describing the physics of fluid flow in porous media recognize spatial variation of hydrologic properties. However, application of these equations has generally been based on simplifying assumptions of homogeneity and isotropy. Simulation of flow systems and estimation of hydrologic properties from flow-system response have typically assumed homogeneous parameters. For example, Theis pumping-well analysis provides a single observation of transmissivity; although often interpreted as a point measurement, it has recently been viewed as an average, or effective, value describing the composite effect within the well's region of influence. Additionally, numerical procedures used to simulate groundwater systems require knowledge of hydrologic properties at network nodes distributed across the aquifer; these parameters

are assumed constant over the area of nodal influence. Recent work (Gelhar et al., 1977; Bakr et al., 1978) has shown that parameter distribution over finite-difference networks implies some spatial correlation structure which previously had gone unrecognized.

Analysis of statistical and spatial distribution of hydrologic properties and the resulting effect on head distribution in flow systems has been the emphasis of much recent work (e.g., Gelhar, 1976; Bakr et al., 1978; Gutjahr et al., 1978; Smith and Freeze, 1979a,b). These and other approaches to the problem of analyzing parameter heterogeneity are briefly discussed in the Literature Review section.

The present work investigates spatial distribution of transmissivity as it affects hydraulic head in two-dimensional, horizontal confined aquifers. Design of observation-well networks under assumption of stochastic head is considered in three illustrative examples.

Statement of Objectives

The general aim of this study is two-fold. First is to determine the spatial structure and statistical characteristics (mean and variance) of piezometric head as modeled by the two-dimensional depth-averaged, aquifer equation, under both steady and transient conditions, assuming a specific description of the statistical structure of the random transmissivity field. Second is to consider the application of these results to the design of simple observation-well networks.

Specific objectives which fall under these general aims are:
(1) Development of the two-dimensional spectral equation for groundwater flow assuming stochastic representation of parameters and using spectral analysis.

(2) Determination of reasonable input spectrum and covariance functions for the ln T (natural log of transmissivity) process.
(3) Comparison of resulting head variance and covariance to those obtained for one- and three-dimensional confined flow by Bakr et al. (1978) and for one- and two-dimensional phreatic flow by Gelhar (1976).
(4) Application of results to estimation of hydraulic gradient and transmissivity from simple observation-well networks with a view toward design of such networks to achieve minimum variance in estimated parameters.

Literature Review

In mathematical descriptions of groundwater flow, hydrologists have always recognized the continuum nature of flow systems. Inability to measure aquifer parameters as continuous processes and the great difficulty of obtaining large numbers of discrete samplings of the parameter field have resulted in assumption of parameter homogeneity and isotropy to simplify solution of flow equations. Development of modern numerical techniques has relaxed the homogeneity assumption through division of the flow region into nodal areas for which aquifer parameters may vary but within which parameter values are constant. Another approach to incorporate parameter inhomogeneity has involved statistical descriptions of the parameter distribution.

A large body of literature has recognized a log-normal distribution for the hydraulic conductivity in soils and aquifers (e.g., Law, 1944; Warren and Price, 1961; McMillan, 1966; Nielson et al., 1973); this literature is summarized by Freeze (1975). Drawing hydraulic conductivity values from a log-normal probability distribution and following a Monte Carlo procedure, Warren and Price (1961) concluded that a geometric

mean is the best effective conductivity value for three-dimensional flow. McMillan (1966) investigated the relationship between hydraulic conductivity fluctuations and variations in head using a numerical model. Regionalization of parameters to overcome data scarcity as discussed by Freeze (1972) emphasized treatment of conductivity observations as if statistically independent. In 1975, Freeze furthered the investigation of parameter heterogeneity effects on steady and unsteady, one-dimensional groundwater flow. Using numerical simulation and Monte Carlo techniques, he considered effects of variability in conductivity, compressibility, and porosity. These and earlier studies of parameter variability ignore spatial correlation structure of parameter distribution.

Inclusion of non-homogeneity effects in analysis of groundwater flow has been emphasized recently by several workers. Each researcher has assumed that aquifer parameters are stochastic random processes whose spatial variability may be described by statistical characteristics such as mean, variance, and covariance. Specific techniques applied include: self-consistent approximation (Dagan, 1979), perturbation analysis (Tang and Pinder, 1977), sensitivity analysis (McElwee and Yukler, 1978), Monte Carlo procedures (Freeze, 1975; Smith, 1978; Smith and Freeze, 1979a,b; Warren and Price, 1961; Vandenburg, 1977; Delhomme, 1979), and spectral methods (Gelhar, 1976; Bakr, 1976; Bakr et al., 1978, Gutjahr et al., 1978; Naff, 1978; Gelhar et al., 1979). Each of these techniques is briefly discussed in the following paragraphs.

Dagan (1979) used the self-consistent method to determine effective hydraulic conductivity, effective storativity, and statistical properties of head and specific discharge. He observes that one-dimensional analysis grossly overestimates gradient and specific discharge variances.

Effective storativity is determined to be the arithmetic average of the heterogeneous values. Effective conductivity is shown to be less than the geometric mean for one-dimensional analyses, equal to the geometric mean for two-dimensional analyses, and slightly larger than the geometric mean for three-dimensional analyses. Dagan was unable to obtain a simple relationship for the two-dimensional self-consistent model.

Perturbation analysis was employed by Tang and Pinder (1977) to study two-dimensional mass transport and well flow. Stochastic random variables in the mass-transport problem are diffusivity and contaminant concentration; in the well-flow problem transmissivity and head are characterized as stochastic variables. In each problem the mean response behaves in the same manner as the deterministic solution.

Sensitivity analysis of well flow was conducted by McElwee and Yukler (1978) using three different modeling approaches: the Theis equation, a radial-flow model, and a two-dimensional model. All three models exhibit similar responses to variations of transmissivity and storativity. Nearer the well, predicted head was more sensitive to variations in transmissivity. Storativity changes were significant over larger areas than were transmissivity changes. As boundary effects became important in the two numerical models, the sensitivity coefficient for transmissivity approached a constant value which was larger for constant-head boundaries than for no-flow boundaries. The sensitivity coefficient for storativity went to zero for constant-head boundaries and to infinity for no-flow boundaries.

Several workers have used Monte Carlo techniques to investigate heterogeneity effects. Warren and Price (1961) conclude that for three-dimensional flow the geometric mean is the best measure of effective

permeability from sand-box and numerical studies in which permeabilities were assigned from a log-normal distribution. Selecting transmissivity values from a normal distribution, Vandenberg (1977) uses a finite difference model to simulate flow to a well. Analyzing water-level drawdown by the Theis method, he found that heterogeneity effects were not noticeable in data near the well and that analysis of segments of simulated drawdown curves produces transmissivity values that cluster around the arithmetic average.

A recent series of Monte Carlo investigations have used one- and two-dimensional numerical models to study heterogeneity effects. Freeze (1975) assumed, as did Warren and Price (1961) and Vandenberg (1977), that assigned values of parameters were uncorrelated; the severity of this limitation was noted by Gelhar et al. (1977). Further investigations by Smith (1978) and Smith and Freeze (1979a,b) incorporated spatial structure of medium properties. These studies produced the following significant results: two-dimensional simulation produces greatly reduced head variances compared to one-dimensional results, output variance is strongly dependent on the variance and correlation scale of input parameters, and the geometric mean is a reasonable value for effective conductivity.

Conditional simulation, a type of Monte Carlo technique, was used by Delhomme (1979) to study effects of transmissivity variation on simulated hydraulic head. He indicates that variability of head due to high transmissivity variance can be reduced by strong boundary constraints on head distribution. The importance of using all available transmissivity and head data is also shown.

Spectral analysis techniques have been used in several recent

studies. Heterogeneity effects in one- and two-dimensional phreatic flow systems were considered by Gelhar (1976). He notes that estimated flow variance is smaller than log-conductivity variance and that two-dimensional head variance is an order-of-magnitude smaller than one-dimensional head variance. Analysis of one- and three-dimensional confined flow was carried out by Bakr (1976), Bakr et al. (1978), and Gutjahr et al. (1978). The papers by Bakr and Bakr et al. indicate strong dependence of head variance on correlation length of the input process, an anisotropic head covariance function despite use of an isotropic input covariance for the log-conductivity process, and a reduction in head variance from the one-dimensional to the three-dimensional case. Investigating limitations of the log-conductivity linearization in the one-dimensional case, Gutjahr et al. (1978) and Bakr (1976) find results to be adequate for small values of standard deviation of log-conductivity although errors increase rapidly as the standard deviation of log-conductivity exceeds one. Gutjahr et al. also consider the question of an effective conductivity value determining the geometric mean to be appropriate for two-dimensional analyses. One-dimensional analysis suggests an effective conductivity smaller than the geometric mean; three-dimensional results indicate an effective conductivity larger than the geometric mean. Spectral analysis has also been applied to dispersive processes in groundwater systems by Naff (1978) and Gelhar et al. (1979).

Spectral analysis of two-dimensional groundwater systems has not been extensive. Gelhar (1976) analyzed two-dimensional phreatic flow for which he chose the two-dimensional autocovariance function proposed by Whittle (1954) to represent the spatial correlation structure of the aquifer variability. Whittle (1954) described this autocovariance

function as "the elementary two-dimensional covariance function paralleling the negative exponential function for one-dimensional analysis." The work of Whittle is based on analysis of agricultural yields. Other two-dimensional processes which have been studied include forest-land surveys (Matern, 1947), mineral deposits (Agterberg, 1974), and precipitation (Rodriguez-Iturbe and Mejia, 1974). In the analysis of precipitation data, Rodriguez-Iturbe and Mejia assume a covariance function which is a product of spatial correlation structure and temporal correlation structure.

Design of observation-well networks for improved estimation of parameters from observed head levels has recently received the attention of several investigators. Gelhar (1976) shows that the normalized one-dimensional phreatic flow variance increases rapidly as the network scale increases with respect to the integral scale of the log-conductivity process. Bakr (1976) and Gutjahr et al. (1978) consider two network problems: flow through a permeameter and flow across an aquitard. For permeameter flow they conclude that error in estimated hydraulic resistivity decreases as the core length increases relative to the correlation length of conductivity. Two significant results were noted in the aquitard flow problem: measurement of aquitard conductivity midway between head measurements produced minimum variance in estimated discharge, and minimum discharge variance was achieved for observation wells separated by a distance of one-fifth to one-half the correlation length.

Procedure

In the analysis of groundwater flow, the stochastic technique conceptualizes parameters (e.g., head and transmissivity) of the

deterministic flow system as random fields which evolve in space according to fixed probability laws. These stochastic processes can then be described probabilistically (Jenkins and Watts, 1968). Complete description of the spatial random fields requires joint probability density functions between each point in space. Data to estimate joint densities will almost never be available; analysis and data requirements are simplified by consideration of only the first and second moments of the joint density, the mean and covariance. Correlation between observations of the spatially continuous parameter process is described by a continuous covariance function which is directly associated with the second moment statistics.

In analysis of groundwater flow, statistical parameters describing the hydraulic head are determined from statistical knowledge of aquifer variability according to the spectral equation of flow. Development of the spectral equation follows procedures discussed by Lumley and Panofsky (1964, p. 16-18). Methods presented by Lumley and Panofsky require that the equation governing the flow system have a zero mean. The zero-mean governing equation for groundwater flow is derived by writing the head and ln T parameters as sums of a mean and fluctuations about the mean; the fluctuation parts are assumed to be zero-mean stationary (statistically homogeneous) processes. Such representations are substituted into the flow equation, and the mean-flow equation (the flow equation formulated in terms of mean parameters) is determined. Extracting the mean-flow equation by subtraction results in the governing flow equation for fluctuations in the parameter field.

The Fourier-Stieltjes integral representation of a zero-mean, stationary stochastic process is

$$p = \int_{-\infty}^{\infty} e^{i\vec{k}\cdot\vec{x}}\, dZ_p(\vec{k}) \qquad (1.1)$$

in which the complex Fourier amplitude of parameter p, dZp, is defined on wave-number space $\vec{k}$. Substituting Fourier-Stieltjes representations for parameters in the zero-mean equation, results in an equation relating the complex Fourier amplitudes of head and ln T. Multiplying the complex Fourier amplitude by its conjugate and taking the expected value

$$\Phi_p(\vec{k})d\vec{k} = E(dZ_p dZ_p^*) \qquad (1.2)$$

leads to the spectral density, or spectrum Φ_p, for the parameter. For simple groundwater systems the spectrum of head is proportional to the ln T spectrum. The spectrum, which indicates the contribution of variations from a specific wave length to the total variance of the process, can be Fourier transformed into the covariance, R,

$$R_p(\vec{\xi}) = \int_{-\infty}^{\infty} e^{i\vec{k}\cdot\vec{\xi}}\, \Phi_p(\vec{k})d\vec{k} \qquad (1.3)$$

As a product of the variance and correlation function, the covariance is indicative of the correlation, or dependence, between parameter

values separated by the lag vector ξ. The correlation function is the covariance normalized by the variance

$$\rho_p(\vec{\xi}) = \frac{R_p(\vec{\xi})}{\sigma_p^2} \tag{1.4}$$

From the correlation function, a length parameter of the correlation structure, called the integral scale or average distance of correlation, can be determined

$$\lambda = \int_0^\infty \rho_p(\xi)\, d\xi \tag{1.5}$$

λ is the integral scale of the correlation function associated with parameter p. This scale offers a convenient way to compare the correlation structure with other length scales.

Assumptions required to apply the technique as outlined are statistical homogeneity and ergodicity. Statistical homogeneity is the property of the random field, which implies that spatial statistical properties are functions only of the separation vector between parameter observation points; statistical homogeneity of spatial processes is equivalent to stationarity for temporal processes. Ergodicity is an assumption that equates spatial and ensemble averages. In other words, the average obtained from observations within a finite space is equal to that which would be obtained by sampling an infinite space.

In reality, equating these two averages is only acceptable if the variance of the finite space average goes to zero as the space over which the average is taken goes to infinity (Lumley and Panofsky, 1964).

Statistical isotropy which implies statistical homogeneity, will be assumed when describing aquifer variability in the following analyses. A statistically isotropic process is one for which the correlation function depends only on the separation distance $\xi \equiv |\vec{\xi}|$ and not on the orientation of $\vec{\xi}$; thus, $R_p(\vec{\xi}) = R_p(\xi)$.

ANALYSIS OF STEADY FLOW

In this section the spectral equation for two-dimensional, steady groundwater flow will be derived. Then mathematically acceptable spectral formulations will be selected to describe the hypothetical log-transmissivity field. From log-transmissivity spectra it is possible to determine the autocovariance functions of the log-transmissivity and head processes and the cross-covariance function between the processes. Comparison of results from the present analysis, the one- and two-dimensional analyses of phreatic flow by Gelhar (1976), and the one- and three-dimensional analyses of confined flow by Bakr (1976) and Bakr et al. (1978) will be made; comparison with the three-dimensional analysis, which is intuitively most realistic, is of special interest.

Spectral-Equation Derivation

The classical, depth-averaged equation for two-dimensional, steady groundwater flow, with heterogeneous transmissivity, is

$$\frac{\partial}{\partial x}\left(T\frac{\partial \phi}{\partial x}\right) + \frac{\partial}{\partial y}\left(T\frac{\partial \phi}{\partial y}\right) = 0 \qquad (2.1)$$

where T is transmissivity and ϕ is hydraulic head. Equation (2.1) can be written in terms of ln T as

$$\frac{\partial^2\phi}{\partial x^2} + \frac{\partial^2\phi}{\partial y^2} + \frac{\partial \ln T}{\partial x}\frac{\partial\phi}{\partial x} + \frac{\partial \ln T}{\partial y}\frac{\partial\phi}{\partial y} = 0 \qquad (2.2)$$

Assuming head and log-transmissivity to be spatial stochastic processes, they may be represented as the sum of a mean part and a fluctuation about the mean

$$\phi(x,y) = H(x) + h(x,y)$$
$$\ln T(x,y) = F + f(x,y) \qquad (2.3)$$

In (2.3) H is a function of only the x direction, implying a unidirectional mean-flow assumption. Unidirectional mean flow is not excessively restrictive; the coordinate system can be oriented so that the x axis and mean-flow directions are parallel. The ln T processes is assumed to have a constant mean, F.

Substituting (2.3) into (2.2) and performing the indicated algebra results in

$$\frac{\partial^2 H}{\partial x^2} + \frac{\partial^2 h}{\partial x^2} + \frac{\partial^2 h}{\partial y^2} + \frac{\partial f}{\partial x}\frac{\partial H}{\partial x} + \frac{\partial f}{\partial x}\frac{\partial h}{\partial x} + \frac{\partial f}{\partial y}\frac{\partial h}{\partial y} = 0 \qquad (2.4)$$

An equation describing the mean-flow condition is found by taking the expectation of (2.4)

$$\frac{\partial^2 H}{\partial x^2} + E\left(\frac{\partial f}{\partial x}\frac{\partial h}{\partial x}\right) + E\left(\frac{\partial f}{\partial y}\frac{\partial h}{\partial y}\right) = 0 \qquad (2.5)$$

The governing equation for perturbations in groundwater flow is given by subtracting (2.5) from (2.4)

$$\frac{\partial^2 h}{\partial x^2} + \frac{\partial^2 h}{\partial y^2} - J_1\frac{\partial f}{\partial x} = 0 \qquad (2.6)$$

in which J_1, the mean gradient, is $-\frac{\partial H}{\partial x}$ and second-order perturbation products are neglected.

An assumption of statistical homogeneity for both ln T and head fluctuations is made. Statistically homogeneous processes are described by statistical properties (covariance and related functions) which depend only on the lag vector separating observations and not on actual locations of observations. Assuming statistical homogeneity allows representation of input f and output h by Fourier-Stieltjes integrals (Lumley and Panofsky, 1964, p. 16).

$$f = \iint_{-\infty}^{\infty} e^{i(k_1 x + k_2 y)} \, dZ_f(k_1, k_2)$$

$$h = \iint_{-\infty}^{\infty} e^{i(k_1 x + k_2 y)} \, dZ_h(k_1, k_2) \qquad (2.7)$$

where dZ_f and dZ_h represent complex Fourier amplitudes of the respective fluctuations over k_1 and k_2, wave-number space. Substituting (2.7) into (2.6) gives, after differentiating,

$$\iint_{-\infty}^{\infty} \left[-k_1^2 dZ_h - k_2^2 dZ_h - iJ_1 k_1 dZ_f \right] e^{i(k_1 x + k_2 y)} = 0$$

which is true only if the bracketed term is zero. Thus, an equation relating the Fourier amplitudes of f and h results

$$dZ_h(k_1,k_2) = \frac{iJ_1k_1}{-(k_1^2 + k_2^2)} \quad dZ_f(k_1,k_2) \tag{2.8}$$

From Lumley and Panofsky (1964, p. 16), the expectation of the product of the Fourier amplitude with its complex-conjugate is the spectrum for the random process. By this procedure a relationship between the spectra of f and h can be derived from (2.8)

$$\Phi_h(k_1,k_2)d\vec{k} = E(dZ_h dZ_h^*) = \frac{k_1^2 J_1^2}{(k_1^2 + k_2^2)} \Phi_f(k_1,k_2)d\vec{k} \tag{2.9}$$

Φ_h and Φ_f are spectra for the head and log-transmissivity processes, and the superscript * denotes the complex-conjugate. Capital Φ designates the spectrum of the indicated stochastic process and lower case φ implies the hydraulic head.

The head spectrum, (2.9), is directly proportional to the ln T spectrum, and the proportionality factor is a function of the mean gradient and wave-number space location. Mathematically, knowledge of either the h or f spectrum would allow evaluation of the other. In the following section, reasonable formulations of the ln T spectrum will be

identified for use as input to (2.9).

In T Spectra and Covariance Functions

A spectrum/covariance pair for two-dimensional spatial processes was proposed by Whittle (1954) based on analysis of agricultural yields. The Whittle spectrum has the form

$$\Phi_W(k_1, k_2) = \frac{N}{a^4(k_1^2 + k_2^2 + \frac{1}{a^2})^2} \quad ; \quad N = \frac{\sigma^2 a^2}{\pi}, \; a = \frac{2\lambda}{\pi} \tag{2.10}$$

where N is a normalizing constant which insures that the covariance function equals the variance when evaluated at zero lag, a is the correlation parameter, λ is the integral scale, and σ^2 is the variance.

The covariance function associated with the Whittle spectrum, obtained by taking the Fourier transform of the spectrum (Lumley and Panofsky, 1964, p. 16), is formulated in terms of a modified Bessel function

$$R_W(\xi) = \sigma^2 \frac{\pi\xi}{2\lambda} K_1\left(\frac{\pi\xi}{2\lambda}\right) \tag{2.11}$$

ξ is the magnitude of the separation, or lag, vector between observation points, $\xi = (\xi_1^2 + \xi_2^2)^{\frac{1}{2}}$, and K_1 is the modified Bessel function of second kind, first order. Whittle (1954, p. 448) describes (2.11), when normalized by the variance, as "the elementary correlation function in two-dimensions, similar to the exponential $e^{-|\xi|/\lambda}$ in one dimension." Gelhar (1976) uses the Whittle spectrum and covariance functions to describe the log-conductivity process when analyzing two-dimensional phreatic flow.

The head variance is to be obtained by using the assumed ln T spectrum, (2.10), in (2.19) and integrating over wave-number space. Note that a singularity at $k_1 = k_2 = 0$ remains in the head spectrum and as a result the integral is divergent. Thus, the Whittle spectrum will not yield a finite variance for two-dimensional confined groundwater flow under the assumption of statistically homogeneous h. As an alternative, consider two spectra, A and B, appropriately modified to eliminate the singularity in the head spectrum

$$\Phi_A(k_1,k_2) = \frac{N\,(k_1^2 + k_2^2)}{a^4(k_1^2 + k_2^2 + \frac{1}{a^2})^3} \quad ; \quad N = \frac{2\sigma^2 a^2}{\pi} \quad , \quad a = \frac{4\lambda}{\pi} \tag{2.12}$$

$$\Phi_B(k_1,k_2) = \frac{N(k_1^2 + K_2^2)^2}{a^4(k_1^2+k_2^2+\frac{1}{a^2})^4} \quad ; \quad N = \frac{3\sigma^2 a^2}{\pi} \quad , \quad a = \frac{16\lambda}{3\pi} \tag{2.13}$$

Spectrum B obviously eliminates the singularities in the spectrum of the head process. Conversion of the head spectrum and spectrum A to polar coordinates clearly shows that spectrum A also eliminates the singularities in (2.9).

The Fourier transform of spectra A and B determines the associated covariance functions (see Appendices I and II)

$$R_A(\xi) = \sigma^2\left[\frac{\pi\xi}{4\lambda} K_1(\frac{\pi\xi}{4\lambda}) - \frac{1}{2}(\frac{\pi\xi}{4\lambda})^2 K_o(\frac{\pi\xi}{4\lambda})\right] \tag{2.14}$$

$$R_B(\xi) = \sigma^2\left[(1 + \frac{1}{8}(\frac{3\pi\xi}{16\lambda})^2)\frac{3\pi\xi}{16\lambda}K_1(\frac{3\pi\xi}{16\lambda}) - (\frac{3\pi\xi}{16\lambda})^2 K_o(\frac{3\pi\xi}{16\lambda})\right] \tag{2.15}$$

Figure 2.1 is a graphical presentation of each spectral function, (2.10), (2.12), and (2.13), discussed above as possible representations for the ln T process, along with the spectrum assumed by Bakr et al. (1978, eq. 26) for ln K in their three-dimensional analysis.

For plotting purposes spectra are normalized by the product $\sigma_f^2\lambda^n$, n = 2 for two-dimensional cases and 3 in the three-dimensional case. This normalized spectrum is plotted against an equivalent dimensionless wave number, which is the wave number multiplied by lag distance at which the associated covariance function is reduced by e^{-1}, λ_e. Assuming the Whittle spectrum to describe the ln T process leads to $\lambda_e = 1.05\lambda$; when using spectrum A $\lambda_e = 1.33\lambda$, using spectrum B $\lambda_e = 1.4\lambda$, and using the three-dimensional spectrum (Bakr et al., 1978) $\lambda_e = \lambda$.

Similar behavior is expressed by the Whittle and three-dimensional spectra. Both exhibit maximum energy levels localized at the origin

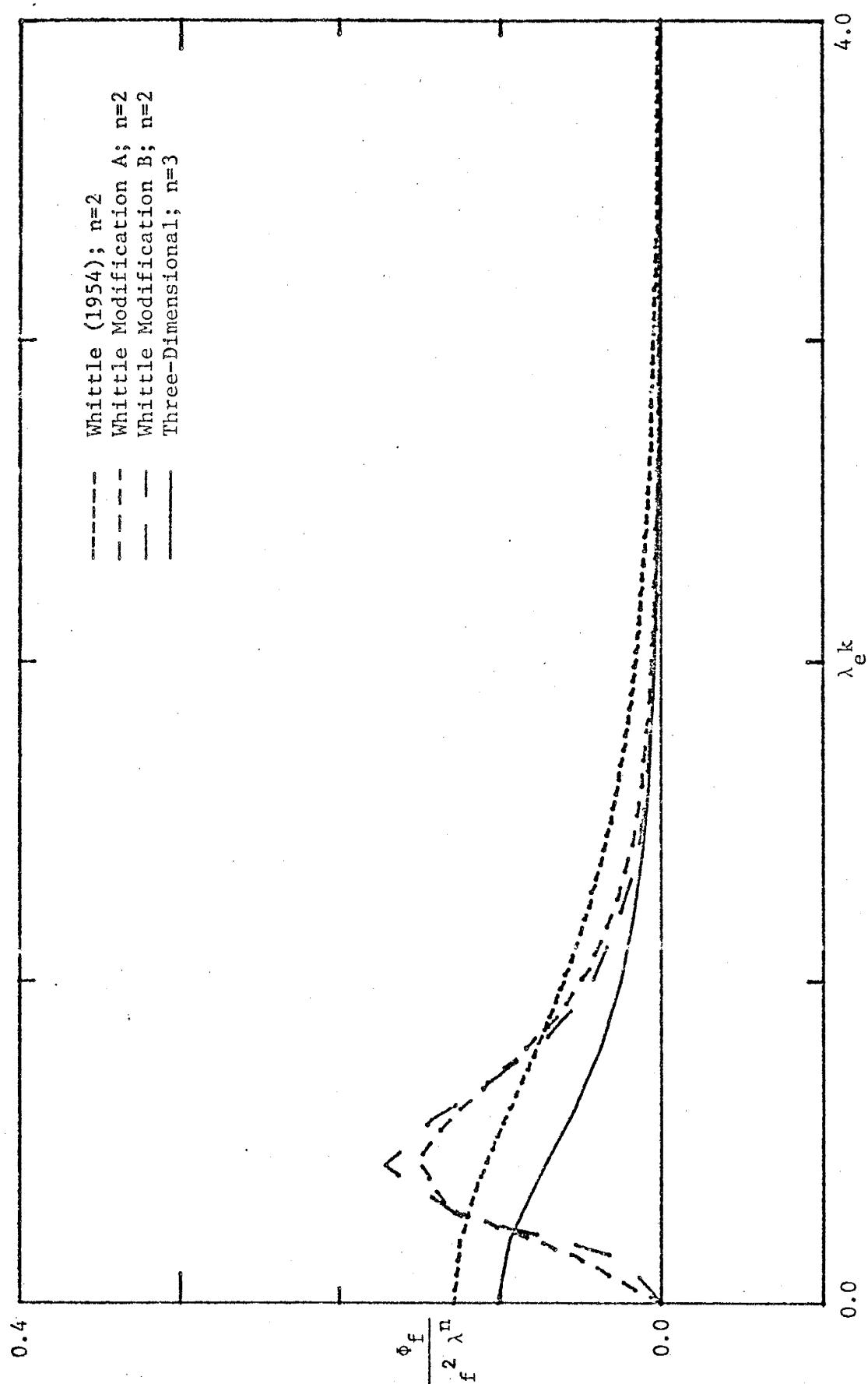

Figure 2.1: Comparision of Potential Two-Dimensional Ln T Spectra with the Three-Dimensional Ln K Spectrum assumed by Bakr et al. (1978)

that decrease monotonically as wave number increases. Spectra A and B have maximum energy levels localized around $\lambda_e k = 0.45$ from which they decrease monotonically with increasing wave number. This shape is similar to that observed for the one-dimensional ln K spectra (Bakr et al., 1978, Fig. 1). The occurrence of a finite spectral density at small wave number implies long wave lengths in ln T fluctuations. The Whittle and three-dimensional spectra imply that there is some contribution to the ln T variance come from variations of indefinitely large wave length; spectra A and B suggest that contributions to the ln T variance come from variations of very large, but finite, wave lengths. Spectra with the form of A or B imply a more structured medium composed of alternating high and low transmissivity regions as indicated by the shape of the correlation functions.

Graphical comparison of the correlation functions discussed above with the three-dimensional form of Bakr et al. (1978, eq. 21) is shown in Figure 2.2. Correlation functions, the covariance functions normalized by their respective variance, are plotted against the equivalent dimensionless lag distance. Equivalent dimensionless lag distance is the lag distance divided by the distance at which the correlation drops to the e^{-1} level.

Above the e^{-1} correlation level the three two-dimensional correlation functions are indistinguishable. Below the e-fold drop of correlation values the Whittle and three-dimensional correlation functions behave quite similarly although the Whittle function has slightly lower values. In this range of low correlation values, correlation functions A and B both exhibit the "hole" phenomena which was also observed in the one-dimensional analysis of Bakr et al. (1978, Fig. 1b). Minima in both

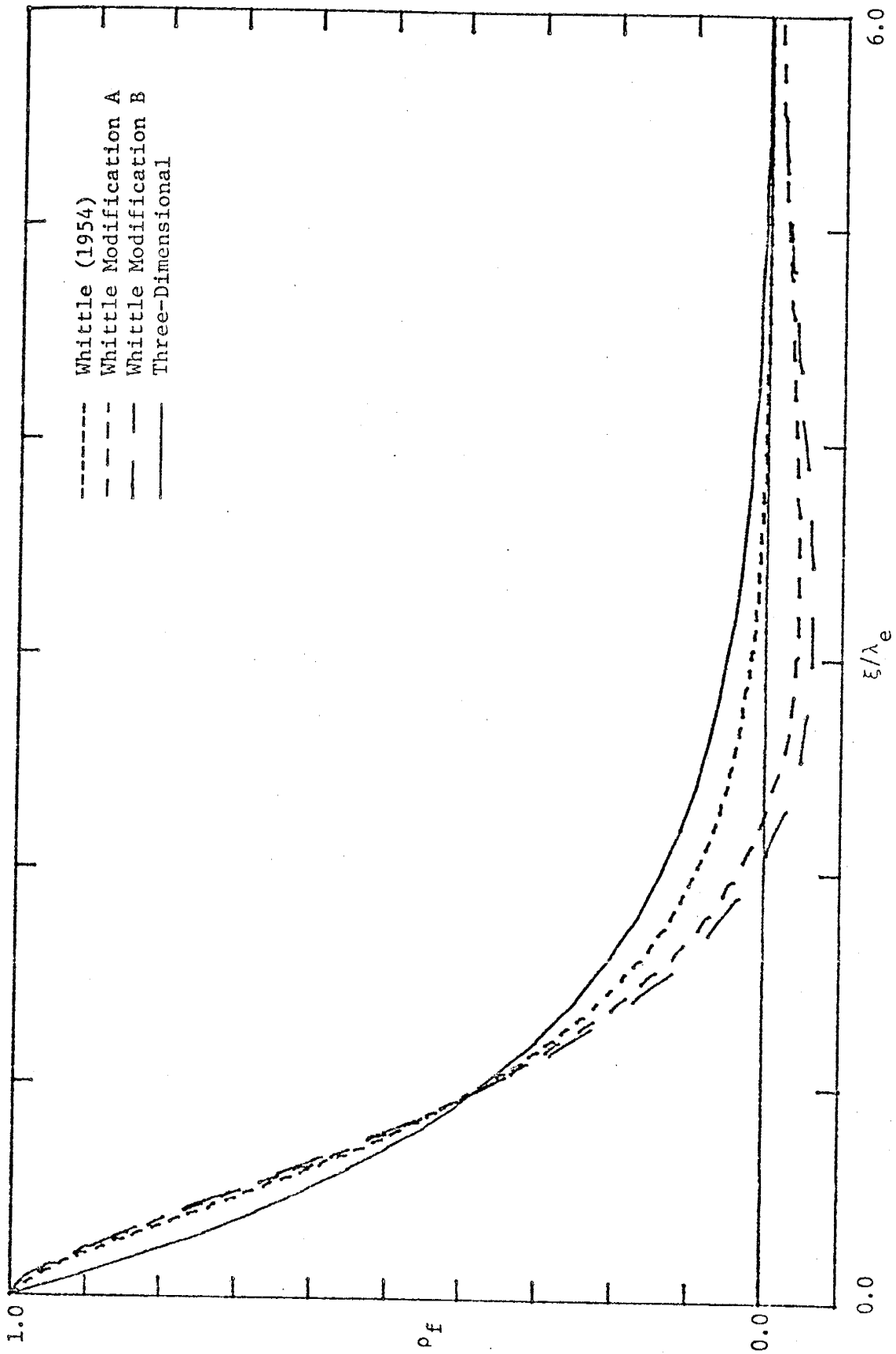

Figure 2.2: Comparison of Potential Two-Dimensional Ln T Correlation Functions with the Three-Dimensional Correlation Function assumed by Bakr et al. (1978)

two-dimensional correlation functions occur at a dimensionless lag distance of about three. This negative correlation implies that regions of high ln T with a scale on the order of λ_e will typically be adjacent to similar regions in which ln T is less than the mean. The "hole" phenomenon observed in the ln K and ln T covariance functions of one- and two-dimensional analyses appears to be a characteristic of the input spectra chosen to eliminate singularities in their respective head spectra. Spectra A and B will both be used in evaluating the head covariance function and the ln T - head cross-covariance function resulting from the steady analysis. The "hole" phenomenon observed in these ln T correlation functions will be accepted as an inherent feature of two-dimensional confined groundwater flows when the head process is assumed to be statistically homogeneous (stationary).

The assumptions have been made throughout this analysis that the ln T process is statistically isotropic and statistically homogeneous. These properties apply to the statistical character of the flow media; it is possible to have a physically heterogeneous aquifer, as indicated in (2.1), which can be described as statistically homogeneous. Statistical properties of the flow system, such as the covariance function, are homogeneous if they are functions of separation distance between observations and not their locations. Stationarity is the temporal equivalent of statistical homogeneity. Statistical isotropy implies dependence of statistical properties on only the magnitude and not on the orientation of separation vectors between observation points. Unlike its physical counterpart, statistical isotropy implies statistical homogeneity. Both statistical homogeneity and statistical isotropy are assumed for the input process to simplify the present analysis.

Statistical homogeneity is assumed for the head process in subsequent analyses.

Head Variance and Covariance Functions

The head covariance function is determined by the Fourier transform of the head spectrum. Variance of the head process may be found either by evaluating the Fourier transform of the spectrum at zero lag or by taking the limit of the covariance function as the lag distance goes to zero.

$$R_h(\xi_1,\xi_2) = \int_{-\infty}^{\infty}\int e^{i(k_1\xi_1 + k_2\xi_2)}\Phi_h(k_1,k_2)dk_1dk_2 \tag{2.16}$$

$$\sigma_h^2 = R_h(0) = \int_{-\infty}^{\infty} \Phi_h(\vec{k})d\vec{k} \tag{2.17}$$

$$= \lim_{\xi_1,\xi_2\to 0} R_h(\xi_1,\xi_2)$$

where the h subscript denotes statistical properties of the head fluctuations and ξ_1 and ξ_2 are components of the lag vector separating observation points of the process.

Substituting (2.9) into (2.16), assuming (2.12) for the ln T spectrum, and performing the integration (see Appendix III) leads to the head covariance function associated with input spectrum A. Written in polar coordinates this head covariance function has the form

$$R_{Ah}(\xi\ x) = \sigma_{Ah}^2\ 4\left\{\cos^2\chi\left[\left(\frac{1}{4}\left(\frac{\pi\xi}{4\lambda}\right)^2 + 2\right)K_o\left(\frac{\pi\xi}{4\lambda}\right)\right.\right.$$

$$\left. + \frac{\pi\xi}{4\lambda}K_1\left(\frac{\pi\xi}{4\lambda}\right) + 4\left(\frac{\pi\xi}{4\lambda}\right)^{-1}K_1\left(\frac{\pi\xi}{4\lambda}\right) - 4\left(\frac{\pi\xi}{4\lambda}\right)^{-2}\right]$$

$$- \left[K_o\left(\frac{\pi\xi}{4\lambda}\right) + \frac{1}{4}\left(\frac{\pi\xi}{4\lambda}\right)K_1\left(\frac{\pi\xi}{4\lambda}\right)\right.$$

$$\left.\left. +2\left(\frac{\pi\xi}{4\lambda}\right)^{-1}K_1\left(\frac{\pi\xi}{4\lambda}\right) - 2\left(\frac{\pi\xi}{4\lambda}\right)^{-2}\right]\right\} \qquad (2.18)$$

where χ is the angle between the lag vector, ξ, and the mean-flow direction and λ is the integral scale associated with Φ_A. Equations (2.17) give the head variance

$$\sigma_{Ah}^2 = \frac{8}{\pi^2}\ J_1^2\ \sigma_f^2\ \lambda^2 \qquad (2.19)$$

Following the same procedure but using (2.13) as the ln T spectrum (see Appendix IV) the head covariance and variance functions are

$$R_{Bh}(\xi,\chi) = \sigma_{Bh}^2 \frac{1}{2}[(2-(\frac{3\pi\xi}{16\lambda})^2\cos^2\chi) \frac{3\pi\xi}{16\lambda} K_1(\frac{3\pi\xi}{16\lambda})$$

$$+ (\frac{3\pi\xi}{16\lambda})^2 K_o(\frac{3\pi\xi}{16\lambda})] \qquad (2.20)$$

$$\sigma_{Bh}^2 = (\frac{8}{3\pi})^2 J_1^2 \sigma_f^2 \lambda^2 \qquad (2.21)$$

Head variances given by (2.19) and (2.21) are plotted in Figure 2.3; head correlation functions associated with (2.18) and (2.20) are plotted in Figures 2.4 and 2.5 respectively.

Head variances resulting from one- and two-dimensional phreatic-flow analyses (Gelhar, 1976), one- and three-dimensional confined-flow analyses (Bakr et al., 1978), and two-dimensional confined-flow analyses, assuming both spectra A and B for the input process, are graphically compared in Figure 2.3. As presented, head variances are normalized by $\sigma_f^2 b^2$, ln T variance multiplied by the square of the aquifer (or saturated) thickness, b, and plotted against a dimensionless ratio, $r = \frac{J_1 \lambda_e}{b}$, using the equivalent scale appropriate to each flow system.

Two-dimensional phreatic head variance is smaller than its one-dimensional counterpart by about two orders-of-magnitude for small values of r and one-half order-of-magnitude for large values of r. For confined

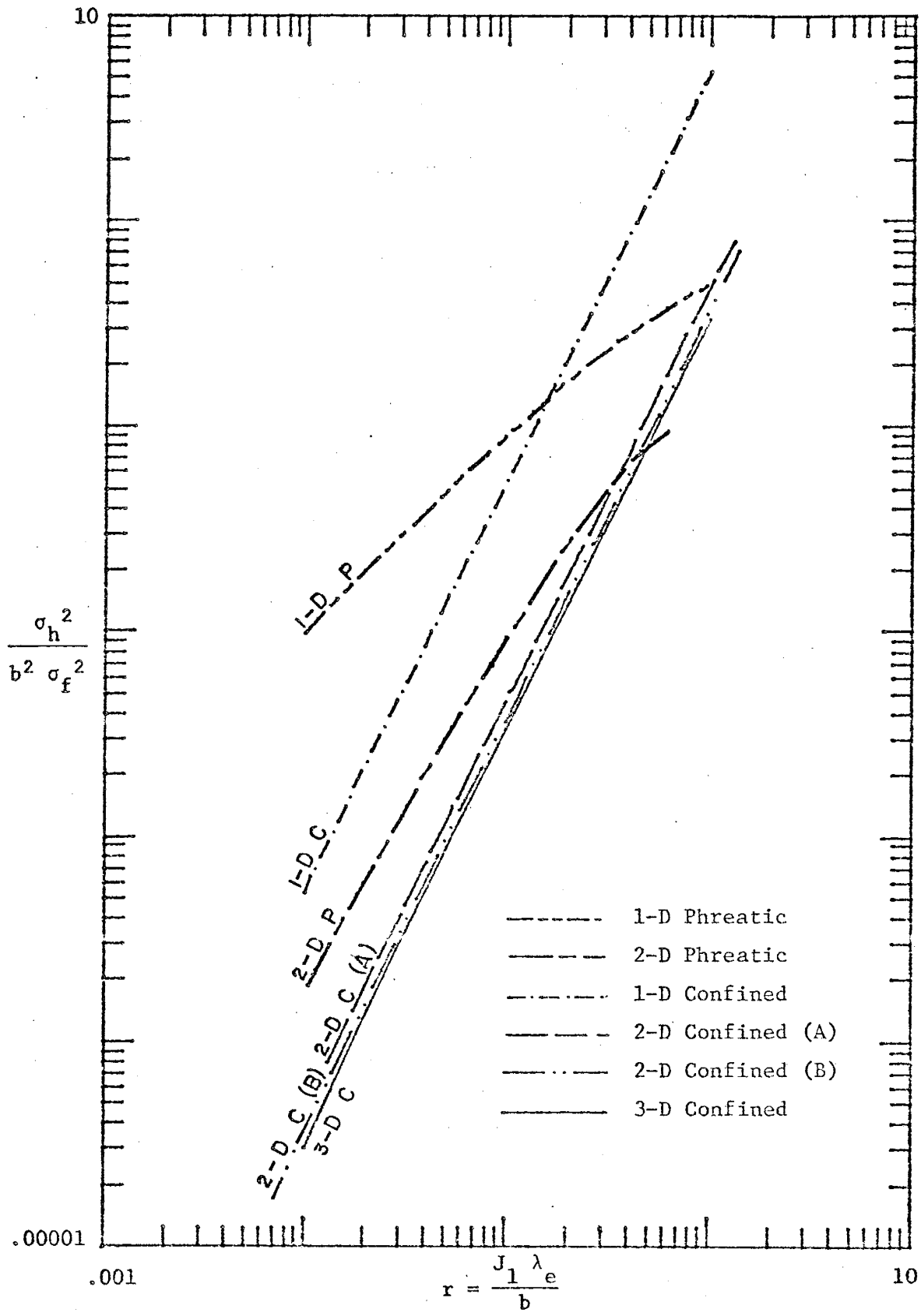

Figure 2.3: Comparison of Steady Head Variances for 1- and 2-Dimensional Phreatic Flow and 1-, 2-, and 3-Dimensional Confined Flow

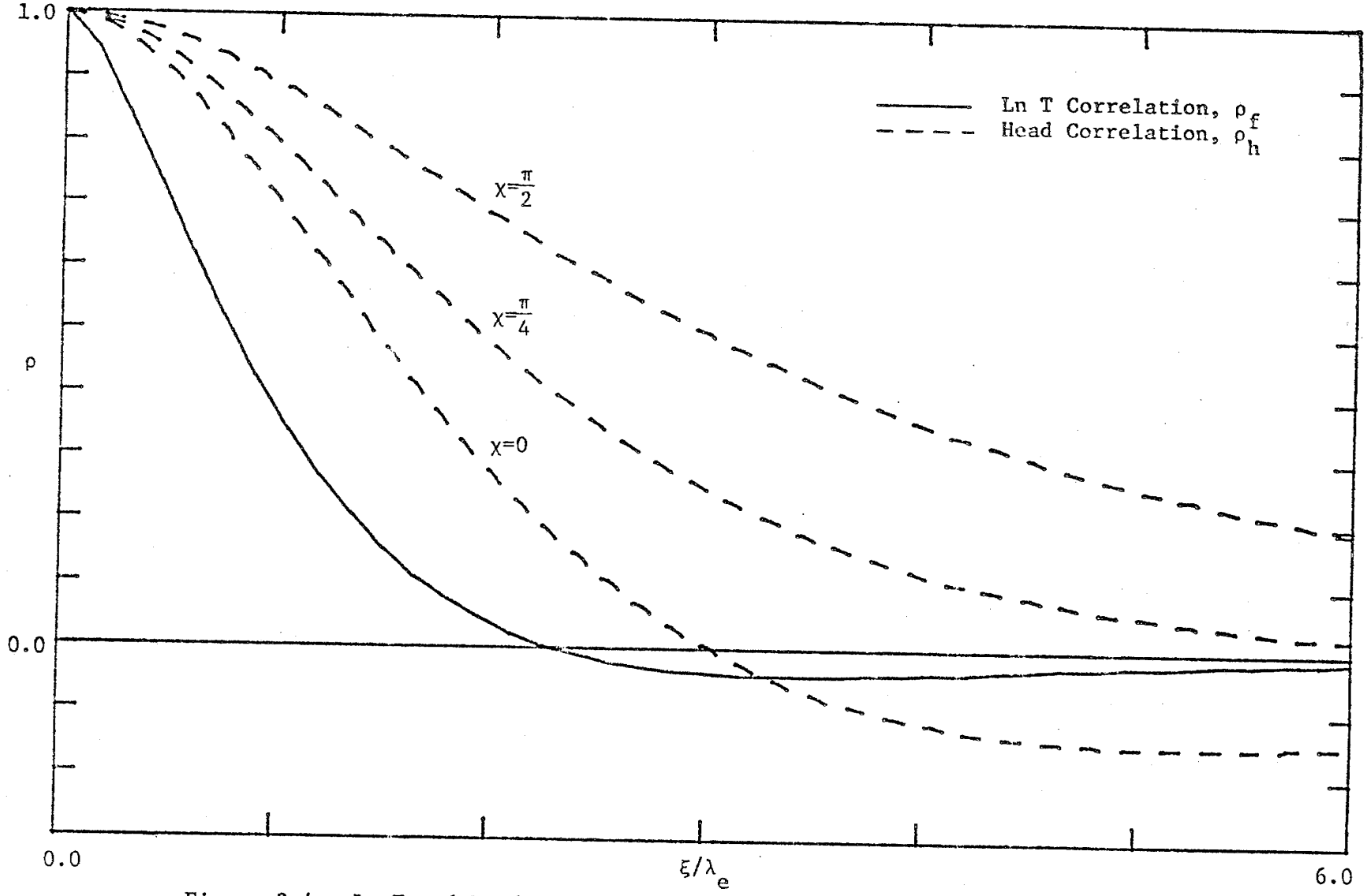

Figure 2.4: Ln T and Head Correlation Functions assuming Input Spectrum A

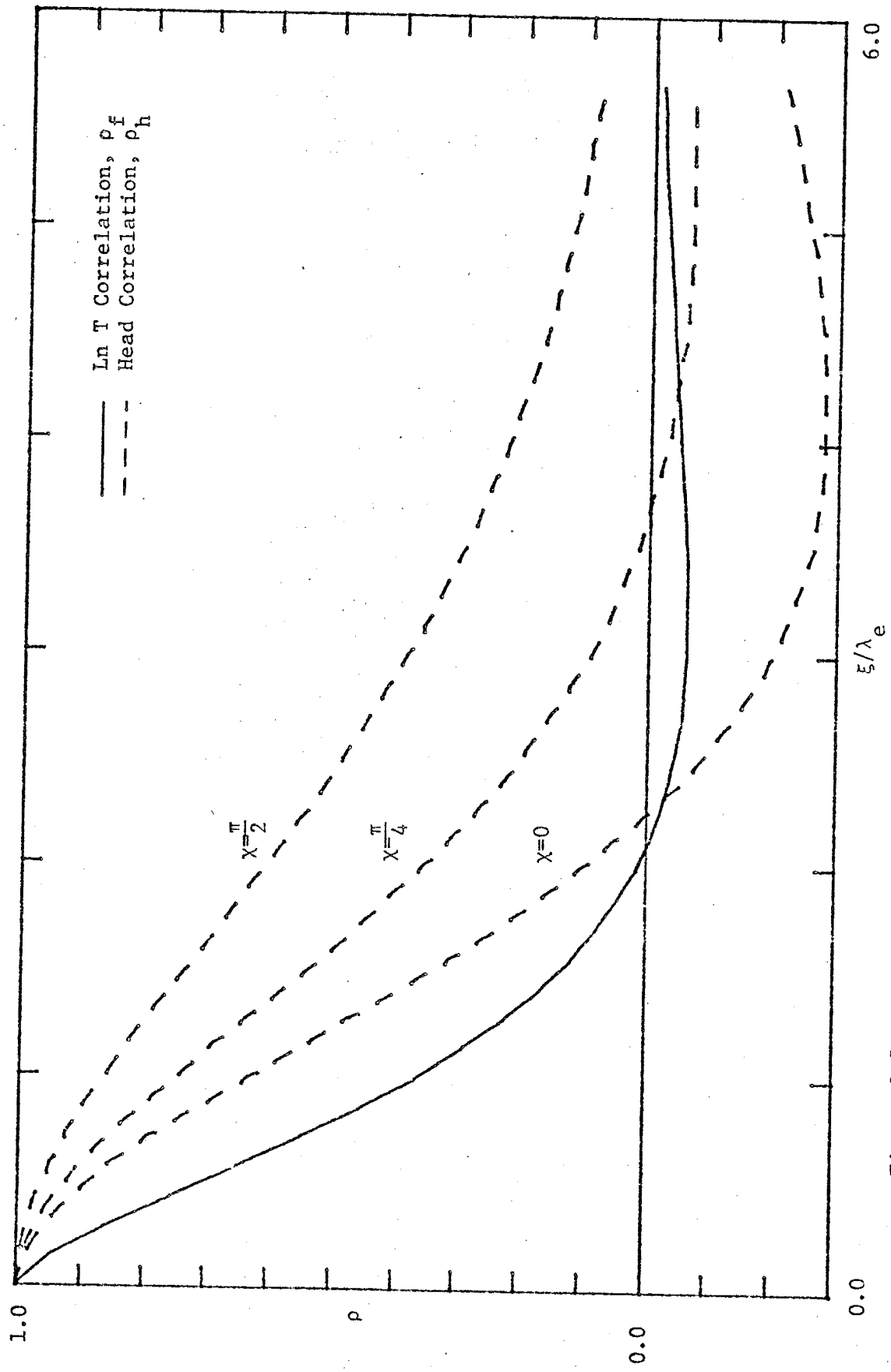

Figure 2.5: Ln T and Head Correlation Functions assuming Input Spectrum B

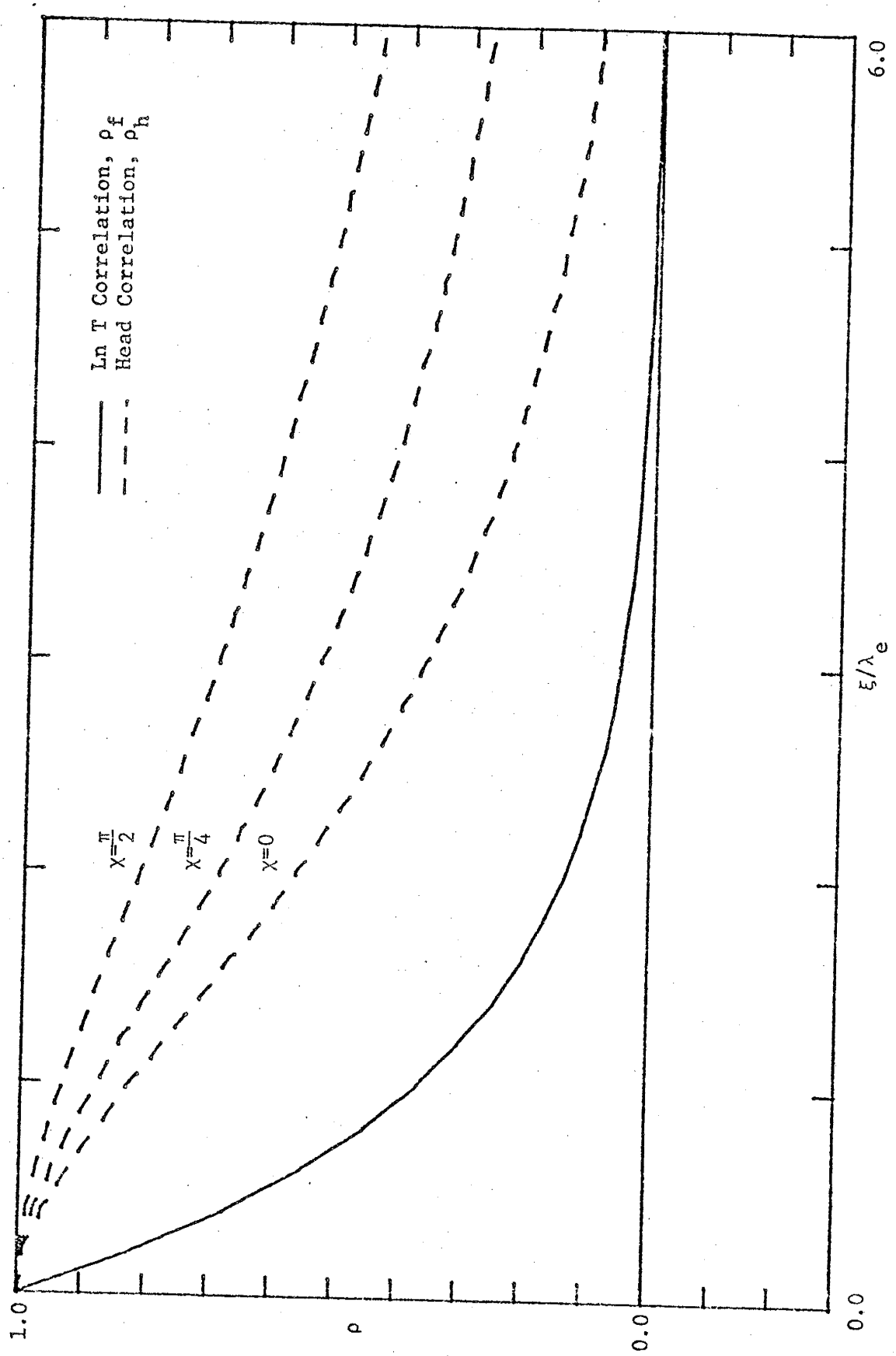

Figure 2.6: Three-Dimensional Ln K and Head Correlation Functions (from Bakr et al., 1978)

flow, multidimensional head variances are about one-and-a-half orders-of-magnitude smaller than the one-dimensional result; all confined head variances have the same slope in the log-log plot. In the analysis of two-dimensional confined flow, assuming input spectrum A produced a slightly larger head variance than assuming input spectrum B. Both two-dimensional head variance results are larger than the three-dimensional result, although the differences are negligible.

Head variance reductions for multidimensional flow analysis may be explained by freedom of water particles to choose one of several alternative flow paths around a local low permeability zone instead of being forced through the obstruction.

Although statistically isotropic ln T correlation functions are assumed to describe the input process, each of the head correlation functions produced is statistically anisotropic. Minimum correlation in the heads occur parallel to mean groundwater flow (see Figs. 2.4, 2.5, and 2.6). Each of the head correlation functions implies that head fluctuations are uncorrelated at large lag distance. The head correlation functions maintain high values over much greater dimensionless lag distances than do the ln T correlation functions - evidence of the smoothing effect of groundwater flow. Both two-dimensional head correlation functions exhibit the "hole" phenomena, indicating negative correlation of head fluctuations at intermediate lag distance. The "hole" resulting from use of spectrum B exhibits stronger negative correlation and continues to exist over a larger range of lag-vector orientation angles than the "hole" resulting from use of spectrum A. Despite the strong similarities between ln T correlation functions A and B the resulting head correlation functions exhibit significant differences in

both magnitude of correlation and correlation scale, the distance over which high correlation levels exist.

Cross-Covariance Functions

Evaluation of the cross-covariance function between head and ln T, a measure of dependence between the two processes at various lag distances, first requires evaluation of the cross-spectrum. Formulation of the cross-spectrum parallels that of the head spectrum previously discussed. The cross-spectrum is given by the expectation of the Fourier amplitude of the head fluctuations, (2.8), multiplied by the complex-conjugate of the ln T Fourier amplitude (Lumley and Panofsky, 1964, p. 21):

$$\Phi_{hf}(k_1,k_2)d\vec{k} = E(dZ_h dZ_f^*) = \frac{-iJ_1k_1}{(k_1^2 + k_2^2)} \Phi_f(k_1,k_2)\, d\vec{k} \qquad (2.22)$$

The cross-covariance function is the Fourier transform of the cross-spectrum. Substituting spectrum A, (2.12), into (2.22) and completing the transform (see Appendix V) gives the associated cross-covariance function which, in polar coordinates, is

$$R_{Ahf}(\xi,\chi) = \sigma_f^2 J_1 \lambda \frac{2}{\pi} \cos\chi \left(\frac{\pi\xi}{4\lambda}\right)^2 K_1\left(\frac{\pi\xi}{4\lambda}\right) \tag{2.23}$$

The cross-covariance function associated with input spectrum B (see Appendix VI) is

$$R_{Bhf}(\xi,\chi) = \sigma_f^2 J_1 \lambda \frac{8}{3\pi} \cos\chi \left(\frac{3\pi\xi}{16\lambda}\right)^2 \left[K_1\left(\frac{3\pi\xi}{16\lambda}\right) - \frac{1}{4}\left(\frac{3\pi\xi}{16\lambda}\right) K_o\left(\frac{3\pi\xi}{16\lambda}\right)\right] \tag{2.24}$$

Both (2.23) and (2.24) are zero valued when $\xi = 0$ or when $\chi = \frac{\pi}{2}$. Thus, head and ln T fluctuations are uncorrelated at zero lag; E(hf) = 0.

Normalized by the term $\sigma_f^2 J_1 \lambda$, equations (2.23) and (2.24) are plotted in Figures 2.7 and 2.8 against equivalent dimensionless lag distance for four values of the angle χ ranging from 0 to 180 degrees. As noted in previous discussions of ln T spectra and covariance functions and head covariance functions, the equations resulting from use of either spectra A or B exhibit similar behavior patterns.

The cross-covariance functions given by (2.23) and (2.24) indicate positive cross-correlation values for lag vectors in the first (and fourth) quadrant, zero cross-correlation perpendicular to mean flow,

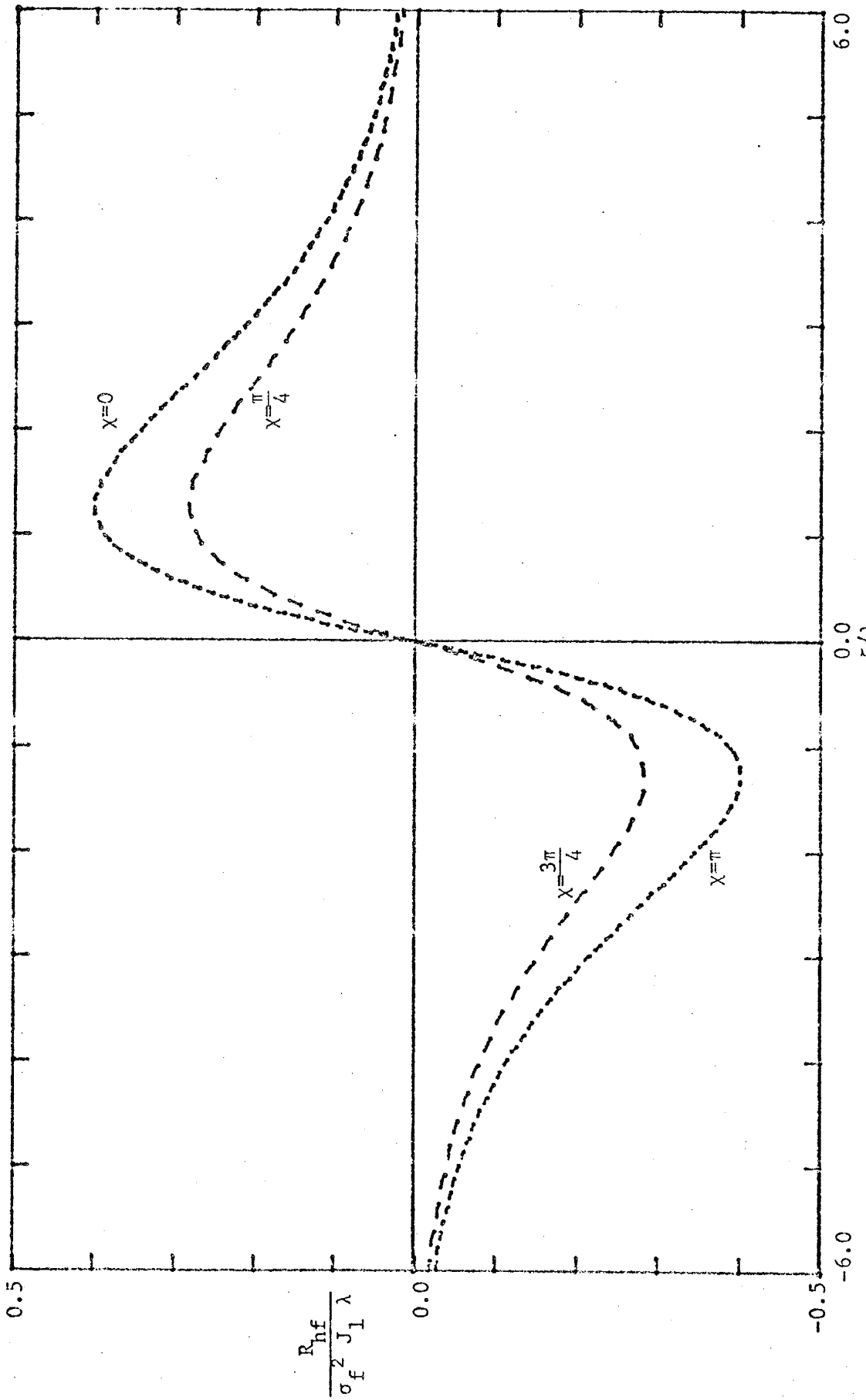

Figure 2.7: Dimensionless Cross-Covariance Function between Ln T and Head assuming Input Spectrum A

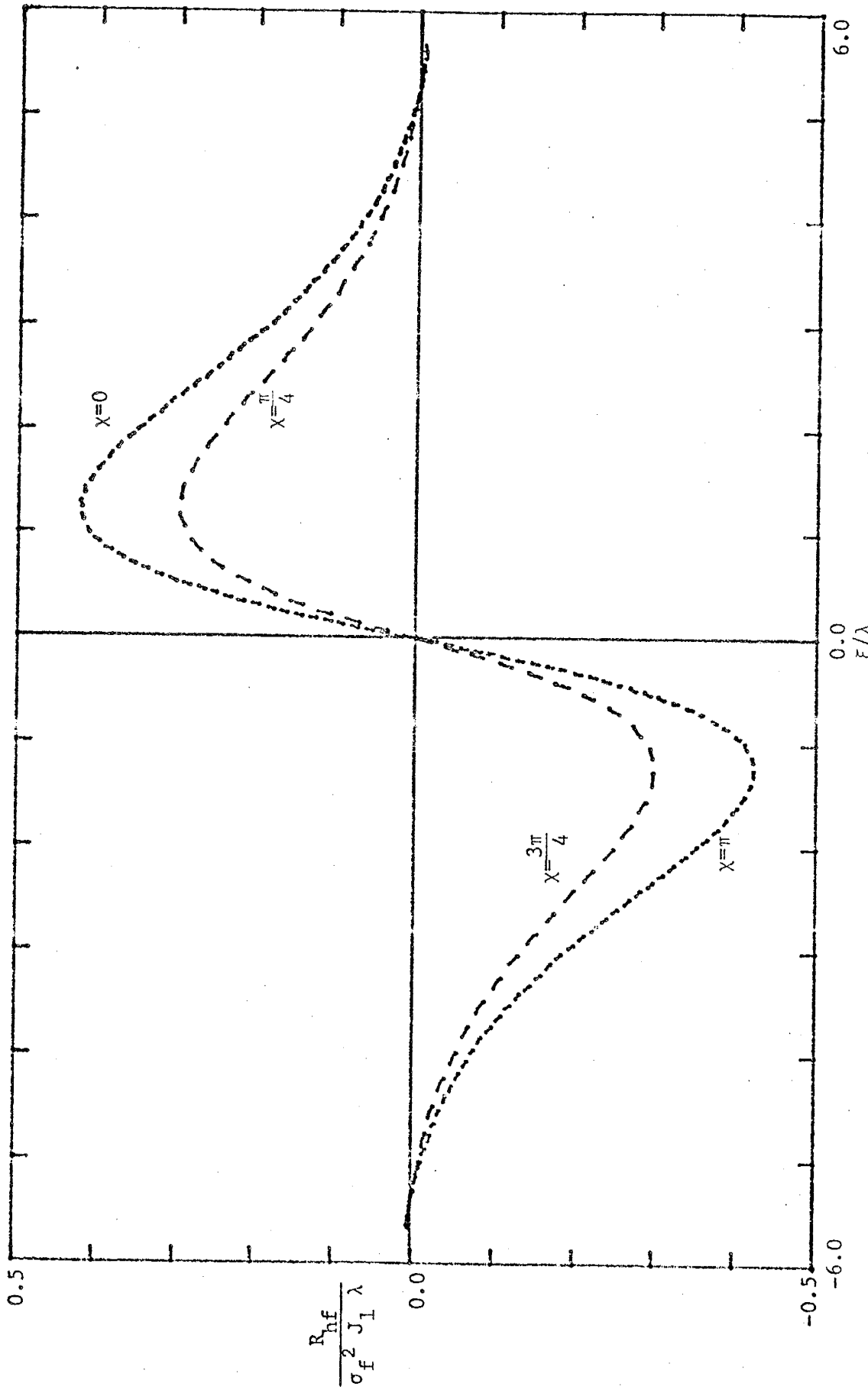

Figure 2.8: Dimensionless Cross-Covariance Function between Ln T and Head assuming Input Spectrum B

and negative cross-correlation values for lag vectors in the second (and third) quadrant. Maximum and minimum correlation values occur at dimensionless lag distance of about 1.25 for all orientations. Both equations exhibit zero cross-correlation values for large lag distances. Small differences in the cross-covariance functions result from use of spectra A and B. Slightly greater maxima and minima and a more rapid decay are seen for the cross-covariance function associated with input spectrum B.

Interpretation of Covariance Functions

Covariance and correlation functions (correlation functions are the covariance function divided by the variance) measure the degree of dependence of information obtained at various lag distances. These functions are constructed by taking the expected value of the product of two observations made at various lag distances (Lumley and Panofsky, 1964, p. 14)

$$\rho(\vec{\xi}) = \frac{R(\vec{\xi})}{\sigma^2} = \frac{E[X(\vec{x}+\vec{\xi})X(\vec{x})]}{\sigma^2}$$

where ρ is the correlation function and X has zero mean. Positive correlation values imply correlation between observations of similar magnitude (high values with high values or low with low), and negative values for the correlation function imply correlation of observations of opposite magnitude (high values with low). Larger absolute values

of correlation indicate stronger dependence between observations at that lag distance. Maximum correlation occurs at zero lag distance because observations are compared with themselves.

ln T correlation functions resulting from use of spectra A and B (Fig. 2.2) exhibit high correlation levels at short lag distances. As lag distance increases these correlation functions decay rapidly, becoming slightly negative before approaching zero. Behavior of the correlation functions implies small-scale spatial correlation structure in the ln T process. The head correlation functions (Figs. 2.4, 2.5, 2.6) exhibit high correlation levels spread over much greater lag distances than was observed for the ln T correlation functions - strong evidence of the smoothing effect of the governing flow equation.

Limitations

The present analysis is limited by several implied and expressed assumptions noted here.

(1) Use of two-dimensional models to represent what is in reality a three-dimensional process implies certain limitations in application of results to "real-world" situations. In the present study the flow process is assumed to be depth-averaged; that is, parameter values assigned at observation points on the aquifer surface are considered to be representative averages of the vertical variations in the parameter.

(2) Assumption of unidirectional variations in mean head first seem rather restrictive. However, orientation of the coordinate system with the principal axis parallel to mean flow is conceptually easy to accomplish.

(3) Steady-flow conditions are generally very restrictive in groundwater

analyses; this condition will be relaxed in the transient analysis to be discussed next.

(4) The assumption of statistical isotropy for ln T and statistical homogeneity for head may be of some legitimate concern. Unfortunately, a check of these properties is not available because statistical analysis of sufficiently large sets of two-dimensional head and log-transmissivity data is lacking.

Summary

A summary of the analysis of two-dimensional, steady groundwater flow and its results are:

(1) Stochastic analysis procedures are used in this study because they recognize the continuum nature and variability of aquifer materials. The spectral technique accounts for this variability by considering statistical properties of flow parameters and variables.

(2) The head spectrum is determined to be a simple function of the ln T spectrum.

(3) Singularities in the head spectrum preclude use of the Whittle spectrum and covariance function to represent the input, ln T, process if heads are assumed to be statistically homogeneous. However, minor modifications of this spectrum can be made which eliminate the singularities.

(4) Head variance is determined to be a function of variance and average correlation distance of the ln T process and mean gradient. This indicates the importance of considering spatial correlation structure as well as variance of the aquifer parameter when evaluating head variance.

(5) Multidimensional head variances are reduced more than an order-of-

magnitude from the one-dimensional head variance as a result of the freedom of water particles to move around low permeability zones.

(6) Two- and three-dimensional head correlation functions reflect the same aspects of the groundwater system; head fluctuations are statistically anisotropic and correlated over much greater distances than are ln T fluctuations. This later point illustrates the smoothing nature of the groundwater system.

(7) Head variance and correlation functions resulting from use of both input spectra A and B exhibit the same basic characteristics; in this general sense the head process is not greatly sensitive to the assumed description of the input, ln T, process. However, specific values of these functions are dependent on the input spectrum used.

(8) The cross-covariance function between ln T and head exhibits positive correlation values in the first and fourth quadrants of the coordinate system, zero correlation perpendicular to mean flow, and negative correlation in the second and third quadrants.

ANALYSIS OF TRANSIENT FLOW

Transient aspects of groundwater flow have not previously been considered in studies using stochastic and spectral techniques. As a first step in this direction, temporal variations of hydraulic head will be restricted to the mean component of the head process. Analytical procedures parallel those followed in the analysis of steady flow: the head spectrum equation is determined, an appropriate form of the ln T spectrum is chosen, and equations for the transient head variance and correlation structure are determined. Transient analysis results will be compared with results obtained from the steady analysis.

Spectral-Equation Development

The transient equation for depth-averaged groundwater flow is formulated by replacing the zero right-hand side of (2.1) by a term describing storage effects

$$\frac{\partial}{\partial x}\left(T\frac{\partial \phi}{\partial x}\right) + \frac{\partial}{\partial y}\left(T\frac{\partial \phi}{\partial y}\right) = S\frac{\partial \phi}{\partial t} \tag{3.1}$$

Rewriting (3.1) in terms of ln T

$$\frac{\partial^2\phi}{\partial x^2} + \frac{\partial^2\phi}{\partial y^2} + \frac{\partial \ln T}{\partial x}\frac{\partial\phi}{\partial x} + \frac{\partial \ln T}{\partial y}\frac{\partial\phi}{\partial y} = \frac{S}{T}\frac{\partial\phi}{\partial t} \tag{3.2}$$

Assuming head and ln T to be stochastic processes, they may be formulated as a mean part plus fluctuations about the mean

$$\phi(x,y,t) = H(x,t) + h(x,y)$$

$$\ln T(x,y) = F + f(x,y) \tag{3.3}$$

Note that in (3.3) the mean part of the head process contains all time dependency observed in the heads and, as in the steady case, spatial variation of the mean head is allowed only in the x direction. Fluctuations in the head process occur in both the x and y directions but have no temporal variation. Representation of ln T in (3.3) is identical to (2.3); mean ln T is constant and fluctuations occur in both spatial directions. The anti-log of ln T gives an equation for the transmissivity in terms of the mean and fluctuations of ln T

$$T = e^{F} e^{f}$$

Transmissivity on the right-hand side of (3.2) can be approximated by

$$\frac{1}{T} \simeq \frac{1}{T_{\ell}} \left(1 - f + \frac{f^2}{2}\right) \tag{3.4}$$

where T_{ℓ} is the transmissivity value associated with mean ln T. Throughout the analysis of transient flow the storage coefficient is assumed to be deterministic because of the relatively small range of values observed for confined systems; such an assumption will simplify computations.

Substituting (3.3) and (3.4) into (3.2) leads to

$$\frac{\partial^2 H}{\partial x^2} + \frac{\partial^2 h}{\partial x^2} + \frac{\partial^2 h}{\partial y^2} + \frac{\partial f}{\partial x}\frac{\partial H}{\partial x} + \frac{\partial f}{\partial x}\frac{\partial h}{\partial x} + \frac{\partial f}{\partial y}\frac{\partial h}{\partial y} = \frac{S}{T_{\ell}} \frac{\partial H}{\partial t}\left(1 - f + \frac{f^2}{2}\right) \tag{3.5}$$

The mean equation of transient flow is determined by taking expectations through (3.5)

$$\frac{\partial^2 H}{\partial x^2} + E\left(\frac{\partial f}{\partial x}\frac{\partial h}{\partial x}\right) + E\left(\frac{\partial f}{\partial y}\frac{\partial h}{\partial y}\right) = \frac{S}{T_\ell}\frac{\partial H}{\partial t}\left(1 + \frac{\sigma_f^2}{2}\right) \tag{3.6}$$

Subtracting (3.6) from (3.5) results in the governing equation of flow formulated in terms of fluctuations of head and ln T

$$\frac{\partial^2 h}{\partial x^2} + \frac{\partial^2 h}{\partial y^2} - J_1\frac{\partial f}{\partial x} = -\frac{S}{T_\ell}\frac{\partial H}{\partial t} f \tag{3.7}$$

where $J_1 = -\frac{\partial H}{\partial x}$ is the mean gradient and second-order perturbation products have been neglected.

Statistical homogeneity will again be assumed for the head and ln T processes. Fluctuations in these processes are represented by Fourier-Stieltjes integrals [recall (2.7)] leading to an equation relating the complex Fourier amplitudes dZ_h and dZ_f

$$dZ_h(k_1,k_2) = \left[\frac{-ik_1J_1}{(k_1^2+k_2^2)} + \frac{\frac{S}{T_\ell}\frac{\partial H}{\partial t}}{(k_1^2+k_2^2)}\right]dZ_f(k_1,k_2) \tag{3.8}$$

Multiplying (3.8) by its complex-conjugate and taking expected values produces an equation for the head spectrum as a function of the ln T spectrum and mean-flow parameters

$$\Phi_h(k_1,k_2) = \left[\frac{k_1^2J_1^2}{(k_1^2+k_2^2)^2} + \frac{(\frac{S}{T_\ell}\frac{\partial H}{\partial t})^2}{(k_1^2+k_2^2)^2}\right]\Phi_f(k_1,k_2) \tag{3.9}$$

The spectral equation for the transient head process, (3.9), assuming steady head fluctuations, is composed of the steady head spectral equation, (2.9), plus an additional term due to transient components of the governing flow equation. The singularity at the wave-number space origin observed in (2.9) appears in (3.9) with increased strength. In the steady head spectrum the singularity behaved as a squared term; however, the transient head spectrum has a fourth-power singularity arising from the new term reflecting the transient component of (3.7). Of the two spectral forms proposed for ln T in the steady analysis only Φ_B, (2.13), eliminates the singularity in (3.9). Assuming statistically

homogeneous head fluctuations, (2.13) is an appropriate form of the ln T spectrum for use in the transient analysis.

Head Variance and Covariance Functions

Having assumed a convenient form for Φ_f, it is possible to determine the equations for transient head variance and covariance (or correlation) by Fourier transformation of the head spectrum equation.

Substituting (2.13) into (3.9) and proceeding according to (2.17) determines the transient head variance (see Appendix VII)

$$\sigma_h^2 = [\frac{J_1^2}{4} + (\frac{S}{T_\ell} \frac{\partial H}{\partial t} \frac{16\lambda}{3\pi})^2] (\frac{16\lambda}{3\pi})^2 \sigma_f^2 \tag{3.10}$$

Solving (3.9) by (2.16) results in the transient head covariance function

$$R_{hh}(\xi,\chi) = \frac{J_1^2}{4} \sigma_f^2 (\frac{16\lambda}{3\pi})^2 \frac{1}{2}[(2-(\frac{3\pi\xi}{16\lambda})^2 \cos^2\chi) \frac{3\pi\xi}{16\lambda} K_1(\frac{3\pi\xi}{16\lambda}) + (\frac{3\pi\xi}{16\lambda})^2 K_o(\frac{3\pi\xi}{16\lambda})]$$

$$+ \frac{S^2}{T_\ell^2}(\frac{\partial H}{\partial t})^2 \sigma_f^2 (\frac{16\lambda}{3\pi})^4 \frac{1}{8} [(8 + (\frac{3\pi\xi}{16\lambda})^2) \frac{3\pi\xi}{16\lambda} K_1(\frac{3\pi\xi}{16\lambda}) + (\frac{3\pi\xi}{16\lambda})^2 K_o(\frac{3\pi\xi}{16\lambda})] \tag{3.11}$$

where ξ and χ are the polar coordinates of the separation vector ξ.

Transient head variance, (3.10), is composed of two terms. The first depends on the mean gradient parameter and is identical to the steady head variance, (2.21), developed previously for the same input spectrum. Parameters associated with transient aspects of the flow system characterize the second term in (3.10); formulation of this term is dependent on the assumption of steady head fluctuations. The importance of considering spatial correlation structure and variability of the ln T process is again illustrated by the transient head variance. A fourth-power dependence on λ occurs in the transient contribution to (3.10) compared with dependence on λ squared in the steady head variance.

Two terms contribute to the transient head covariance function, (3.11). As with the head spectrum and variance equations one part of the covariance function is characterized by the mean gradient; this term is identical to the steady head covariance function, (2.20), using input spectrum B. The second portion of (3.11) is dependent on mean transient parameters. In the correlation function these two terms sum according to a weighting factor, Ω, which is determined by the relative magnitude of the mean gradient and mean transient parameters

$$\Omega = \frac{\frac{J_1^2}{4}}{\frac{J_1^2}{4} + \left(\frac{S}{T_\ell}\frac{\partial H}{\partial t}\frac{16\lambda}{3\pi}\right)^2} \qquad (3.12)$$

When $\Omega = 1$, contributions to the transient head correlation function

come exclusively from the mean-gradient term; and (3.11) is identical to (2.20), the steady head correlation function. Only the term reflecting transient flow parameters contributes when $\Omega = 0$.

Figures 3.1 and 3.2 illustrate the transient head correlation function. In Figure 3.1 each of the contributing correlation functions is plotted. The J_1, mean-gradient, term is anisotropic, with minimum values parallel to mean flow and maximum values perpendicular to mean flow. Isotropic contributions arise from the S/T term; correlation values from this term are large, of the same magnitude as the mean-gradient term evaluated at $\chi = \frac{\pi}{2}$. Both contributions indicate much larger correlation distances for head fluctuations than suggested by the assumed correlation function for ln T. Effects of varying Ω are shown in Figure 3.2 for $\chi = 0$. Smaller values of Ω produce higher correlation levels over longer distances. Recall that the mean-gradient contribution has minimum values when evaluated parallel to mean flow ($\chi = 0$) so the correlation functions illustrated in Figure 3.2 will increase as χ increases to 90 degrees.

Comparison of Transient and Steady Analyses

Results of the transient analysis are composed of the steady result plus an additional term which incorporates transient parameters when steady head fluctuations are assumed and when the same input spectrum is used for both steady and transient analyses. Transient effects reflected in the spectral, variance, and correlation functions are summarized:

(1) In the transient head spectrum, (3.9), the S/T term is isotropic and further limits options for Φ_f because of increased severity of the

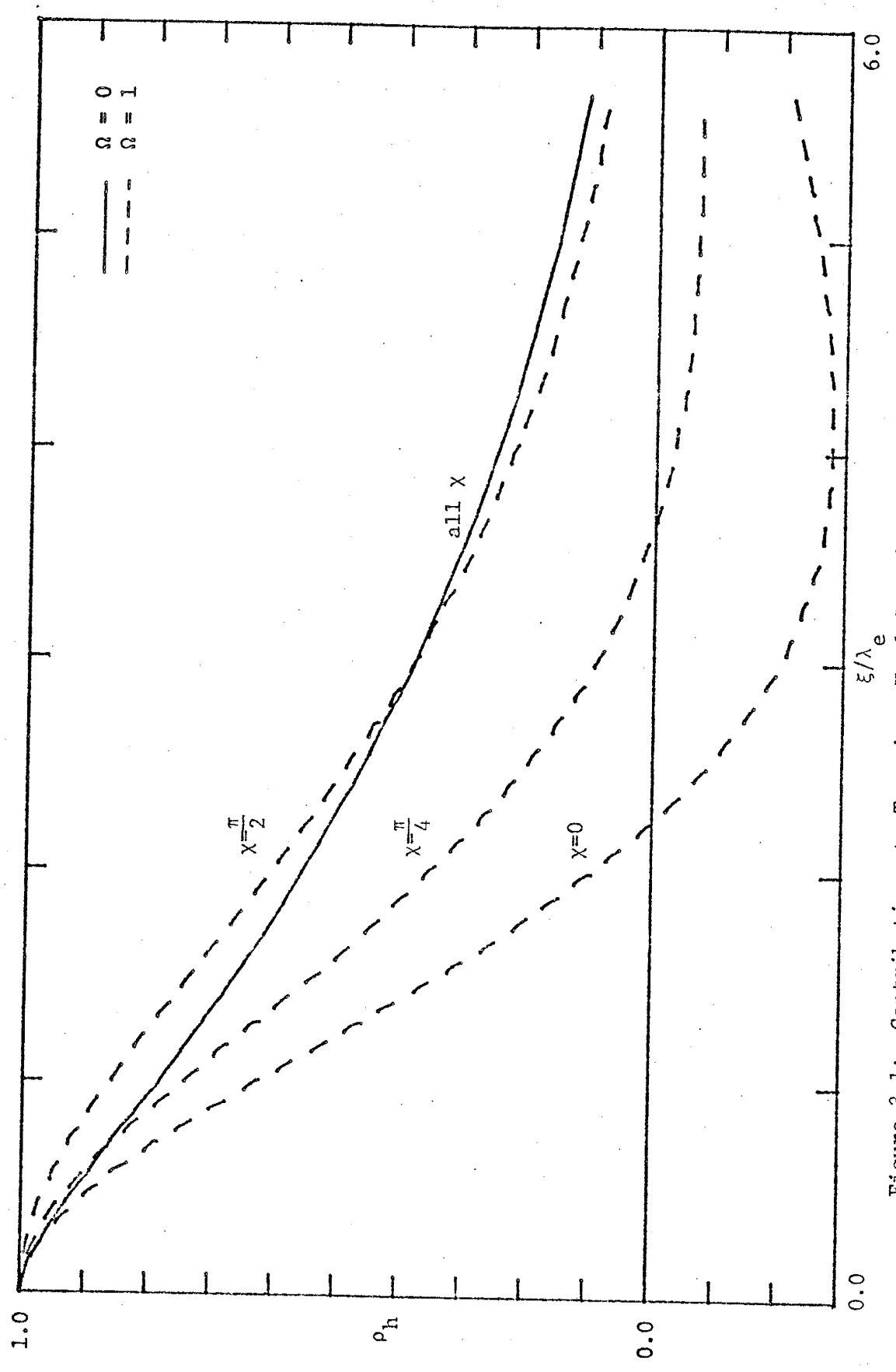

Figure 3.1: Contributions to Transient Head Correlation Function from terms reflecting the Mean-Gradient and Mean-Transient Parameters

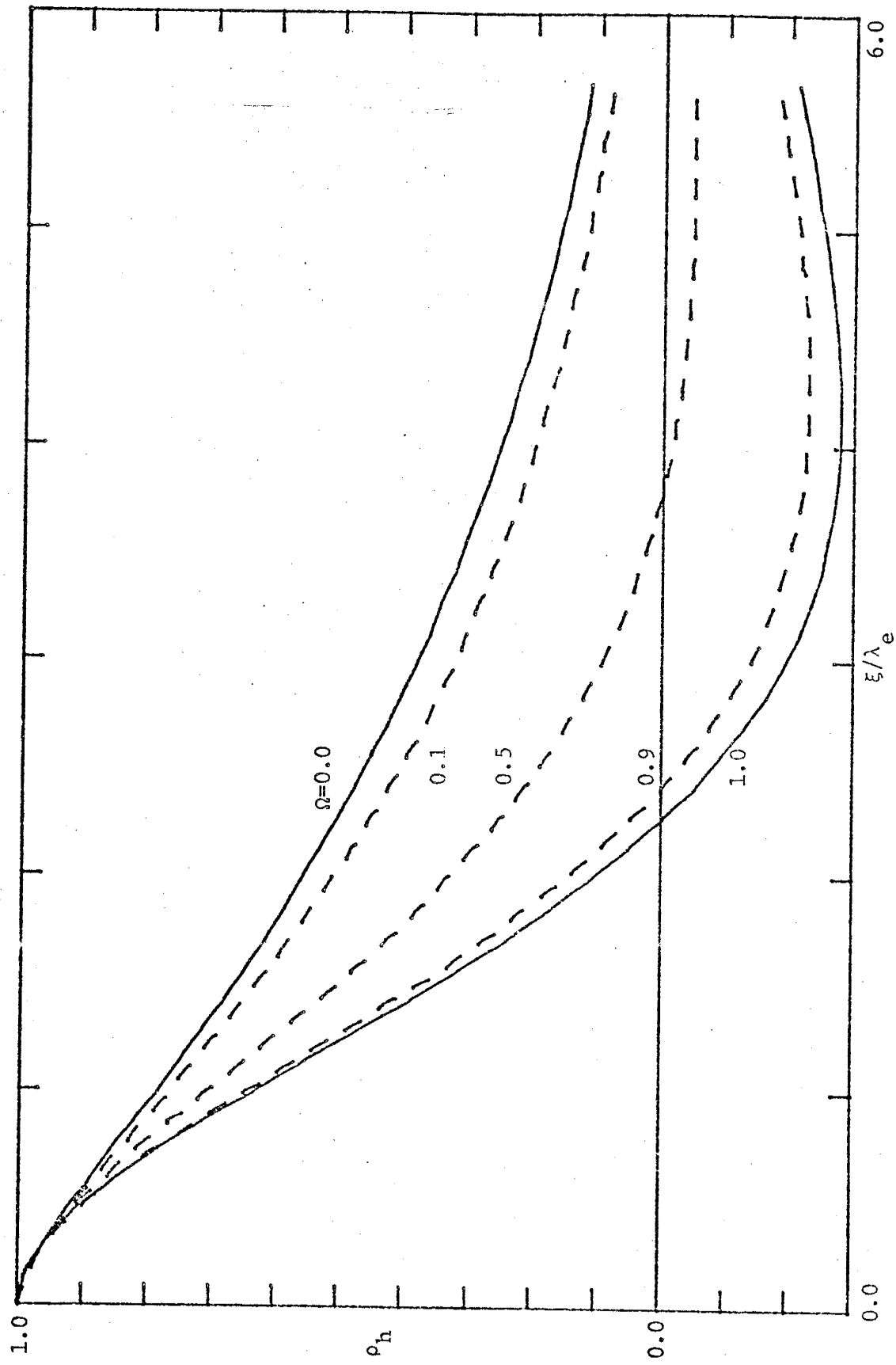

Figure 3.2: Transient Head Correlation Function evaluated for several values of Ω at χ = 0.0

singularity at the origin of wave-number space.

(2) The S/T term in the transient head variance, (3.10), reflects a significantly increased dependence on spatial correlation structure of the ln T process.

(3) An isotropic S/T term with high correlation values contributes to the transient head correlation function; when the S/T term dominates, the correlation function exhibits greater correlation of observations over longer distances.

Summary

Application of stochastic analysis to two-dimensional transient flow serves to reiterate conclusions of the steady analysis.

(1) The transient head spectrum is a function of the ln T spectrum in which the proportionality coefficient incorporates the mean parameters and wave-number space location.

(2) A stronger singularity exists in the transient head spectrum equation than was observed in the steady head spectrum equation. To maintain statistical homogeneity of the head fluctuations a modified form of the Whittle spectrum must be used to represent the ln T spectrum.

(3) Transient head variance is composed of contributions dependent on the mean gradient and mean-transient parameters when all temporal variability of the head process is contained in the mean head. The mean-gradient term is identical to the steady head variance.

(4) Head variance is strongly dependent on spatial correlation structure and variability of ln T. The spatial correlation parameter, λ, appears as a fourth-power factor in the contribution of transient parameters to the variance.

(5) The transient head correlation function is also composed of two parts, one characterized by the mean gradient and the other by mean transient parameters. The mean-gradient contribution is identical to the steady head correlation function. The transient contribution is statistically isotropic. Both parts combine as a weighted sum in which the weighting factor is determined by the relative magnitude of mean gradient and mean transient parameters.

(6) The transient head correlation function indicates correlation of head observations over much greater distances than ln T observations - again suggestive of the smoothing nature of the groundwater system.

APPLICATIONS TO NETWORK DESIGN

Water-level observations are often used to estimate flow parameters such as gradient and transmissivity. Hydraulic gradient may be determined from head surface maps or water levels recorded in a specific network of wells. Estimation of aquifer transmissivity from observed water levels is a classical problem of groundwater hydrology that has received much attention in the recent literature.

A technique for estimating local transmissivity from water-level observations proposed by Stallman (1956) approximates the two-dimensional groundwater equation by a finite difference formulation. This procedure has been applied to non-homogeneous aquifers and aquifers of variable thickness by Weeks and Sorey (1973) with varying degrees of success. Approaching the inverse problem on a regional scale, Sagar et al. (1975) suggest interpolation of head data by spline or Lagrange polynomials from which derivatives of the flow equation can be determined. A direct solution to the regional inverse problem proposed by Tang and Pinder (1979) requires knowledge of transmissivity along a line which traverses all streamlines in the model region. Cooley (1977, 1979) uses non-linear regression to estimate hydraulic parameters and then evaluates reliability and significance of parameters and resulting head simulations with statistical goodness-of-fit tests. Knowledge of the regional head distribution is employed by Emsellem and deMarsilly (1971) to find the best regional distribution of hydraulic parameters. Neuman and Yakowitz (1979) follow a statistically based approach to estimate spatial variability of transmissivity which incorporates prior information about transmissivity.

Design of well networks to achieve optimum estimation of parameters has not been considered. In the following examples, variability of estimated parameters will be related to network size by incorporating stochastic representation of hydraulic head in the parameter estimating equation. Estimation of three flow parameters will be discussed: gradient magnitude, gradient direction, and ln T. The gradient magnitude and direction problems will be based on three-point observations of an assumed plane surface, and the ln T problem will follow the Stallman (1956) estimation procedure.

In each case the estimating equation is first formulated, then stochastic representation of hydraulic head is substituted; after some algebraic manipulation, an equation for variance of the estimated parameter in terms of head variance and correlation function results. Substitution of appropriate correlation functions leads to an equation defining variance of the estimated parameter as a function of dimensionless network scale, network size divided by the average correlation distance of the aquifer. From this relationship, it is possible to design an observation-well network for optimal estimation of flow parameters. Alternatively, these results can also be used to evaluate the variance of a parameter estimated from an existing network, indicating reliability of the estimated parameter.

The procedure is illustrated by application to an extensively instrumented irrigation and drainage study area at San Acacia, New Mexico.

Variance in Estimated Gradient Magnitude

In the first network problem estimation of groundwater gradient magnitude from observed water levels will be investigated. A simple

hydraulic surface approximated by an inclined plane is assumed within the area of the observation network. Estimation of this surface from three observation points is based on the three-point equation for a plane. Gradient magnitude is determined from the plane equation.

The gradient estimating equation is formulated as a function of observed head, ϕ_i, at three observation points

$$\hat{\vec{J}} = \vec{a}_1\phi_1 + \vec{a}_2\phi_2 + \vec{a}_3\phi_3 \qquad (4.1)$$

$\hat{\vec{J}}$, estimated gradient, is also a function of the network geometry, represented in (4.1) by the coefficient vectors $\vec{a}_i$. Development of (4.1) is presented in Appendix VIII.

Conceptualized as a stochastic process, head is represented as the sum of a mean part, H, and fluctuations about the mean; because the network analysis deals with measured head levels, fluctuations about mean head will incorporate actual variations in head, h, plus potential measurement error, ε,

$$\phi_i = H_i + h_i + \varepsilon_i \qquad (4.2)$$

Substituting (4.2) into (4.1) and taking expectations produces a mean gradient estimate

$$E(\hat{\vec{J}}) = \bar{\vec{J}} = \vec{a}_1 H_1 + \vec{a}_2 H_2 + \vec{a}_3 H_3 \tag{4.3}$$

The zero-mean property of h and ε has been recognized. An estimating equation for gradient fluctuations results when (4.3) is subtracted from (4.2). Variance of estimated gradient magnitude is determined by taking the expected value of the squared magnitude of estimated gradient fluctuations

$$\sigma_J^2 = E(|\hat{\vec{J}} - \bar{\vec{J}}|^2) \tag{4.4}$$

Completing the expectation process after substituting (4.1) and (4.3) for the estimated and mean gradients leads to formulation of (4.4) in terms of variance and correlation functions of head plus a term representing measurement error

$$\sigma_J^2 = \frac{\sigma_h^2}{L^2}\left[4 - 2(\rho_{h_1h_2}(\xi,\chi) + \rho_{h_1h_2}(\xi,\chi)) + 4\frac{\sigma_\varepsilon^2}{\sigma_h^2}\right] \tag{4.5}$$

L is the network scale. In obtaining (4.5) the following relations have been recognized

$$E(h_i^2) = \sigma_h^2 \tag{4.6a}$$

$$E(h_i h_j) = R_{h_i h_j} = \sigma_h^2 \rho_{h_i h_j},\ i \neq j \tag{4.6b}$$

$$E(\varepsilon_i^2) = \sigma_\varepsilon^2 \tag{4.6c}$$

$$E(\varepsilon_i \varepsilon_j) = 0,\ i \neq j \tag{4.6d}$$

$$E(h_i \varepsilon_j) = 0,\ \text{all } i \text{ and } j \tag{4.6e}$$

Assumption of a specific network geometry, an isosceles-right triangle (Figure 4.1) with observation points at each apex, was used

to simplify evaluation of equation (4.5). Orientation of the network with the right angle at the origin of the coordinate system whose x axis parallels mean flow is convenient. The angle, γ, formed between the principal network side and mean flow, defines the degree of network rotation.

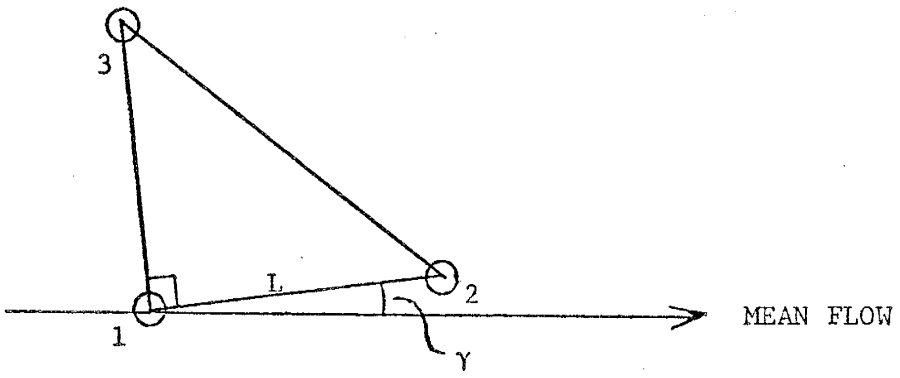

Figure 4.1: Three-Point Observation-Well Network for Estimating Gradient Magnitude and Direction.

Head correlation functions are defined in terms of the separation vector between observation points: for the configuration illustrated in Figure 4.1 the separation vector between observation points 1 and 2, in polar coordinates, is $\xi = L$ and $\chi = \gamma$; between observation points 1 and 3, $\xi = L$ and $\chi = \gamma + \frac{\pi}{2}$. When head correlation function (2.20) is inserted into (4.5) with the appropriate separation vector coordinates the following equation for variance of estimated gradient magnitude results.

$$\sigma_J^2 = \frac{\sigma_h^2}{L^2}\left[4 - \left(4-\left(\frac{3\pi L}{16\lambda}\right)^2\right)\frac{3\pi L}{16\lambda} K_1\left(\frac{3\pi L}{16\lambda}\right)\right.$$

$$\left. -2\left(\frac{3\pi L}{16\lambda}\right)^2 K_o\left(\frac{3\pi L}{16\lambda}\right) + 4\frac{\sigma_\varepsilon^2}{\sigma_h^2}\right] \qquad (4.7)$$

Equation (4.7), normalized by $\frac{\sigma_h^2}{\lambda^2}$, is plotted in Figure 4.2 as a function of $\frac{L}{\lambda}$ for several values of the measurement error factor $\frac{\sigma_\varepsilon^2}{\sigma_h^2}$. The solid curve results when $\frac{\sigma_\varepsilon^2}{\sigma_h^2} = 0$; for $\frac{L}{\lambda}$ less than 0.4, this curve has a constant value of 0.7. At small values of dimensionless network scale, measurement error effects increase as the network size decreases; beyond $\frac{L}{\lambda} = 0.4$ the measurement error factor exerts insignificant influence. As the network size increases relative to the aquifer scale the normalized variance of estimated gradient magnitude decreases rapidly. Note that the error in gradient magnitude is independent of the network orientation.

The graph in Figure 4.2 may be used to aid design of an observation-well network for estimation of gradient magnitude or to interpret reliability of estimates made from an existing network. In the first instance one would determine an acceptable value for σ_J^2 and enter the graph to find the network size required to achieve that desired variance. Determination of the reliability of an estimate made from an existing network would be accomplished by entering the graph with the known value of $\frac{L}{\lambda}$ and finding the associated variance of estimated gradient magnitude.

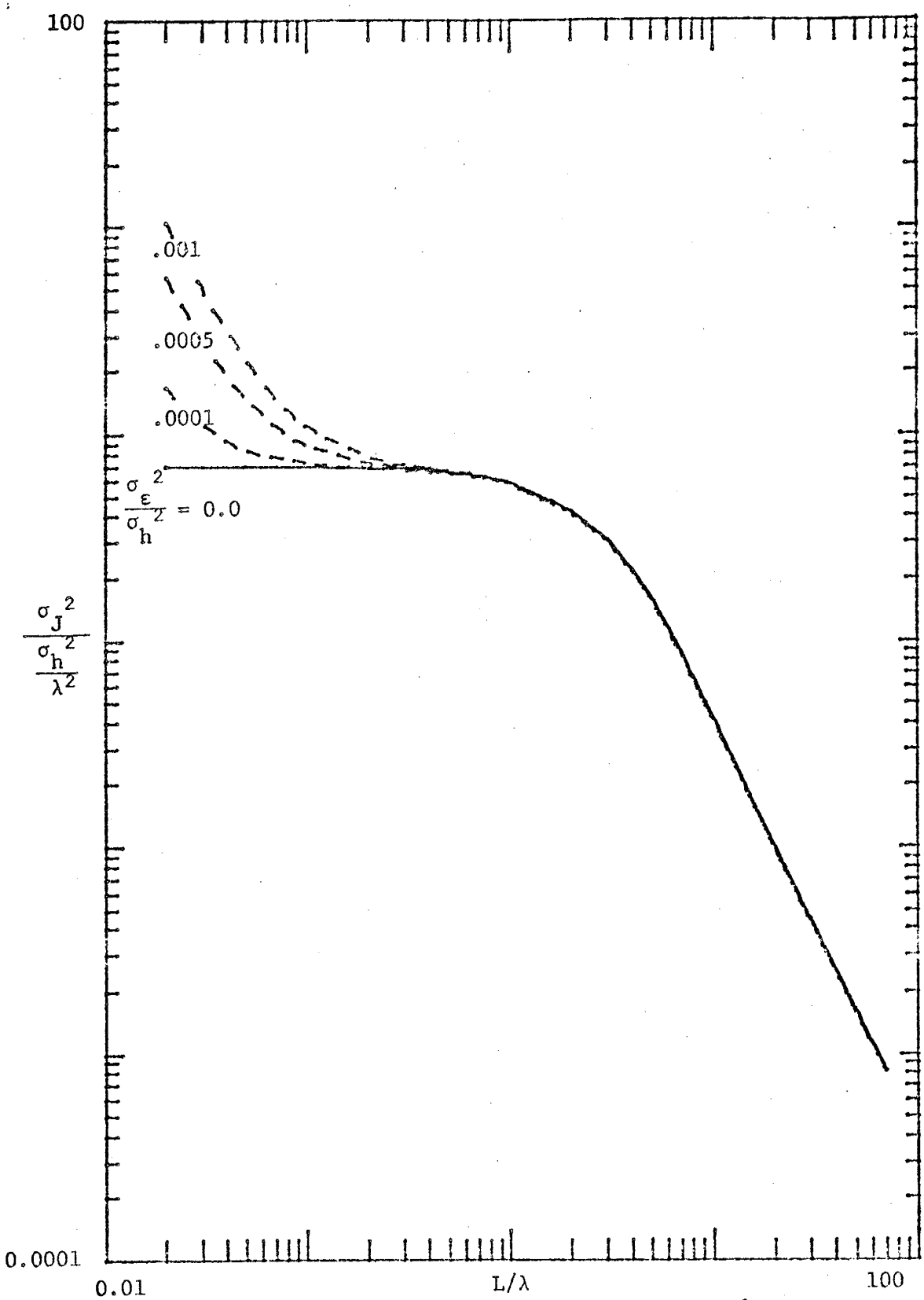

Figure 4.2: Normalized Variance of Estimated Gradient Magnitude

Figure 4.2 has been used to evaluate the variance of the gradient magnitude estimated from data collected in an irrigation and drainage study conducted at San Acacia, New Mexico. The mean gradient magnitude in the San Acacia study is estimated to be 1.2×10^{-3}; from Figure 4.2 the variance of this estimate is 9.3×10^{-7}. Thus, the standard deviation, $\sigma_J = 9.6 \times 10^{-4}$, of the estimate is practically equal to the estimated gradient. Parameters required for this calculation are evaluated in Appendix XI.

Error in Estimated Gradient Direction

In considering design of an observation-well network for estimation of gradient direction, the hydraulic surface will again be approximated by an inclined plane. Observation wells will be located at the corners of an isosceles-right triangle network as in the gradient-magnitude case (Figure 4.1). Gradient direction is estimated according to procedures used to estimate dip of geologic formations from three observation points. A brief review of this procedure is included in Appendix IX.

The sine of the angle formed by the estimated gradient direction and the true gradient direction is a convenient measure of the error of estimated gradient direction. Formulated in terms of observed water levels and network geometry the equation for sine of the angle of deviation is

$$\sin(\phi) = \frac{\cos\gamma - (\cos\gamma + \sin\gamma)\left(\frac{\phi_1-\phi_2}{\phi_3-\phi_2}\right)}{\left[2\left(\frac{\phi_1-\phi_2}{\phi_3-\phi_2}\right)^2 - 2\left(\frac{\phi_1-\phi_2}{\phi_3\ \phi_2}\right) + 1\right]^{\frac{1}{2}}} \tag{4.8}$$

Before formulating the mean square error of (4.8) in terms of the head process statistics and network size, consideration must be given to testing the estimating equation for possible bias. If exact knowledge of the head surface is assumed and the true flow direction is parallel to the x axis ($\theta = 0$), the head differences in (4.8) can be written as the product of the x component of the vector separating observation points and the gradient magnitude, J,

$$\phi_1 - \phi_2 = (x_2 - x_1)J_1 = L\cos\gamma$$

$$\phi_3 - \phi_2 = (x_2 - x_3)J_1 = L(\sin\gamma + \cos\gamma) \tag{4.9}$$

Subscripted x's refer to x-coordinates of particular observation points. Replacing the head-difference terms in (4.8) by (4.9) leads to $\sin(\theta) = 0$ when the head surface is exactly known; thus, (4.8) is an unbiased estimator of $\sin(\theta)$.

Functional dependence of (4.8) on the observed heads is very complicated. Statistical analysis of (4.8) requires that the head dependence

be simplified. Recognizing the stochastic nature of hydraulic head, first-order analysis techniques produce the following approximation to (4.8)

$$\sin(\theta) \simeq \left.\frac{\partial \sin\theta}{\partial \phi_1}\right|_{\vec{H}} (\phi_1 - H_1) + \left.\frac{\partial \sin\theta}{\partial \phi_2}\right|_{\vec{H}} (\phi_2 - H_2) + \left.\frac{\partial \sin\theta}{\partial \phi_3}\right|_{\vec{H}} (\phi_3 - H_3) \tag{4.10}$$

where $\vec{H} = (\vec{H}_1, H_2, H_3)$ represents evaluation at the mean head. Replacing the observed heads in (4.10) by (4.2), squaring, and taking expectations results in an equation for the mean square error of estimated gradient direction

$$E(\sin^2\theta) = \sigma_h^2 \left[\left(\left(\frac{\partial \sin\theta}{\partial \phi_1}\right)^2 + \left(\frac{\partial \sin\theta}{\partial \phi_2}\right)^2 + \left(\frac{\partial \sin\theta}{\partial \phi_3}\right)^2 \right|_{\vec{H}} \left(1 + \frac{\sigma_\varepsilon^2}{\sigma h^2}\right) \right.$$

$$+ 2 \left.\frac{\partial \sin\theta}{\partial \phi_1}\right|_{\vec{H}} \left.\frac{\partial \sin\theta}{\partial \phi_2}\right|_{\vec{H}} \rho_{h_1 h_2}(\xi,\chi) + 2 \left.\frac{\partial \sin\theta}{\partial \phi_1}\right|_{\vec{H}} \left.\frac{\partial \sin\theta}{\partial \phi_3}\right|_{\vec{H}} \rho_{h_1 h_3}(\xi,\chi)$$

$$\left. + 2 \left.\frac{\partial \sin\theta}{\partial \phi_2}\right|_{\vec{H}} \left.\frac{\partial \sin\theta}{\partial \phi_3}\right|_{\vec{H}} \rho_{h_2 h_3}(\xi,\chi) \right] \tag{4.11}$$

In (4.10) and (4.11) the vertical line following the derivatives indicates that the result of the differentiation is evaluated when mean heads are substituted for the random-head variables.

$$\left.\frac{\partial \sin\theta}{\partial \phi_1}\right|_{\vec{H}} = \frac{-(\sin\gamma + \cos\gamma)}{LJ_1}$$

$$\left.\frac{\partial \sin\theta}{\partial \theta_2}\right|_{\vec{H}} = \frac{\sin\gamma}{LJ_1}$$

$$\left.\frac{\partial \sin\theta}{\partial \phi_3}\right|_{\vec{H}} = \frac{\cos\gamma}{LJ_1} \qquad (4.12)$$

As in the gradient-magnitude case, the normalized form of (2.20) will be assumed for the head correlation functions. For specific network geometry shown in Figure 4.1, coordinates ξ and χ of the separation vector between observation points 1 and 2 have the values L and γ; between observation points 1 and 3, $\xi = L$ and $\chi = \gamma + \frac{\pi}{2}$; between observation points 2 and 3, $\xi = \sqrt{2}\,L$ and $\chi = \gamma + \frac{3\pi}{4}$. Substituting (4.12) and appropriate head correlation functions into (4.11) leads to an equation for mean squared error of estimated gradient direction as a function of head variance, measurement-error variance, and network size

$$E(\sin^2\theta) = \frac{\sigma_h^2}{J_1^2 L^2}\left\{2 - 2\left(\frac{3\pi L}{16\lambda}\right) K_1\left(\frac{3\pi L}{16\lambda}\right) - \left(\frac{3\pi L}{16\lambda}\right)^2 K_o\left(\frac{3\pi L}{16\lambda}\right)\right.$$

$$+ \cos\gamma\sin\gamma\left[2 + \left[\left(\frac{3\pi L}{16\lambda}\right)^2 - 4\right]\frac{3\pi L}{16\lambda} K_1\left(\frac{3\pi L}{16\lambda}\right)\right.$$

$$+ \left[2 - \tfrac{1}{2}\left(\frac{3\pi\sqrt{2}L}{16\lambda}\right)^2\right]\frac{3\pi\sqrt{2}L}{16\lambda} K_1\left(\frac{3\pi\sqrt{2}L}{16\lambda}\right)$$

$$\left.\left. -2\left(\frac{3\pi L}{16\lambda}\right)^2 K_o\left(\frac{3\pi L}{16\lambda}\right) + \left(\frac{3\pi\sqrt{2}L}{16\lambda}\right)^2 K_o\left(\frac{3\pi\sqrt{2}L}{16\lambda}\right)\right]\right.$$

$$+ \cos^2\gamma\sin^2\gamma\left[2\left(\frac{3\pi L}{16\lambda}\right)^3 K_1\left(\frac{3\pi L}{16\lambda}\right) - \left(\frac{3\pi\sqrt{2}L}{16\lambda}\right)^3 K_1\left(\frac{3\pi\sqrt{2}L}{16\lambda}\right)\right]$$

$$\left. + \frac{\sigma_\varepsilon^2}{\sigma_h}(2\cos\gamma\sin\gamma + 2)\right\} \qquad (4.13)$$

After normalizing by $\frac{\sigma_h^2}{J_1^2\lambda^2}$, (4.13) is evaluated as a function of the dimensionless network scale, L/λ, and presented in graphical form in Figure 4.3. The solid line represents the normalized mean square error when evaluated for zero measurement-error variance and a network rotation angle of zero or 90 degrees (both give the same result). In general, the normalized mean squared error exhibits a maximum for small networks ($L/\lambda < 1.$); this value is nearly constant and equals 0.17349 in the limit as L goes to zero. Beyond $L/\lambda = 1.$, the normalized

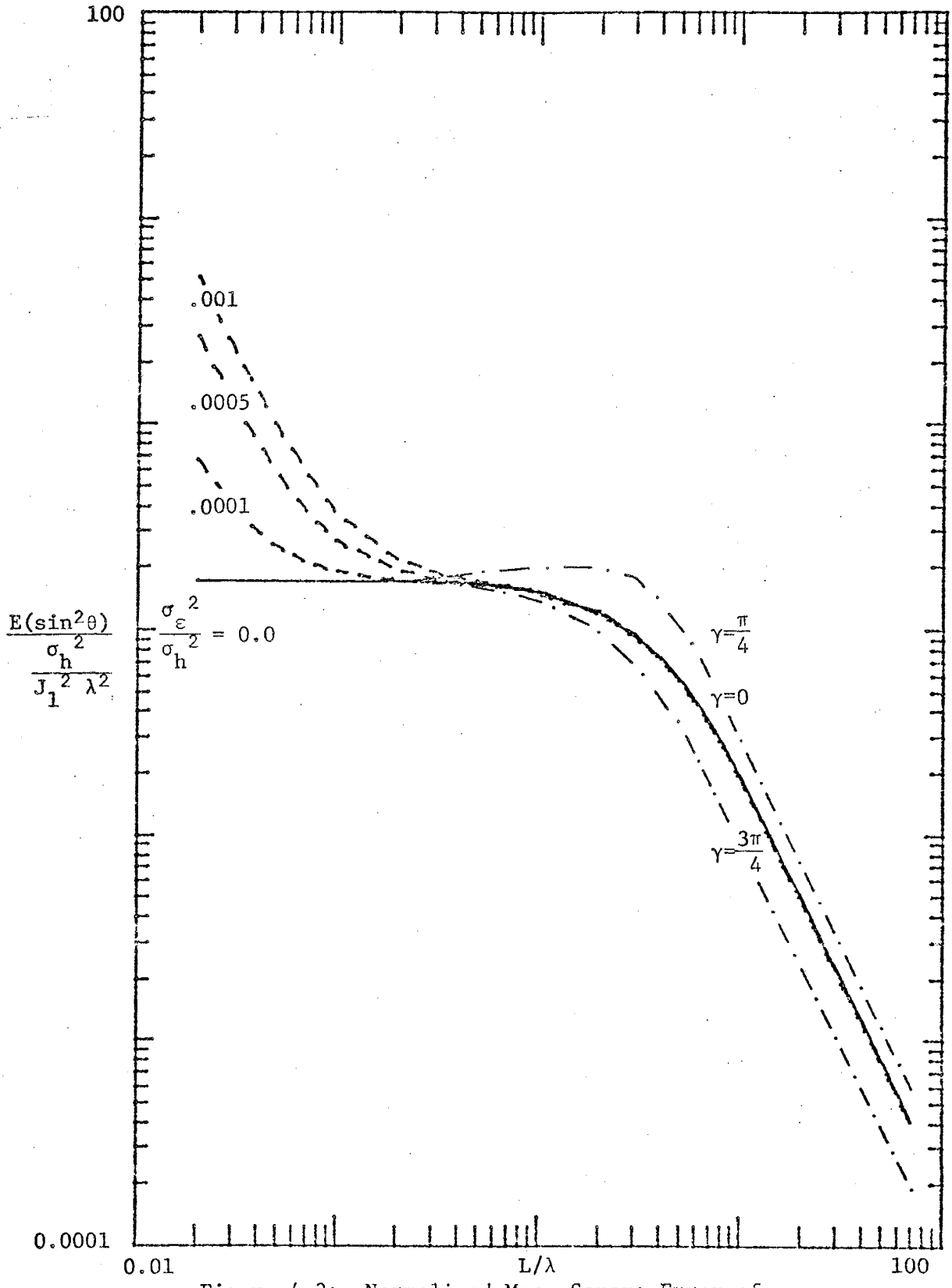

Figure 4.3: Normalized Mean Square Error of Estimated Gradient Direction

mean squared error decreases rapidly as the dimensionless network scale increases. Dashed lines at small values of dimensionless network scale reflect the influence of a typical range of the measurement-error variance. This effect diminishes with increasing network size, becoming negligible when $L/\lambda = 0.4$. Network rotational effects are reflected in the dot-dash lines at large values of network scale. Networks rotated 135 or 315 degrees are bisected by the mean-flow direction and produce minimum values of the error measure; rotation angles which are integer multiples of 90 degrees produce intermediate values of the normalized mean square error and networks rotated 45 or 215 degrees give maximum values.

Application of Figure 4.3 is again illustrated using data collected from the irrigation and drainage study at San Acacia, New Mexico (see Appendix XI for the flow parameters). The average gradient direction estimated from water-level observations in wells 3, 4, and 5 over the 1977-1978 winter season is -8.7 degrees. Entering Figure 4.3 at $L/\lambda = 1$ the mean square error of estimated gradient direction is 0.14. This implies a rms error of 0.37 for $\sin(\theta)$ or approximately 22 degrees for θ.

Variance in Estimated ln T

Estimation of transmissivity from observed head levels, the inverse problem in hydrogeology, has been approached in various ways by many workers. For purposes of illustration, a procedure proposed by Stallman (1956) to estimate transmissivity from water levels observed in a five-well network will be used here. The estimation equation will be modified slightly to give ln T because this form of the parameter appears in the

modified flow equation.

The equation for estimating ln T (see Appendix X), developed for uniform spacing of observation wells, is

$$\ln \hat{T} = -\ln (\phi_1 + \phi_2 + \phi_3 + \phi_4 - 4\phi_5) + \ln(L^2 S\frac{\partial \phi}{\partial t} - L^2 W) \qquad (4.14)$$

Substitution of (4.2), representing the observed heads as the sum of mean, fluctuation, and measurement error terms leads to the following first order approximation:

$$\ln \hat{T} = -\ln(H_1 + H_2 + H_3 + H_4 - 4H_5) + \ln(L^2 S\frac{\partial \phi}{\partial t} - L^2 W)$$

$$- \left(\frac{h_1 + h_2 + h_3 + h_4 - 4h_5 + \varepsilon_1 + \varepsilon_2 + \varepsilon_3 + \varepsilon_4 - 4\varepsilon_5}{H_1 + H_2 + H_3 + H_4 - 4H_5}\right) \qquad (4.15)$$

Taking the expected value of (4.15),

$$E(\ln \hat{T}) = -\ln[H_1 + H_2 + H_3 + H_4 - 4H_5] + \ln(L^2 S\frac{\partial H}{\partial t} - L^2 W)$$

and subtracting leaves an equation for fluctuations of the ln T estimate

$$\hat{f} = (\ln \hat{T} - \ln T_\ell) = -\left(\frac{h_1 + h_2 + h_3 + h_4 - 4h_5 + \varepsilon_1 + \varepsilon_2 + \varepsilon_3 + \varepsilon_4 - 4\varepsilon_5}{H_1 + H_2 + H_3 + H_4 - 4H_5}\right) \tag{4.16}$$

where $\ln T_\ell = E(\ln T)$. Variance of estimated ln T, as a function of head variance and correlation functions, is developed by squaring (4.16) and taking expectations

$$\sigma^2_{\hat{f}} = \frac{\sigma_h^2}{(\Sigma H)^2}\Big[20 + 2\Big\{\rho_{h_1h_2}(\xi,\chi) + \rho_{h_1h_3}(\xi,\chi) + \rho_{h_1h_4}(\xi,\chi) - 4\,\rho_{h_1h_5}(\xi,\chi)$$

$$+ \rho_{h_2h_3}(\xi,\chi) + \rho_{h_2h_4}(\xi,\chi) - 4\,\rho_{h_2h_5}(\xi,\chi)$$

$$+ \rho_{h_3h_4}(\xi,\chi) - 4\,\rho_{h_4h_5}(\xi,\chi)$$

$$- \rho_{h_4h_5}(\xi,\chi)\Big\}$$

$$+ 20\frac{\sigma_\varepsilon^2}{\sigma_h^2}\Big] \tag{4.17}$$

where $\Sigma H = H_1 + H_2 + H_3 + H_4 - 4H_5$. The transient head correlation function, (3.11) normalized by (3.10), will be used in (4.17); coordinates for the various separation vectors required are presented in Table 4.1.

TABLE 4.1

Polar Coordinates of Separation Vectors
required in determination of Variance of Estimated Ln T

OBSERVATION PAIR	ξ (ft)	χ (degrees)
1 and 2	$\sqrt{2}$ L	$\gamma + \frac{5\pi}{4}$
2 and 3	$\sqrt{2}$ L	$\gamma + \frac{3\pi}{4}$
3 and 4	$\sqrt{2}$ L	$\gamma + \frac{\pi}{4}$
4 and 1	$\sqrt{2}$ L	$\gamma + \frac{7\pi}{4}$
1 and 3	2L	$\gamma + \pi$
2 and 4	2L	$\gamma + \frac{\pi}{2}$
1 and 5	L	$\gamma + \pi$
2 and 5	L	$\gamma + \frac{3\pi}{4}$
3 and 5	L	γ
4 and 5	L	$\gamma + \frac{\pi}{2}$

Incorporating appropriate forms of the transient head correlation function in (4.17) and working through some algebra produces the variance of estimated ln T in terms of dimensionless network scale, L/λ,

$$\sigma_f^2 = \frac{\sigma_h^2}{(\Sigma H)^2} \{20 + \Omega\Big[3(\frac{3\pi\sqrt{2}L}{16\lambda})^2 K_o(\frac{3\pi\sqrt{2}L}{16\lambda}) - 3(\frac{3\pi\sqrt{2}L}{16\lambda})^3 K_1(\frac{3\pi\sqrt{2}L}{16\lambda})$$

$$+ \frac{3}{2}(\frac{3\pi 2L}{16\lambda})^2 K_0(\frac{3\pi 2L}{16\lambda}) - \frac{3}{2}(\frac{3\pi 2L}{16\lambda})^3 K_1(\frac{3\pi 2L}{16\lambda})$$

$$- 12(\frac{3\pi L}{16\lambda})^2 K_0(\frac{3\pi L}{16\lambda}) + 12(\frac{3\pi L}{16\lambda})^3 K_1(\frac{3\pi L}{16\lambda})\Big]$$

$$+ [8\,\frac{3\pi\sqrt{2}L}{16\lambda} + (\frac{3\pi\sqrt{2}L}{16\lambda})^3] K_1(\frac{3\pi\sqrt{2}L}{16\lambda}) + (\frac{3\pi\sqrt{2}L}{16\lambda})^2 K_0(\frac{3\pi\sqrt{2}L}{16\lambda})$$

$$+ [4\,\frac{3\pi 2L}{16\lambda} + (\frac{3\pi 2L}{16\lambda})^3] K_1(\frac{3\pi 2L}{16\lambda}) + (\frac{3\pi 2L}{16\lambda})^2 K_0(\frac{3\pi 2L}{16\lambda})$$

$$- [32\,\frac{3\pi L}{16\lambda} + 4(\frac{3\pi L}{16\lambda})^3] K_1(\frac{3\pi L}{16\lambda}) - 4(\frac{3\pi L}{16\lambda})^2 K_0(\frac{3\pi L}{16\lambda})$$

$$+ 20\,\frac{\sigma_\varepsilon^2}{\sigma_h^2}\} \qquad (4.18)$$

Equation (4.18), normalized by $\dfrac{\sigma_h^2}{\left(\lambda^2 \dfrac{S}{T_\ell} \dfrac{\partial H}{\partial t}\right)^2}$, has been plotted against L/λ in Figure 4.4 for $\Omega = 1$ and several typical values of the measurement-error factor. From the transient analysis a weighting factor, Ω, of one implies that contributions to the head correlation function come exclusively from the mean-gradient term, producing the same result as if steady flow were assumed. Figure 4.4 illustrates that measurement-error effects are significant only for networks of

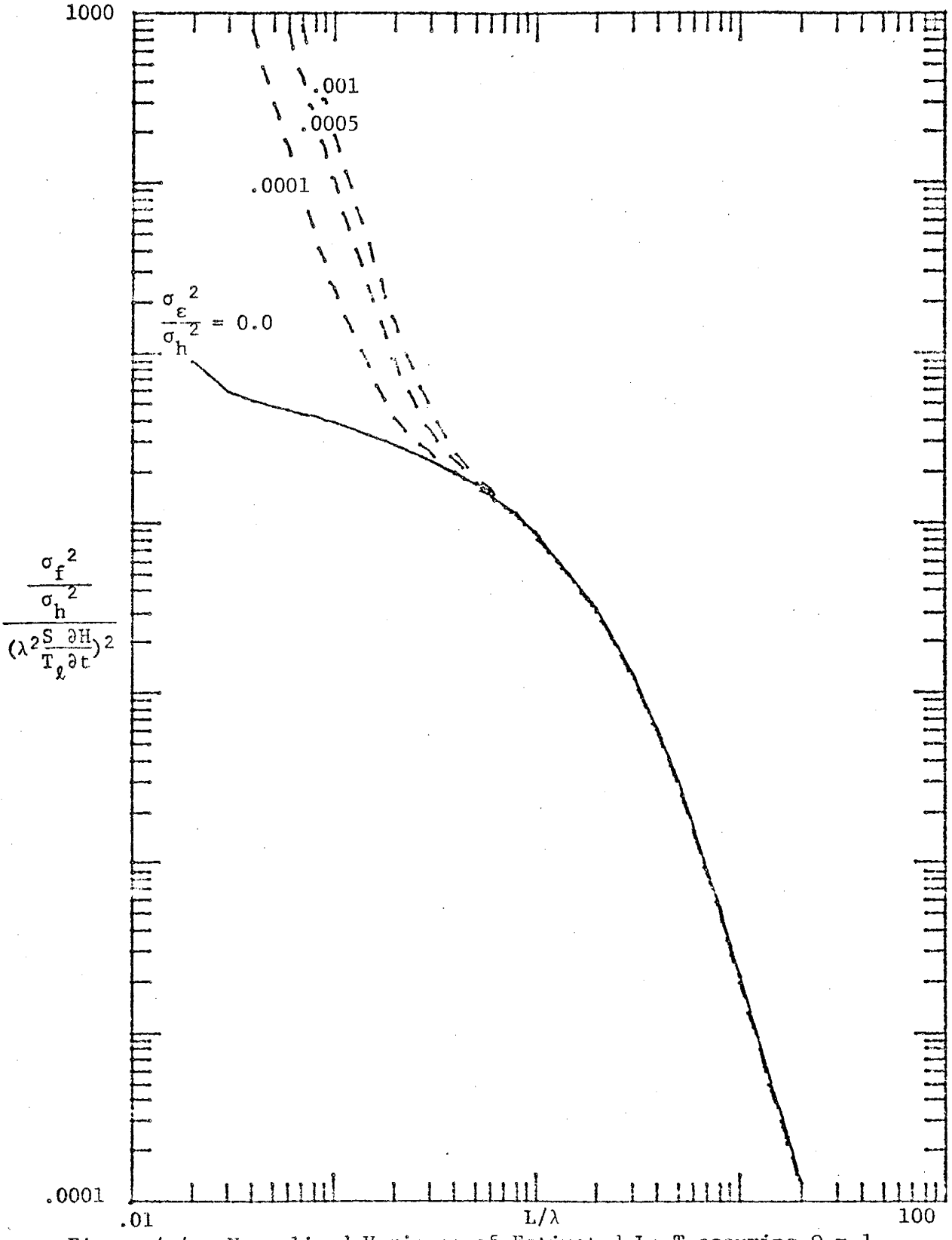

Figure 4.4: Normalized Variance of Estimated Ln T assuming $\Omega = 1$ and a typical range of Measurement-Error values

small dimensionless scale. The network rotation angle, γ, does not appear in (4.18), indicating no dependence of variance of estimated ln T on network orientation relative to the mean flow. Effects of various values of the weighting factor, Ω, are shown in Figure 4.5 where the normalized form of (4.18) is plotted as a function of L/λ for $\frac{\sigma_\varepsilon^2}{\sigma_h^2} = 0.0$.

The normalized variance of estimated ln T decreases as the network scale increases with respect to the integral scale of the aquifer variability. Smaller values of the variance of estimated ln T imply greater confidence in the transmissivity estimated from analysis of network data. As network scale increases the terms truncated in approximating the second order spatial derivatives of (X.1) become increasingly more important. Enlargement of the observation network, which reduces $\sigma^2_{\ln T}$, leads to excessive errors in the numerical approximation making the Stallman estimation technique inappropriate. Some optimum network size would be anticipated, but this value has not been determined. Increases in the normalized variance of estimated ln T as network size decreases, illustrated by Figure 4.5 leads to questions regarding the minimum network size for which Stallman's (1956) technique is applicable.

Figure 4.5 is used to determine the variance of ln T estimated from the five-point network on the farm at San Acacia, New Mexico. Parameters of the flow system at the farm are reviewed and tabulated in Appendix XI.

The transient weighting factor, Ω, was determined to be 0.15 for the summer and 0.95 for the winter period. The nearness of $\Omega = 0.95$ to 1.0 indicates the winter flow system to be nearly in steady state; as a result, one would not anticipate good results from analysis of winter

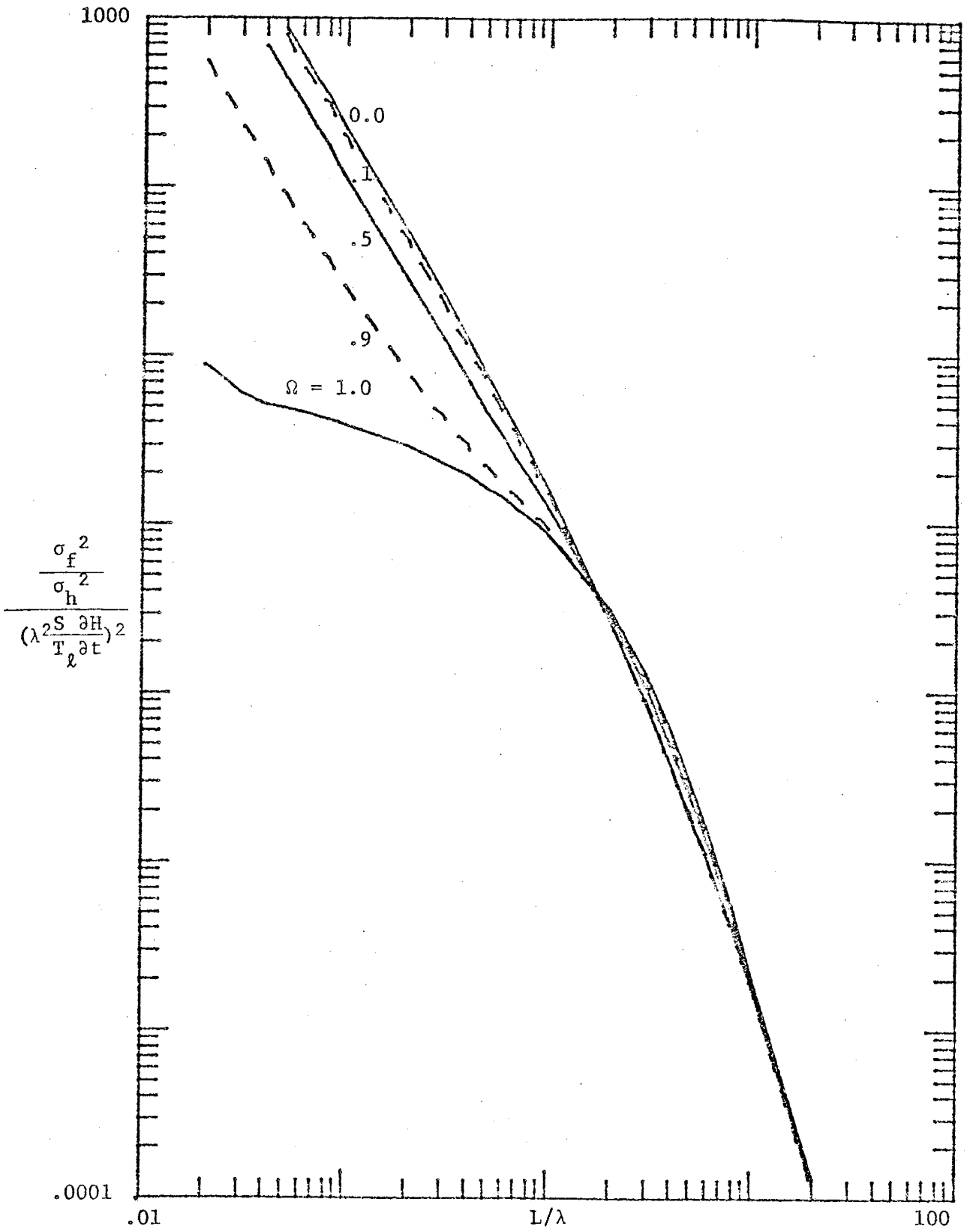

Figure 4.5: Normalized Variance of Estimated Ln T illustrating effects of various values of Ω with zero Measurement-Error

data using the Stallman technique (see Figure XI.2).

By interpolation from Figure 4.5 the normalized variance of estimated ln T is 1.5 for the summer and 0.9 for the winter. Thus, for the summer $\sigma^2_{\ln T} = 17.6$, $\sigma_{\ln T} = 4.2$ and the coefficient of variation is 0.5. Using winter data $\sigma^2_{\ln T} = 204.8$ and $\sigma_{\ln T} = 14.31$ and with $\tilde{T} = 4000$ ft^2/day (from Appendix XI) the coefficient of variation is 1.7. As expected the variance of estimated ln T, using winter data, implies little confidence in the transmissivity estimate. Results for the summer data are much better though not exceptionally good.

Summary

A summary of application of stochastic groundwater analysis to observation-well-network design and notable results is itemized below.

(1) Variances of parameters estimated from observed heads can be formulated as functions of dimensionless network scale, measurement-error variance, head variance, and parameters of mean flow.

(2) Variances of estimated parameters normalized by a term incorporating head variance, can be used to suggest the network size required to achieve a desired variance for the estimated parameter or to indicate variance of estimates made from existing networks.

(3) Variance of both estimated gradient magnitudes and direction decrease as the dimensionless network scale increases.

(4) Variance of estimated ln T decreases as dimensionless network scale increases.

(5) Effects due to measurement error are significant only for networks of small dimensionless scale.

CONCLUSIONS AND RECOMMENDATIONS

Conclusions

Analysis of steady flow using two similar correlation functions for the ln T process leads to some initial conclusions regarding sensitivity of the head process. The spectral and correlation functions of each of the alternative descriptions of ln T exhibit similar behavior; they differ only in magnitude. The resulting head correlation and cross-covariance functions also exhibit the same general characteristics and differ only in magnitude. Basic differences in the ln T description are reflected in the statistical description of the head process.

The length scale of aquifer variability is again shown to be significant. This reiterates the conclusions of Gelhar (1976), Bakr et al. (1978), and Gutjahr et al. (1978). Head variance of steady flow is a function of the ln T integral scale squared; for the transient case head variance is a fourth-order polynomial of the ln T integral scale.

Head correlation functions resulting from analysis of both steady and transient flow are smoother than the ln T correlation function. This result indicates that the head process is correlated over greater distances than is the ln T process; the head process is a much smoother surface and has less variability than the ln T process.

The dimensionless network scale is an important variable in the optimum design of observation-well networks for estimation of flow parameters from water-level measurements. Variance of estimated parameters can be minimized when aquifer variability is incorporated in the design procedure.

Recommendations

Application of stochastic and spectral techniques to groundwater flow is still relatively new. Work to date has generally assumed steady flow and zero recharge. Future research should investigate the effects of time-dependent fluctuations of the head process and spatial and temporal distribution of recharge. Incorporation of stochastic representation for storativity will also be of interest. Relaxation of the statistical homogeneity assumption is of considerable interest and is currently under investigation. Despite the extensive data requirements, estimation of correlation functions from observed data in some typical aquifers would provide an important confirmation of the assumed correlation functions employed in these analyses.

REFERENCES

Abramowitz, M. and I. A. Stegun, Handbook of Mathematical Functions, 1046 pp., Dover Publications, Inc., New York, 1972.

Agterberg, F. P., Developments in Geomathematics, 596 pp., Elsevier Pub. Co., Ltd., Amsterdam, 1974.

Bakr, A. A. M., Stochastic analysis of the effect of spatial variations of hydraulic conductivity on groundwater flow, Ph.D. dissertation, New Mexico Institute of Mining and Technology, Socorro, 1976.

Bakr, A. A. M., L. W. Gelhar, A. L. Gutjahr, and J. R. MacMillan, Stochastic analysis of spatial variability in subsurface flows, Part I. Comparison of one- and three-dimensional flows, Water Resour. Res., 14(2), 263-272, 1978.

Bartlett, M. S., An Introduction to Stochastic Processes, 2d. ed., 362 pp., Cambridge University Press, London, 1966.

Billings, M. P., Structural Geology, 606 pp., Prentice-Hall, Inc., Englewood Cliffs, New Jersey, 1972.

Boas, M. L., Mathematical Methods in the Physical Sciences, 778 pp., John Wiley and Sons, New York, 1966.

Cooley, R. L., A method of estimating parameters and assessing reliability for models of steady state groundwater flow, 1. Theory and numerical properties, Water Resour. Res., 13(2), 318-325, 1977.

Cooley, R. L., A method of estimating parameters and assessing reliability of models of steady state groundwater flow, 2. Application of statistical analysis, Water Resour. Res., 15(3), 603-617, 1979.

Dagan, G., Models of groundwater flow in statistically homogeneous porous formations, Water Resour. Res., 15(1), 47-63, 1979.

Delhomme, J. P., Spatial variability and uncertainty in groundwater flow parameters: A geostatistical approach, Water Resour. Res., 15(2), 269-280, 1979.

Emsellem, Y., and G. de Marsily, An automatic solution to the inverse problem, Water Resour. Res., 7(5), 1264-1283, 1971.

Erdelyi, A., ed., Tables of Integral Transforms, Volume I, 391 pp., McGraw-Hill, New York, 1954.

Freeze, R. A., Regionalization of hydrologic parameters for use in mathematical models of groundwater flow, 24th International Geological Congress, Sec. 11, 177-190, 1972.

Freeze, R. A., A stochastic-conceptual analysis of one-dimensional groundwater flow in nonuniform homogeneous media, Water Resour. Res., 11(5), 725-741, 1975.

Gelhar, L. W., Effects of hydraulic conductivity variations on groundwater flow, Proceedings, Second International IAHR Symposium on Stochastic Hydraulics, Lund, Sweden, 1976.

Gelhar, L. W., A. A. Bakr, A. L. Gutjahr, and J. R. MacMillan, Comments on 'A stochastic-conceptual analysis of one-dimensional groundwater flow in nonuniform homogeneous media' by R. Allan Freeze, Water Resour. Res., 13(2), 477-479, 1977.

Gelhar, L. W., A. L. Gutjahr, and R. L. Naff, Stochastic analysis of macrodispersion in a stratified aquifer, Water Resour. Res., 15(6), 1387-1397, 1979.

Gelhar, L. W., P. J. Wierenga, C. J. Duffy, K. R. Rehfeldt, R. B. Senn, M. Simonett, T-C. Yeh, A. L. Gutjahr, W. R. Strong, and A. Bustamante, Irrigation return flow studies at San Acacia, New Mexico: Monitoring, modeling and variability, Rpt. No. H-3, Hydrology Research Program, New Mexico Institute of Mining and Technology, Socorro, 1980.

Gutjahr, A. L., L. W. Gelhar, A. A. Bakr, and J. R. MacMillan, Stochastic analysis of spatial variability in subsurface flows Part II. Evaluation and application, Water Resour. Res., 14(5), 953-960, 1978.

Jenkins, G. M., and D. G. Watts, Spectral Analysis and its applications, 525 pp., Holden-Day, San Francisco, 1968.

Law, J., A statistical approach to the interstitial heterogeneity of sand reservoirs, Trans. AIME, 155, Petrol. Div., 202-222, 1944.

Lumley, J. L., and H. A. Panofsky, The Structure of Atmospheric Turbulence, 239 pp., John Wiley and Sons, Inc., New York, 1964.

Matern, B., Metoder att uppskatta noggrannheten vid linjeoch provytetaxering (Methods of estimating the accuracy of line and sample plot surveys), Meddelanden fran Statens Skogsforskningsinstitut, 36, 1-117, 1947.

McElwee, C. D. and M. A. Yukler, Sensitivity of groundwater models with respect to variations in transmissivity and storage, Water Resour. Res., 14(3), 451-460, 1978.

McMillan, W. D., Theoretical analysis of groundwater basins operations, Tech. Rpt. No. 6-25, 168 pp., Hydraulic Lab., University of California, Berkeley, 1966.

Naff, R. L., A continuum approach to the study and determination of field longitudinal dispersion coefficients, Ph.D. dissertation, New Mexico Institute of Mining and Technology, Socorro, 1978.

Neuman, S. P., and S. Yakowitz, A statistical approach to the inverse problem of aquifer hydrology 1. Theory, Water Resour. Res., 15(4), 845-860, 1979.

Nielson, D. R., J. W. Biggar, and K. T. Erh, Spatial variability of field-measured soil-water properties, Hilgardia, 42(7), 215-259, 1973.

Oberhettinger, F., Fourier Transforms of Distributions and Their Inverses, 167 pp., Academic Press, New York, 1973.

Rodrigues-Iturbe, I. and J. M. Mejia, The design of rainfall networks in time and space, Water Resour. Res., 10(4), 713-728, 1974.

Sagar, B., S. Yakowitz, and L. Duckstein, A direct method for the identification of the parameters of dynamic nonhomogeneous aquifers, Water Resour. Res., 11(4), 563-570, 1975.

Smith, L., A stochastic analysis of steady-state groundwater flow in a bounded domain, Ph.D. dissertation, University of British Columbia, Vancouver, B.C., Canada, 1978.

Smith, L., and R. A. Freeze, Stochastic analysis of steady state groundwater flow in a bounded domain 1. One-dimensional simulations, Water Resour. Res., 15(3), 521-528, 1979a.

Smith, L., and R. A. Freeze, Stochastic analysis of steady state groundwater flow in a bounded domain 2. Two-dimensional simulations, Water Resour. Res., 15(6), 1543-1559, 1979b.

Stallman, R. W., Numerical analysis of regional water levels to define aquifer hydrology, Trans. Am. Geophysical Union, EOS, 37(4), 451-460, 1956.

Tang, D. H., and G. F. Pinder, Simulation of groundwater flow and mass transport under uncertainty, Advances in Water Resour., 1(1), 25-30, 1977.

Tang, D. H., and G. F. Pinder, A direct solution to the inverse problem in groundwater flow, Advances in Water Resour., 2(2), 97-99, 1979.

Vandenberg, A., Pump testing in heterogeneous aquifers, Journal of Hydrology, 34, 45-62, 1977.

Warren, J. E., and H. S. Price, Flow in heterogeneous porous media, Soc. Petrol. Eng. J., 1, 153-169, 1961.

Wierenga, P. J., C. Duffy, R. Kselik, R. Senn, and W. Strong, Impacts of irrigated agriculture on water quality in the Rio Grande below Albuquerque, Engineering Experiment Station, Dept. of Agronomy, New Mexico State University, Las Cruces, 1979.

Weeks, E. P., and M. L. Sorey, Use of finite-difference arrays of observation wells to estimate evapotranspiration from ground water in the Arkansas River valley, Colorado, Geological Survey Water-Supply Paper 2029-C, 27 pp., 1973.

Whittle, P., On stationary processes in the plane, Biometrika, 41, 434-449, 1954.

APPENDIX I

DERIVATION OF THE COVARIANCE FUNCTION ASSOCIATED WITH SPECTRUM A

The covariance function of a stochastic process is given by the Fourier transform of the spectrum for the process, (1.3). The covariance function, R_A, associated with Spectrum A, (2.12), is

$$R_A(\xi_1,\xi_2) = \frac{N}{a^4}\iint_{-\infty}^{\infty} e^{i(k_1\xi_1+k_2\xi_2)} \frac{k_1^2}{(k_1^2 + k_2^2 + \frac{1}{a^2})^3} dk_1dk_2$$

$$+ \frac{N}{a^4} \iint_{-\infty}^{\infty} e^{i(k_1\xi_1+k_2\xi_2)} \frac{k_2^2}{(k_1^2 + k_2^2 + \frac{1}{a^2})^3} dk_1dk_2 \qquad (I.1)$$

Both parts of (I.1) have identical forms; completion of one will enable solution of the second by a simple change of variable.

Consider the first Fourier transform

$$I_1 = \frac{N}{a^4} \int_{-\infty}^{\infty} e^{ik_2\xi_2} \int_{-\infty}^{\infty} e^{ik_1\xi_1} \frac{k_1^2}{(k_1^2 + b)^3} dk_1dk_2 \qquad (I.2)$$

where $b = k_2^2 + \frac{1}{a^2}$. Solution of the transform over k_1 is given by Oberhettinger (1973, p. 20, #33)

$$\int_{-\infty}^{\infty} e^{ik_1\xi_1} \frac{k_1^2}{(k_1^2 + b)^3}\, dk_1 =$$

$$- \frac{\pi}{8}[\xi_1^2(k_2^2+\tfrac{1}{a^2})^{-\frac{1}{2}} - \xi_1(k_2^2+\tfrac{1}{a^2})^{-1} - (k_2^2+\tfrac{1}{a})^{-\frac{3}{2}}]\, e^{-\xi_1(k_2^2 + \frac{1}{a^2})^{\frac{1}{2}}} \qquad (I.3)$$

Substituting this result into (I.2) gives

$$I_1 = \frac{-N\pi}{8a^4}\left(\xi_1^2\int_{-\infty}^{\infty} e^{ik_2\xi_2}\, (k_2^2 + \tfrac{1}{a^2})^{-\frac{1}{2}}\, e^{-\xi_1(k_2^2 + \frac{1}{a^2})^{\frac{1}{2}}}\, dk_2\right.$$

$$\left. -\int_{-\infty}^{\infty} e^{ik_2\xi_2}\, [\xi_1(k_2^2 + \tfrac{1}{a^2})^{-1} + (k_2^2 + \tfrac{1}{a^2})^{-\frac{3}{2}}]\, e^{-\xi_1(k_2^2 + \frac{1}{a^2})^{\frac{1}{2}}}\, dk_2\right) \qquad (I.4)$$

The second transform in (I.4) can be formulated as a derivative of the first

$$I_1 = \frac{-N\pi}{8a^4}\left(\xi_1^2\int_{-\infty}^{\infty} e^{ik_2\xi_2}\, (k_2^2 + b^2)^{-\frac{1}{2}}\, e^{-\xi_1(k_2^2 + b^2)^{\frac{1}{2}}}\, dk_2\right.$$

$$\left. + a\frac{d}{db}\int_{-\infty}^{\infty} e^{ik_2\xi_2}\, (k_2^2 + b^2)^{-\frac{1}{2}}\, e^{-\xi_1(k_2^2 + b^2)^{\frac{1}{2}}}\, dk_2\right) \qquad (I.5)$$

where $b = \frac{1}{a}$.

The Fourier transform in (I.5) is found in Oberhettinger (1973, p. 26, #95). Thus

$$I_1 = \frac{-N\pi}{8a^4}\left\{\xi_1^2 K_o\left(\frac{1}{a}(\xi_1^2 + \xi_2^2)^{\frac{1}{2}}\right) - a(\xi_1^2 + \xi_2^2)^{\frac{1}{2}} K_1\left(\frac{1}{a}(\xi_1^2 + \xi_2^2)^{\frac{1}{2}}\right)\right\} \qquad (I.6)$$

Now, consider the remaining transform in (I.1)

$$I_2 = \frac{N}{a}\int_{-\infty}^{\infty} e^{ik_1\xi_1}\int_{-\infty}^{\infty} e^{ik_2\xi_2}\frac{k_2^2}{(k_2^2 + b)^3}\,dk_2 dk_1 \qquad (I.7)$$

where $b = \left(k_1^2 + \frac{1}{a^2}\right)$. This equation is identical in form to (I.2); following a change in variable and the same procedure as above, it is found to be

$$I_2 = \frac{-N\pi}{4a^4}\left\{\xi_2^2 K_o\left(\frac{1}{a}(\xi_1^2 + \xi_2^2)^{\frac{1}{2}}\right) - a(\xi_1^2 + \xi_2^2)^{\frac{1}{2}} K_1\left(\frac{1}{a}(\xi_1^2 + \xi^2)^{\frac{1}{2}}\right)\right\} \qquad (I.8)$$

Combining (I.6) and (I.8) completes the transformation of spectrum A; the covariance function is

$$R_A(\xi_1,\xi_2) = \frac{-N\pi}{4a^4}\left[(\xi_1^2 + \xi_2^2)K_o(\frac{1}{a}(\xi_1^2 + \xi_2^2)^{\frac{1}{2}}) - 2a(\xi_1^2 + \xi_2^2)^{\frac{1}{2}}K_1(\frac{1}{a}(\xi_1^2 + \xi_2^2)^{\frac{1}{2}})\right] \tag{I.9}$$

Written in polar coordinates, where $\xi = \left(\xi_1^2 + \xi_2^2\right)^{\frac{1}{2}}$, (I.9) becomes

$$R_A(\xi) = \frac{-N\pi}{4a^4}\left[\xi^2 K_o(\frac{\xi}{a}) - 2a\xi K_o(\frac{\xi}{a})\right] \tag{I.10}$$

The variance associated with spectrum A is determined by solving (I.1) when $\xi_1 = \xi_2 = 0$

$$\sigma^2 = R_A(0,0) = \frac{N}{a^4}\int_{-\infty}^{\infty}\int \frac{k_1^2 + k_2^2}{(k_1^2 + k_2^2 + \frac{1}{a^2})^3}\, dk_1 dk_2 \tag{I.11}$$

or in polar coordinates

$$\sigma^2 = \frac{N}{a^4}\int_o^{2\pi}\int_o^{\infty} \frac{k^2}{(k^2 + \frac{1}{a^2})^3}\, k dk d\chi$$

Integrating over χ, the angle between the separation vector and mean flow direction, and then twice integrating over k by parts produces

$$\sigma^2 = \frac{N\pi}{2a^2} \tag{I.12}$$

Substituting for N in (I.10)

$$R_A(\xi) = \sigma^2 \frac{1}{2a^2} \left[2a\xi K_1(\frac{\xi}{a}) - \xi^2 K_o(\frac{\xi}{a})\right] \tag{I.13}$$

Solving, now, for the integral scale associated with spectrum A using (1.5)

$$\lambda = \int_o^\infty \frac{1}{2a^2} \left[2a\xi K_1(\frac{\xi}{a}) - \xi^2 K_o(\frac{\xi}{a})\right] d\xi$$

This can be written as a Fourier Cosine transform where y = 0

$$\lambda = \frac{1}{a}\int_o^\infty \xi K_1(\frac{\xi}{a})\cos(\xi y)d\xi + \frac{1}{2a^2}\frac{d^2}{dy^2}\int_o^\infty K_o(\frac{\xi}{a})\cos(\xi y)d\xi \tag{I.14}$$

Each Cosine transform in (I.14) is given in Erdelyi (1954, p. 49) by entries 40 and 41 $\left[\text{Note: } \Gamma\left[\frac{3}{2}\right] = \frac{\pi^{\frac{1}{2}}}{2}\right]$

$$\lambda = \frac{1}{a^2}\frac{\pi}{2}\left(\frac{1}{a^2} + y\right)^{-\frac{3}{2}} + \frac{1}{2a^2}\frac{d^2}{dy^2}\left[\frac{\pi}{2}\left(\frac{1}{a^2} + y^2\right)^{\frac{1}{2}}\right]$$

Completing the differentiation and evaluating the result at y = 0 gives

$$\lambda = \frac{\pi a}{4} \tag{I.15}$$

Substituting for a in (I.13) gives the completed form of the covariance function associated with spectrum A

$$R_A(\xi) = \sigma^2\left[\frac{\pi\xi}{4\lambda} K_1\left(\frac{\pi\xi}{4\lambda}\right) - \frac{1}{2}\left(\frac{\pi\xi}{4\lambda}\right)^2 K_o\left(\frac{\pi\xi}{4\lambda}\right)\right] \tag{2.14}$$

APPENDIX II

DERIVATION OF THE COVARIANCE FUNCTION ASSOCIATED WITH SPECTRUM B

The covariance function of a stochastic process is given by the Fourier transform of the spectrum for the process, (1.3). The covariance function, R_B , associated with spectrum B, (2.13), is

$$R_B(\xi_1,\xi_2) = \frac{N}{a^4} \iint_{-\infty}^{\infty} e^{i(k_1\xi_1 + k_2\xi_2)} \frac{(k_1^2 + k_2^2)^2}{(k_1^2 + k_2^2 + \frac{1}{a^2})^4} dk_1 dk_2 \qquad \text{(II.1)}$$

Changing to polar coordinates and integrating over the angle leaves

$$R_B(\xi) = \frac{2\pi N}{a^4} \int_{-\infty}^{\infty} e^{ik\xi} \frac{k^4}{(k^2 + \frac{1}{a^2})^4} kdk \qquad \text{(II.2)}$$

where $k = \left(k_1^2 + k_2^2\right)^{\frac{1}{2}}$ and $\xi = \left(\xi_1^2 + \xi_2^2\right)^{\frac{1}{2}}$. Because the spectrum is symmetric in k (II.2) can be written as a Hankel transform (Bartlett, 1966, p. 211)

$$R_B(\xi) = \frac{2\pi N}{a^4} \int_{0}^{\infty} J_0(k\xi) \frac{k^4}{(k^2 + \frac{1}{a^2})^4} kdk \qquad \text{(II.3)}$$

where J_o designates the zero order Bessel function of the first kind.

Partial fractionizing $\dfrac{k^4}{\left(k^2 + \frac{1}{a^2}\right)^4}$ leads to

$$R_B(\xi) = \frac{2\pi N}{a^4}\left[\int_o^\infty J_o(k\xi)\frac{k}{(k^2+\frac{1}{a^2})^2}\,dk - \frac{2}{a^2}\int_o^\infty J_o(k\xi)\frac{k}{(k^2+\frac{1}{a^2})^3}\,dk\right.$$

$$\left. + \frac{1}{a^2}\int_o^\infty J_o(k\xi)\frac{k}{(k^2+\frac{1}{a^2})^4}\,dk\right] \qquad \text{(II.4)}$$

The general form of the Hankel transform is

$$H_n = \int_o^\infty J_o(k\xi)\,\frac{k}{(k^2+\frac{1}{a^2})^n}\,dk$$

and the specific forms required to solve (II.4) are

$$H_1 = \int_o^\infty J_o(k\xi)\,\frac{k}{(k^2+b^2)}\,dk = K_o(b\xi) \qquad \text{(II.5a)}$$

$$H_2 = -\frac{a}{2}\frac{\partial H_1}{\partial b} = \frac{a\xi}{2}K_1(b\xi) \qquad \text{(II.5b)}$$

$$H_3 = -\frac{a}{4}\frac{\partial H_2}{\partial b} = \frac{a^3\xi}{8}\left[2K_1(b\xi) - b\xi K_o(b\xi)\right] \qquad \text{(II.5c)}$$

$$H_4 = -\frac{a}{6}\frac{\partial H_3}{\partial b} = \frac{a^3\xi}{48}\left[(8a^2 + \xi^2)K_1(b\xi) + 4a\xi K_o(b\xi)\right] \qquad \text{(II.5d)}$$

where $b = \frac{1}{a}$.

Substituting (II.5b), (II.5c), and (II.5d) into (II.4) and simplifying produces

$$R_B(\xi) = \frac{2\pi N}{6a^3}\left[(1 + \frac{1}{8}\frac{\xi^2}{a^2})\xi K_1(\frac{\xi}{a}) - \frac{\xi^2}{a}K_o(\frac{\xi}{a})\right] \qquad \text{(II.6)}$$

The variance associated with spectrum B is determined by solving (II.1) when $\xi_1 = \xi_2 = 0$

$$\sigma^2 = R_B(0,0) = \frac{N}{a^4}\int_{-\infty}^{\infty}\int \frac{(k_1^2 + k_2^2)^2}{(k_1^2 + k_2^2 + \frac{1}{a^2})^4}\, dk_1 dk_2 \qquad \text{(II.7)}$$

in polar coordinates (II.7) becomes

$$\sigma^2 = \frac{N}{a^4} \int_0^{2\pi} \int_0^{\infty} \frac{k^4}{(k^2 + \frac{1}{a^2})^4} \, k dk d\chi \tag{II.8}$$

Integrating over χ , the angle between the separation vector and the mean flow direction, produces a 2π . Then integrating over k by parts, three times, gives

$$\sigma^2 = \frac{\pi N}{3a^2} \tag{II.9}$$

Substituting for N in (II.6)

$$R_B(\xi) = \sigma^2 \left[(1 + \frac{1}{8} \frac{\xi^2}{a^2}) \frac{\xi}{a} K_1(\frac{\xi}{a}) - (\frac{\xi}{a})^2 K_o(\frac{\xi}{a}) \right] \tag{II.10}$$

The integral scale associated with spectrum B is found by integrating the correlation function as indicated in (1.5).

$$\lambda = \int_0^{\infty} \left[(1 + \frac{1}{8} \frac{\xi^2}{a^2}) \frac{\xi}{a} K_1(\frac{\xi}{a}) - (\frac{\xi}{a})^2 K_o(\frac{\xi}{a}) \right] d\xi \tag{II.11}$$

Equation (II.11) can be written as a Fourier Cosine transform in which $y = 0$

$$\lambda = \frac{1}{a}\int_0^\infty \xi K_1(\frac{\xi}{a})\cos(\xi y)\,d\xi - \frac{1}{8a^3}\frac{d^2}{dy^2}\int_0^\infty \xi K_1(\frac{\xi}{a})\cos(\xi y)\,d\xi$$

$$+ \frac{1}{a^2}\frac{d^2}{dy^2}\int_0^\infty K_o(\frac{\xi}{a})\cos(\xi y)\,d\xi \qquad \text{(II.12)}$$

The transforms in (II.12) are given in Erdelyi (1954, p. 49) by entries 40 and 41

$$\lambda = \frac{\pi}{2a^2}(\frac{1}{a^2} + y^2)^{-\frac{3}{2}} - \frac{1}{8a^3}\frac{d^2}{dy^2}\left[\frac{\pi}{2a}(\frac{1}{a^2} + y^2)^{-\frac{3}{2}}\right] + \frac{1}{a^2}\frac{d^2}{dy^2}\left[\frac{\pi}{2}(\frac{1}{a^2} + y^2)^{-\frac{1}{2}}\right]$$

(II.13)

Evaluating the derivatives in (II.13) and substituting $y = 0$

$$\lambda = \frac{3\pi a}{16} \qquad \text{(II.14)}$$

Substituting for a in (II.10) gives

$$R_B(\xi) = \sigma^2\left[(1 + \frac{1}{8}(\frac{3\pi\xi}{16\lambda})^2)\frac{3\pi\xi}{16\lambda}K_1(\frac{3\pi\xi}{16\lambda}) - (\frac{3\pi\xi}{16\lambda})^2 K_o(\frac{3\pi\xi}{16\lambda})\right] \qquad \text{(2.15)}$$

APPENDIX III

DERIVATION OF THE HEAD COVARIANCE FUNCTION ASSUMING INPUT SPECTRUM A

The head covariance function is given by the Fourier transform of the head spectrum, (2.16). Assuming spectrum A for the ln T spectrum, the head spectrum, (2.9), becomes

$$\Phi_h(k_1,k_2) = \frac{k_1^2 J_1^2 N}{a^4 (k_1^2 + k_2^2) (k_1^2 + k_2^2 + \frac{1}{a^2})^3} \qquad \text{(III.1)}$$

Thus, the head covariance function is

$$R_{Ah}(\xi_1,\xi_2) = \frac{J_1^2 N}{a^4} \int_{-\infty}^{\infty} e^{ik_1\xi_1} k_1^2 \int_{-\infty}^{\infty} e^{ik_2\xi_2} \frac{dk_2}{(k_1^2 + k_2^2) (k_1^2 + k_2^2 + \frac{1}{a^2})^3} dk_1 \qquad \text{(III.2)}$$

Consider, first, the transform over k_2

$$I_1 = \int_{-\infty}^{\infty} e^{ik_2\xi_2} \frac{dk_2}{(k_2^2 + b^2) (k_2^2 + c^2)^3}$$

where $b^2 = k_1^2$ and $c^2 = k_1^2 + \frac{1}{a^2}$. Partial fractionizing leads to

$$I_1 = \frac{1}{(c^2 - b^2)^3} \left(\int_{-\infty}^{\infty} e^{ik_2\xi_2} \frac{dk_2}{(k_2^2 + b^2)} - \int_{-\infty}^{\infty} e^{ik_2\xi_2} \frac{(c^2 - b^2)^2}{(k_2^2 + c^2)^3} dk_2 \right.$$

$$\left. - \int_{-\infty}^{\infty} e^{ik_2\xi_2} \frac{(c^2 - b^2)}{(k_2^2 + c^2)^2} dk_2 - \int_{-\infty}^{\infty} e^{ik_2\xi_2} \frac{dk_2}{(k_2^2 + c^2)} \right) \qquad \text{(III.3)}$$

Each of the transforms in (III.3) are found in Oberhettinger (1973) from entries 7 (p. 17) and 42 (p. 21)

$$I_1 = (c^2 - b^2)^{-3} \left(\frac{\pi}{b} e^{-b\xi_2} - (c^2 - b^2)^2 \frac{1}{4}\left(\frac{\pi}{2}\right)^{\frac{1}{2}} c^{-\frac{5}{2}} \xi_2^{\frac{5}{2}} K_{\frac{5}{2}}(c\xi_2) \right.$$

$$\left. - (c^2 - b^2)\left(\frac{\pi}{2}\right)^{\frac{1}{2}} c^{-\frac{3}{2}} \xi_2^{\frac{3}{2}} K_{\frac{3}{2}}(c\xi_2) - \frac{\pi}{c} e^{-c\xi_2} \right) \qquad \text{(III.4)}$$

Substituting for b and c (III.2) becomes

$$R_{Ah}(\xi_1,\xi_2) = \frac{J_1^2 N}{a^4}\left[a^6\pi \int_{-\infty}^{\infty} e^{ik_1\xi_1}\, k_1\, e^{-\xi_2 k_1}\, dk_1 \right.$$

$$+ \frac{a^2}{4}\left(\frac{\pi}{2}\right)^{\frac{1}{2}} \xi_2^{\frac{5}{2}} \frac{\partial^2}{\partial\xi_1^2}\int_{-\infty}^{\infty} e^{ik_1\xi_1}\, (k_1^2 + \frac{1}{a^2})^{-\frac{5}{4}}\, K_{\frac{5}{2}}(\xi_2(k_1^2 + \frac{1}{a^2})^{\frac{1}{2}})dk_1$$

$$+ a^4\left(\frac{\pi}{2}\right)^{\frac{1}{2}} \xi_2^{\frac{3}{2}} \frac{\partial^2}{\partial\xi_1^2}\int_{-\infty}^{\infty} e^{ik_1\xi_1}\, (k_1^2 + \frac{1}{a^2})^{-\frac{3}{4}}\, K_{\frac{3}{2}}(\xi_2(k_1^2 + \frac{1}{a^2})^{\frac{1}{2}})dk_1$$

$$\left. + a^6\pi \frac{\partial^2}{\partial\xi_1^2}\int_{-\infty}^{\infty} e^{ik_1\xi_1}\, (k_1^2 + \frac{1}{a^2})^{-\frac{1}{2}}\, e^{-\xi_2(k_1^2 + \frac{1}{a^2})^{\frac{1}{2}}}\, dk_1 \right] \qquad \text{(III.5)}$$

Entries 65, 449, and 95 on pages 23, 64, and 26, respectively, of Oberhettinger (1973) give the Fourier transforms in (III.5). Thus

$$R_{Ah}(\xi_1,\xi_2) = \frac{J_1^2 N}{a^4}\left[a^6\pi\, 2\, (\xi_1^2 + \xi_2^2)^{-1}\, (1 - 2\cos^2\chi) \right.$$

$$+ a^4\, \frac{\pi}{4}\, \frac{\partial^2}{\partial\xi_1^2}[(\xi_1^2 + \xi_2^2)\, K_2(\frac{1}{a}(\xi_1^2 + \xi_2^2)^{\frac{1}{2}})]$$

$$+ a^5\, \pi\, \frac{\partial^2}{\partial\xi_1^2}[(\xi_1^2 + \xi_2^2)^{\frac{1}{2}}\, K_1(\frac{1}{a}(\xi_1^2 + \xi_2^2)^{\frac{1}{2}})]$$

$$\left. + 2a^6\, \pi\, \frac{\partial^2}{\partial\xi_1^2}[K_0(\frac{1}{a}(\xi_1^2 + \xi_2^2)^{\frac{1}{2}})] \right] \qquad \text{(III.6)}$$

where χ is the angle between the separation vector and the mean flow direction.

The recurrence relations for Bessel functions (Abramowitz and Stegun, 1972) are used to formulate the second order modified Bessel function as a sum of zero and first order modified Bessel functions, then the derivative formulas are used to evaluate terms in (III.6). Incorporating these results (III.6) becomes

$$R_{Ah}(\xi_1,\xi_2) = \frac{J_1^2 N}{a^4}\Bigg[\, a^4\,\frac{\pi}{4}\,\Big[\Big(\Big(\frac{\xi_1^2}{a}\Big) + 2\Big)K_o\Big(\frac{1}{a}(\xi_1^2+\xi_2^2)^{\frac{1}{2}}\Big)$$

$$- \Big(\frac{1}{a}(\xi_1^2+\xi_2^2)^{\frac{1}{2}} + \frac{2\xi_1^2}{a}(\xi_1^2+\xi_2^2)^{-\frac{1}{2}}\,K_1\Big(\frac{1}{a}(\xi_1^2+\xi_2^2)^{\frac{1}{2}}\Big)\Big]$$

$$+ a^5\,\frac{3\pi}{2}\,\Big[\Big(\frac{\xi_1}{a}\Big)^2\,(\xi_1^2+\xi_2^2)^{-\frac{1}{2}}\,K_1\Big(\frac{1}{a}(\xi_1^2+\xi_2^2)^{\frac{1}{2}}\Big)$$

$$- \frac{1}{a}\,K_o\Big(\frac{1}{a}(\xi_1^2+\xi_2^2)^{\frac{1}{2}}\Big)\Big]$$

$$+ a^6\,2\pi\,\Big[\Big(\frac{\xi_1}{a}\Big)^2\,(\xi_1^2+\xi_2^2)^{-1}\,K_o\Big(\frac{1}{a}(\xi_1^2+\xi_2^2)^{\frac{1}{2}}\Big)$$

$$+ \Big(\frac{2\xi_1^2}{a}(\xi_1^2+\xi_2^2)^{-\frac{3}{2}} - \frac{1}{a}(\xi_1^2+\xi_2^2)^{-\frac{1}{2}}\,K_1\Big(\frac{1}{a}(\xi_1^2+\xi_2^2)^{\frac{1}{2}}\Big)\Big]$$

$$- a^6\,2\pi\,(\xi_1^2+\xi_2^2)^{-1}\,(2\cos\chi - 1)\Bigg] \qquad \text{(III.7)}$$

Substituting for N and a, (I.12) and (I.15), simplifying and changing to polar coordinates

$$R_{Ah}(\xi,\chi) = \frac{8}{\pi^2} J_1^2 \sigma_f^2 \lambda^2 4\Big\{ \cos^2\chi[(\tfrac{1}{4}(\tfrac{\pi\xi}{4\lambda})^2 + 2)K_o(\tfrac{\pi\xi}{4\lambda}) + \tfrac{\pi\xi}{4\lambda} K_1(\tfrac{\pi\xi}{4\lambda}) + 4(\tfrac{\pi\xi}{4\lambda})^{-1}K_1(\tfrac{\pi\xi}{4\lambda}) - 4(\tfrac{\pi\xi}{4\lambda})^{-2}] - [K_o(\tfrac{\pi\xi}{4\lambda}) + (\tfrac{1}{4}(\tfrac{\pi\xi}{4\lambda}) + 2(\tfrac{\pi\xi}{4\lambda})^{-1})K_1(\tfrac{\pi\xi}{4\lambda}) - 2(\tfrac{\pi\xi}{4\lambda})^{-2}] \Big\} \qquad (2.18)$$

The head variance resulting from use of spectrum A to represent the ln T spectrum is evaluated from (III.2) when $\xi_1 = \xi_2 = 0$

$$\sigma_{Ah}^2 = R_{Ah}(0,0) = \frac{J_1^2 N}{a^4} \int\int_{-\infty}^{\infty} \frac{k_1^2}{(k_1^2 + k_2^2)\ (k_1^2 + k_2^2 + \frac{1}{a^2})^3} dk_1 dk_2 \qquad (III.8)$$

Written in polar coordinates (III.8) is

$$\sigma_{Ah}^2 = \frac{J_1^2 N}{a^4} \int_o^{2\pi} \int_o^{\infty} \frac{\cos^2\chi}{(k^2 + \frac{1}{a^2})^3} k dk d\chi \qquad (III.9)$$

Completing the integrations and substituting for a and N

$$\sigma_{Ah}^2 = \frac{8}{\pi^2} J_1^2 \sigma_f^2 \lambda^2 \qquad (2.19)$$

APPENDIX IV

DERIVATION OF THE HEAD COVARIANCE FUNCTION ASSUMING INPUT SPECTRUM B

The head covariance function is given by the Fourier transform of the head spectrum, (2.16). Assuming spectrum B for the ln T spectrum, the head spectrum, (2.9), becomes

$$\Phi_h(k_1,k_2) = \frac{k_1^2 J_1^2 N}{a^4(k_1^2 + k_2^2 + \frac{1}{a^2})^4} \tag{IV.1}$$

Then the head covariance function is

$$R_{Bh}(\xi_1,\xi_2) = \frac{J_1^2 N}{a^4} \int_{-\infty}^{\infty} e^{ik_1\xi_1} k_1^2 \int_{-\infty}^{\infty} e^{ik_2\xi_2} \frac{dk_2}{(k_2^2 + b^2)^4} dk_1 \tag{IV.2}$$

where $b^2 = k_1^2 + \frac{1}{a^2}$.

The transform over k_2 is (Oberhettinger, 1973, p. 21, #42)

$$\int_{-\infty}^{\infty} e^{ik_2\xi_2} \frac{dk_2}{(k_2^2 + b^2)^4} = \frac{\pi^{\frac{1}{2}} \xi_2^{\frac{7}{2}}}{3 \cdot 2^{\frac{7}{2}}} (k_1^2 + \frac{1}{a^2})^{-\frac{7}{4}} K_{\frac{7}{2}}(\xi_2(k_1^2 + \frac{1}{a^2})^{\frac{1}{2}})$$

Substituting this into (IV.2)

$$R_{Bh}(\xi_1,\xi_2) = -\frac{J_1^2 N}{a^4}\frac{\pi^{\frac{1}{2}}\xi_2^{\frac{7}{2}}}{3\cdot 2^{\frac{7}{2}}}\frac{\partial^2}{\partial\xi_1^2}\int_{-\infty}^{\infty} e^{ik_1\xi_1}\,(k_1^2+\frac{1}{a^2})^{-\frac{7}{4}}\,K_{\frac{7}{2}}(\xi_2^2(k_1^2+\frac{1}{a^2})^{\frac{1}{2}})\,dk_1 \tag{IV.3}$$

From entry 449 in Oberhettinger (1973, p. 64) the transform in (IV.3) is evaluated and

$$R_{Bh}(\xi_1,\xi_2) = -\frac{J_1^2 N}{a^4}\frac{\pi^{\frac{1}{2}}\xi_2^{\frac{7}{2}}}{3\cdot 2^{\frac{7}{2}}}\frac{\partial^2}{\partial\xi_1^2}[2\,(\frac{\pi}{2a})^{\frac{1}{2}}\,(\frac{\xi_2}{a})^{-\frac{7}{2}}\,(\xi_1^2+\xi_2^2)^{\frac{3}{2}}\,K_3(\frac{1}{a}(\xi_1^2+\xi_2^2)^{\frac{1}{2}})] \tag{IV.4}$$

Using the recurrence relations and derivative formulas from Abramowitz and Stegun (1972) to write the third order modified Bessel functions in terms of zero and first order modified Bessel functions and evaluate the resulting derivatives gives

$$R_{Bh}(\xi_1,\xi_2) = \frac{J_1^2 N\pi}{24a}\Big[(2-(\frac{\xi_1}{a})^2)\,(\xi_1^2+\xi_2^2)^{\frac{1}{2}}\,K_1(\frac{1}{a}(\xi_1^2+\xi_2^2)^{\frac{1}{2}})$$

$$+\frac{1}{a}\,(\xi_1^2+\xi_2^2)\,K_o(\frac{1}{a}(\xi_1^2+\xi_2^2)^{\frac{1}{2}})\Big]$$

Substituting for N and a, (II.9) and (II.14), simplifying and changing to polar coordinates results in

$$R_{Bh}(\xi,\chi) = (\frac{8}{3\pi})^2 J_1^2 \sigma_f^2 \lambda^2 \frac{1}{2}\Big[(2 - (\frac{3\pi\xi}{16\lambda})^2 \cos^2\chi) \frac{3\pi\xi}{16\lambda} K_1(\frac{3\pi\xi}{16\lambda}) + (\frac{3\pi\xi}{16\lambda})^2 K_o(\frac{3\pi\xi}{16\lambda})\Big] \qquad (2.20)$$

The head variance resulting from use of spectrum B is determined by evaluating (IV.2) at $\xi_1 = \xi_2 = 0$.

$$\sigma_{Bh}^2 = R_{Bh}(0,0) = \frac{J_1^2 N}{a^4} \iint_{-\infty}^{\infty} \frac{k_1^2}{(k_1^2 + k_2^2 + \frac{1}{a^2})^4} dk_1 dk_2 \qquad (IV.5)$$

In polar coordinates (IV.5) becomes

$$\sigma_{Bh}^2 = \frac{J_1^2 N}{a^4} \int_o^{2\pi} \int_o^{\infty} \frac{k^2 \cos^2\chi}{(k^2 + \frac{1}{a^2})^4} k dk d\chi$$

Integrating and then substituting for a and N

$$\sigma_{Bh}^2 = (\frac{8}{3\pi})^2 J_1^2 \sigma_f^2 \lambda^2 \qquad (2.21)$$

APPENDIX V

DERIVATION OF THE CROSS-COVARIANCE FUNCTION BETWEEN HEAD AND ln T ASSUMING INPUT SPECTRUM A

Replacing the ln T spectrum in (2.22) by spectrum A, (2.12), the cross-covariance between the head and ln T processes is given by (1.3)

$$R_{Ahf}(\xi_1,\xi_2) = \frac{-iJ_1N}{a^4} \iint_{-\infty}^{\infty} e^{i(k_1\xi_1 + k_2\xi_2)} \frac{k_1}{(k_1^2 + k_2^2 + \frac{1}{a^2})^3} dk_1dk_2 \qquad (V.1)$$

Equation (V.1) can be written as the sum of Fourier Cosine and Sine transforms. The resulting Fourier Cosine transform is recognized as the symmetric integral of an odd function and thus to be zero valued. Expansion of the Fourier Sine transform according to angle-sum relations gives

$$R_{Ahf}(\xi_1,\xi_2) = \frac{J_1N}{a^4} \left(\iint_{-\infty}^{\infty} \sin(k_1\xi_1)\cos(k_2\xi_2) \frac{k_1\, dk_1dk_2}{(k_1^2 + k_2^2 + \frac{1}{a^2})^3} \right.$$

$$\left. + \iint_{-\infty}^{\infty} \cos(k_1\xi_1)\sin(k_2\xi_2) \frac{k_1\, dk_1dk_2}{(k_1^2 + k_2^2 + \frac{1}{a^2})^3} \right) \qquad (V.2)$$

Again, the second term in (V.2) is a symmetric integral of an odd integrand and so is zero. Rewriting (V.2)

$$R_{Ahf}(\xi_1,\xi_2) = \frac{J_1 N}{a^4} \int_{-\infty}^{\infty} \cos(k_2\xi_2) \int_{-\infty}^{\infty} \sin(k_1\xi_1) \frac{k_1}{(k_1^2 + b^2)^3} dk_1 dk_2 \qquad (V.3)$$

where $b^2 = k_2^2 + \frac{1}{a^2}$.

The Fourier Sine transform over k_1 in (V.3) is obtained from Erdelyi (1954, p. 67, #37)

$$\int_{-\infty}^{\infty} \sin(k_1\xi_1) \frac{k_1\, dk_1}{(k_1^2 + b^2)^3} = 2 \frac{(-1)\, \pi^{\frac{1}{2}}}{2^{\frac{5}{2}} b^{\frac{5}{2}} \Gamma(3)} \frac{\partial}{\partial \xi_1} (\xi_1^{\frac{5}{2}} K_{\frac{5}{2}}(\xi_1 b))$$

and (V.3) becomes

$$R_{Ahf}(\xi_1,\xi_2) = \frac{J_1 N}{a^4} \frac{1}{4} (\frac{\pi}{2})^{\frac{1}{2}} \xi_1^{\frac{5}{2}}\, 2 \int_0^{\infty} \cos(k_2\xi_2)(k_2^2 + \frac{1}{a^2})^{-\frac{3}{4}} K_{\frac{3}{2}}(\xi_1(k_2^2 + \frac{1}{a^2})^{\frac{1}{2}})\, dk_2$$

This Fourier Cosine transform is also found in Erdelyi (1954, p. 56, #45) and

$$R_{Ahf}(\xi_1,\xi_2) = \frac{J_1 N}{a^4} \frac{1}{4} (\frac{\pi}{2})^{\frac{1}{2}} \xi_1^{\frac{5}{2}}\, 2 \left((\frac{\pi}{2})^{\frac{1}{2}} \xi_1^{-\frac{7}{2}} a(\xi_1^2 + \xi_2^2)^{\frac{1}{2}} K_1(\frac{1}{a}(\xi_1^2 + \xi_2^2)^{\frac{1}{2}}) \right) \qquad (V.4)$$

Substituting N and a, (I.12) and (I.15), simplifying, and changing to polar coordinates (V.4) becomes

$$R_{Ahf}(\xi,\chi) = \sigma_f^2 \, J_1 \, \lambda \, \frac{2}{\pi} \cos\chi \, (\frac{\pi\xi}{4\lambda})^2 \, K_1(\frac{\pi\xi}{4\lambda}) \qquad (2.23)$$

APPENDIX VI

DERIVATION OF THE CROSS-COVARIANCE FUNCTION BETWEEN HEAD AND ln T ASSUMING INPUT SPECTRUM B

Replacing the lnT spectrum in (2.22) by spectrum B, (2.13), the cross-covariance function between the head and ln T processes is given by

$$R_{Bhf}(\xi_1,\xi_2) = \frac{-iJ_1N}{a^4} \iint_{-\infty}^{\infty} e^{i(k_1\xi_1 + k_2\xi_2)} \frac{k_1 (k_1^2 + k_2^2)}{(k_1^2 + k_2^2 + \frac{1}{a^2})^4} dk_1dk_2 \qquad \text{(VI.1)}$$

Writing (VI.1) as the sum of a Fourier Cosine transform and a Fourier Sine transform one will note that the Cosine transform is a symmetric integral of an odd integrand and thus is zero. The remaining Sine transform is expanded according to the angle-sum formula producing

$$R_{Bhf}(\xi_1,\xi_2) = \frac{J_1N}{a^4} \left[\iint_{-\infty}^{\infty} \sin(k_1\xi_1) \cos(k_2\xi_2) \frac{k_1 (k_1^2 + k_2^2)}{(k_1^2 + k_2^2 + \frac{1}{a^2})^4} dk_1dk_2 \right.$$

$$\left. + \iint_{-\infty}^{\infty} \cos(k_1\xi_1) \sin(k_2\xi_2) \frac{k_1 (k_1^2 + k_2^2)}{(k_1^2 + k_2^2 + \frac{1}{a^2})^4} dk_1dk_2 \right] \qquad \text{(IV.2)}$$

The second term in (VI.2) is also a symmetric integral of an odd integrand and is zero. Rewriting the rest of (VI.2)

$$R_{Bhf}(\xi_1,\xi_2) = \frac{J_1 N}{a^4}\, 2 \int_{-\infty}^{\infty} \cos(k_2\xi_2) \left(\int_0^{\infty} \sin(k_1\xi_1)\, \frac{k_1^3}{(k_1^2 + k_2^2 + \frac{1}{a^2})^4}\, dk_1 \right.$$

$$\left. + \int_0^{\infty} \sin(k_1\xi_1)\, \frac{k_1\, k_2^2\, dk_1}{(k_1^2 + k_2^2 + \frac{1}{a^2})^4} \right) dk_2$$

Partial fractionizing $\dfrac{k_1 k_2^2}{\left[k_1^2 + k_2^2 + \frac{1}{a^2}\right]^4}$ with respect to k_2 leads to

$$R_{Bhf}(\xi_1,\xi_2) = \frac{J_1 N}{a^4}\, 2 \int_{-\infty}^{\infty} \cos(k_2\xi_2) \left(\int_0^{\infty} \sin(k_1\xi_1)\, \frac{k_1\, dk_1}{(k_1^2 + k_2^2 + \frac{1}{a^2})^3} \right.$$

$$\left. - \int_0^{\infty} \sin(k_1\xi_1)\, \frac{k_1\, dk_1}{(k_1^2 + k_2^2 + \frac{1}{a^2})^4} \right) dk_2 \quad \text{(VI.3)}$$

Solutions to the Fourier Sine transforms in (VI.3) are found in Erdelyi (1954, p. 67, #37). Substituting the transform solutions in (VI.3) gives

$$R_{Bhf}(\xi_1,\xi_2) = \frac{J_1 N}{a^4}\, 4\left[\frac{1}{8} \left(\frac{\pi}{2}\right)^{\frac{1}{2}} \xi_1^{\frac{5}{2}} \int_0^{\infty} \cos(k_2\xi_2)\left(k_2^2 + \frac{1}{a^2}\right)^{-\frac{3}{4}} K_{\frac{3}{2}}\left(\xi_1\left(k_2^2 + \frac{1}{a^2}\right)^{\frac{1}{2}}\right) dk_2 \right.$$

$$\left. - \frac{1}{a^2}\, \frac{1}{48} \left(\frac{\pi}{2}\right)^{\frac{1}{2}} \xi_1^{\frac{7}{2}} \int_0^{\infty} \cos(k_2\xi_2)\left(k_2^2 + \frac{1}{a^2}\right)^{-\frac{5}{4}} K_{\frac{5}{2}}\left(\xi_1\left(k_2^2 + \frac{1}{a^2}\right)^{\frac{1}{2}}\right) dk_2 \right] \qquad \text{(VI.4)}$$

The Fourier Cosine transforms in (VI.4) are also obtained from Erdelyi (1954), entry 45, page 56.

$$R_{Bhf}(\xi_1,\xi_2) = \frac{J_1 N}{a^4}\, 4\left[\frac{1}{8} \left(\frac{\pi}{2}\right)^{\frac{1}{2}} \xi_1^{\frac{5}{2}} \left[\left(\frac{\pi}{2}\right)^{\frac{1}{2}} a\, \xi_1^{-\frac{3}{2}} \left(\xi_1^2 + \xi_2^2\right)^{\frac{1}{2}} K_1\left(\frac{1}{a}\left(\xi_1^2 + \xi_2^2\right)^{\frac{1}{2}}\right)\right]\right.$$

$$\left. - \frac{1}{a^2}\, \frac{1}{48} \left(\frac{\pi}{2}\right)^{\frac{1}{2}} \xi_1^{\frac{7}{2}} \left[\left(\frac{\pi}{2}\right)^{\frac{1}{2}} \xi_1^{-\frac{5}{2}} a^2 \left(\xi_1^2 + \xi_2^2\right) K_2\left(\frac{1}{a}\left(\xi_1^2 + \xi_2^2\right)^{\frac{1}{2}}\right)\right]\right] \qquad \text{(VI.5)}$$

Using the recurrence relations (Abramowitz and Stegun, 1972) the second order modified Bessel function in (VI.5) is written as a sum of zero and first order modified Bessel functions. Then substituting for N and a, (II.9) and (II.14), simplifying, and changing to polar coordinates (VI.5) becomes

$$R_{Bhf}(\xi,\chi) = \sigma_f^2\, J_1\lambda\, \frac{8}{3\pi} \cos\chi \left(\frac{3\pi\xi}{16\lambda}\right)^2 \left[K_1\left(\frac{3\pi\xi}{16\lambda}\right) - \frac{1}{4}\left(\frac{3\pi\xi}{16\lambda}\right) K_o\left(\frac{3\pi\xi}{16\lambda}\right)\right] \qquad (2.24)$$

APPENDIX VII

DERIVATION OF THE COVARIANCE FUNCTION FOR HEAD IN THE TRANSIENT ANALYSIS ASSUMING INPUT SPECTRUM B

The head covariance function for the transient analysis is formulated as the Fourier transform of the transient head spectrum, (3.9); assuming spectrum B, (2.13), to represent the ln T spectrum leads to

$$R_h(\xi_1,\xi_2) = \int_{-\infty}^{\infty}\int e^{i(k_1\xi_1 + k_2\xi_2)} \frac{k_1^2 J_1^2 N}{a^4(k_1^2 + k_2^2 + \frac{1}{a^2})^4} dk_1 dk_2$$

$$+ \int_{-\infty}^{\infty}\int e^{i(k_1\xi_1 + k_2\xi_2)} \frac{(\frac{S}{T_\ell}\frac{\partial H}{\partial t})^2 N}{a^4(k_1^2 + k_2^2 + \frac{1}{a^2})^4} dk_1 dk_2 \qquad \text{(VII.1)}$$

The first transform in (VII.1) is identical to that obtained for the steady head covariance function with spectrum B as input, (IV.2), thus

$$\int_{-\infty}^{\infty}\int e^{i(k_1\xi_1 + k_2\xi_2)} \frac{k_1^2 J_1^2 N}{a^4(k_1^2 + k_2^2 + \frac{1}{a^2})^4} dk_1 dk_2$$

$$= (\frac{8}{3\pi})^2 J_1^2 \sigma_f^2 \lambda^2 \frac{1}{2}\left[[2 - (\frac{3\pi\xi}{16\lambda})^2 \cos^2\chi] \frac{3\pi\xi}{16\lambda} K_1(\frac{3\pi\xi}{16\lambda}) + (\frac{3\pi\xi}{16\lambda})^2 K_o(\frac{3\pi\xi}{16\lambda})\right]$$

(2.20)

and

$$\iint_{-\infty}^{\infty} \frac{k_1^2 J_1^2 N}{a^4(k_1^2 + k_2^2 + \frac{1}{a^2})^4} dk_1 dk_2 = (\frac{8}{3\pi})^2 J_1^2 \sigma_f^2 \lambda^2 \qquad (2.21)$$

Consider the second transform in (VII.1)

$$I(\xi_1,\xi_2) = \iint_{-\infty}^{\infty} e^{i(k_1\xi_1 + k_2\xi_2)} \frac{(\frac{S}{T_\ell} \frac{\partial H}{\partial t})^2 N}{a^4(k_1^2 + k_2^2 + \frac{1}{a^2})^4} dk_1 dk_2$$

$$= (\frac{S}{T_\ell} \frac{\partial H}{\partial t})^2 \frac{N}{a^4} \int_{-\infty}^{\infty} e^{ik_1\xi_1} \int_{-\infty}^{\infty} e^{ik_2\xi_2} \frac{dk_2}{(k_2^2 + b^2)^4} dk_1 \qquad (VII.2)$$

where $b^2 = \left(k_1^2 + \frac{1}{a^2}\right)$. The transform on k_2 is (Oberhettinger, 1973, p. 21, #42)

$$I(\xi_1,\xi_2) = (\frac{S}{T_\ell} \frac{\partial H}{\partial t})^2 \frac{N}{a^4} \int_{-\infty}^{\infty} e^{ik_1\xi_1} \frac{\xi_2^{\frac{7}{2}}}{24} (\frac{\pi}{2})^{\frac{1}{2}} (k_1^2 + \frac{1}{a^2})^{-\frac{7}{4}} K_{\frac{7}{2}}(\xi_2(k_1^2 + \frac{1}{a^2})^{\frac{1}{2}}) dk_1$$

(VII.3)

Oberhettinger (1973) gives this Fourier transform on page 64 (entry 449)

$$I(\xi_1,\xi_2) = \left(\frac{S}{T_\ell}\frac{\partial H}{\partial t}\right)^2 \frac{N}{a^4}\frac{\xi_2^{\frac{7}{2}}}{24}\left(\frac{\pi}{2}\right)^{\frac{1}{2}}\left[2\left(\frac{\pi}{2a}\right)^{\frac{1}{2}}\left(\frac{\xi_2}{a}\right)^{-\frac{7}{2}}(\xi_1^2+\xi_2^2)^{\frac{3}{2}}K_3\left(\frac{1}{a}(\xi_1^2+\xi_2^2)^{\frac{1}{2}}\right)\right] \tag{VII.4}$$

Using the recurrence relations (Abramowitz and Stegun, 1972) the third order modified Bessel function in (VII.4) is formulated as the sum of zero and first order modified Bessel functions. Then substituting for N and a, (II.9) and (II.14), simplifying, and changing to polar coordinates

$$I(\xi_1,\xi_2) = \left(\frac{S}{T_\ell}\frac{\partial H}{\partial t}\right)^2 \sigma_f^2 \left(\frac{16\lambda}{3\pi}\right)^4 \frac{1}{8}\left[\left(8+\left(\frac{3\pi\xi}{16\lambda}\right)^2\right)\frac{3\pi\xi}{16\lambda}K_1\left(\frac{3\pi\xi}{16\lambda}\right) + \left(\frac{3\pi\xi}{16\lambda}\right)^2 K_0\left(\frac{3\pi\xi}{16\lambda}\right)\right] \tag{VII.5}$$

Evaluating (VII.2) at $\xi_1 = \xi_2 = 0$ gives the contribution of this additional term to the head variance in the transient analysis.

$$I(0,0) = \left(\frac{S}{T_\ell}\frac{\partial H}{\partial t}\right)^2 \frac{N}{a^4}\int_{-\infty}^{\infty}\int \frac{dk_1\,dk_2}{(k_1^2+k_2^2+\frac{1}{a^2})^4} \tag{VII.6}$$

In polar coordinates (VII.6) is

$$I(0,0) = \left(\frac{S}{T_\ell}\frac{\partial H}{\partial t}\right)^2 \frac{N}{a^4} \int_0^{2\pi}\int_0^{\infty} \frac{k\,dk}{\left(k^2 + \frac{1}{a^2}\right)^4}\, d\chi$$

Completing the integrals and substituting for a and N

$$I(0,0) = \left(\frac{S}{T_\ell}\frac{\partial H}{\partial t}\right)^2 \left(\frac{16\lambda}{3\pi}\right)^4 \sigma_f^2 \qquad \text{(VII.7)}$$

Combining (2.20) and (VII.5) gives the head covariance function for the transient analysis

$$R_h(\xi,\chi) = \frac{J_I^2}{4}\sigma_f^2 \left(\frac{16\lambda}{3\pi}\right)^2 \frac{1}{2}\left[\left(2 - \left(\frac{3\pi\xi}{16\lambda}\right)^2 \cos^2\chi\right) \frac{3\pi\xi}{16\lambda} K_1\left(\frac{3\pi\xi}{16\lambda}\right) + \left(\frac{3\pi\xi}{16\lambda}\right)^2 K_o\left(\frac{3\pi\xi}{16\lambda}\right)\right]$$

$$+ \left(\frac{S}{T_\ell}\frac{\partial H}{\partial t}\right)^2 \sigma_f^2 \left(\frac{16\lambda}{3\pi}\right)^4 \frac{1}{8}\left[\left(8 + \left(\frac{3\pi\xi}{16\lambda}\right)^2\right) \frac{3\pi\xi}{16\lambda} K_1\left(\frac{3\pi\xi}{16\lambda}\right) + \left(\frac{3\pi\xi}{16\lambda}\right)^2 K_o\left(\frac{3\pi\xi}{16\lambda}\right)\right] \qquad (3.11)$$

Equations (2.21) and (VII.7) give the head variance for the transient analysis

$$\sigma_h^2 = \left[\frac{J_I^2}{4} + \left(\frac{S}{T_\ell}\frac{\partial H}{\partial t}\right)^2 \left(\frac{16\lambda}{3\pi}\right)^2\right] \left(\frac{16\lambda}{3\pi}\right)^2 \sigma_f^2 \qquad (3.10)$$

APPENDIX VIII

GRADIENT-MAGNITUDE ESTIMATION

The equation for a plane surface observed at three points is a standard mathematical formulation discussed in most math texts (e.g., Boas, 1966). The derivation outlined in the following discussion is based on linear and vector algebra techniques although other approaches to the problem are available.

Consider observations ϕ_1, ϕ_2, ϕ_3, of the plane surface at points A, B, and C, which have coordinates (x_1,y_1), (x_2,y_2), and (x_3,y_3) in the x-y coordinate system. The vectors separating points A and B and points A and C are given by

$$\vec{AB} = (x_2 - x_1)i + (y_2 - y_1)j + (\phi_2 - \phi_1)k$$

$$\vec{AC} = (x_3 - x_1)i + (y_3 - y_1)j + (\phi_3 - \phi_1)k \qquad \text{(VIII.1)}$$

i, j, and k are unit vectors in the x, y, and ϕ directions. The cross product of vectors $\vec{AB}$ and $\vec{AC}$ produces the vector $\vec{N}$ normal to the plane at point A

$$\vec{N} = \vec{AB} \times \vec{AC} = \begin{vmatrix} i & j & k \\ x_2 - x_1 & y_2 - y_1 & \phi_2 - \phi_1 \\ x_3 - x_1 & y_3 - y_1 & \phi_3 - \phi_1 \end{vmatrix}$$

$$\vec{N} = [(y_3 - y_2)\phi_1 + (y_1 - y_3)\phi_2 + (y_2 - y_1)\phi_3]i$$
$$+ [(x_2 - x_3)\phi_1 + (x_3 - x_1)\phi_2 + (x_1 - x_2)\phi_3]j$$
$$+ [x_2y_3 - x_3y_2 + x_1y_2 - x_2y_1 + x_3y_1 - x_1y_3]k \qquad \text{(VIII.2)}$$

The equation for the plane at B with the surface normal $\vec{N}$ is given by the dot product of $\vec{N}$ and any vector in the plane, which has the components $x - x_2$, $y - y_2$, and $\phi - \phi_2$. After some algebraic manipulation, this dot product leads to an equation of the plane in the form

$$\phi = \{[(y_2 - y_3)\phi_1 + (y_3 - y_1)\phi_2 + (y_1 - y_2)\phi_3]x$$
$$+ [(x_3 - x_2)\phi_1 + (x_1 - x_3)\phi_2 + (x_2 - x_1)\phi_3]y$$
$$+ (y_2\phi_3 - y_3\phi_2)x_1 + (y_3\phi_1 - y_1\phi_3)x_2 + (y_1\phi_2 - y_2\phi_1)x_3\}$$
$$\div [x_2y_3 - x_3y_2 + x_1y_2 - x_2y_1 + x_3y_1 - x_1y_3] \qquad \text{(VIII.3)}$$

The gradient of the plane is determined by applying the gradient operator, $\nabla = i\frac{\partial}{\partial x} + j\frac{\partial}{\partial y}$, to (I.3)

$$\nabla\phi = i\frac{\partial\phi}{\partial x} + j\frac{\partial\phi}{\partial y}$$

$$= \Big\{[(y_2 - y_3)\phi_1 + (y_3 - y_1)\phi_2 + (y_1 - y_2)\phi_3]i + [(x_3 - x_2)\phi_1 + (x_1 - x_3)\phi_2 + (x_2 - x_1)\phi_3]j\Big\} \div [x_2y_3 - x_3y_2 + x_1y_2 - x_2y_1 + x_3y_1 - x_1y_3] \qquad \text{(VIII.4)}$$

$$\therefore \hat{\vec{J}} = -\nabla\phi = \vec{a}_1\phi_1 + \vec{a}_2\phi_2 + \vec{a}_3\phi_3 \qquad \text{(VIII.5)}$$

where $$\vec{a}_1 = \frac{(y_3 - y_2)i + (x_2 - x_3)j}{[x_2y_3 - x_3y_2 + x_1y_2 - x_2y_1 + x_3y_1 - x_1y_3]}$$

$$\vec{a}_2 = \frac{(y_1 - y_3)i + (x_3 - x_1)j}{[x_2y_3 - x_3y_2 + x_1y_2 - x_2y_1 + x_3y_1 - x_1y_3]}$$

$$\vec{a}_3 = \frac{(y_2 - y_1)i + (x_1 - x_2)j}{[x_2y_3 - x_3y_2 + x_1y_2 - x_2y_1 + x_3y_1 - x_1y_3]}$$

APPENDIX IX

GRADIENT-DIRECTION ESTIMATION

Gradient direction is estimated using the three-point technique of structural geology for determining strike and dip; the method treats the horizon of interest as an inclined plane. For a discussion of the procedure and example problems see Billings (1972).

Application of this procedure requires the water-level elevation at three points and the distance between observation points. Location of a point on the line joining maximum and minimum observed elevations, which has an elevation equal to that of the intermediate point, is determined by ratio of differences in observed elevations. The line joining two points on the same horizon which have equal elevations is the strike. The dip, or gradient, direction is perpendicular to the strike. The angle, θ , formed between the estimated and true gradient, or down-dip, directions can be formulated in terms of geometry of the observation network

$$\theta = 90^{\circ} - (\gamma + \psi) \qquad \text{(IX.I)}$$

where γ is the network rotation angle and ψ is the angle between the principal network side and the strike direction (see Figure 4.1).

The sine of the angle of deviation, the error in estimated gradient

direction, may be written

$$\sin\theta = \cos\psi\sin\gamma - \sin\psi\cos\gamma \qquad \text{(IX.2)}$$

In accordance with the Law of Cosines and other trigonometric relationships, (IX.2) can be formulated as a function of separation distance between observation points and observed water levels

$$\sin\theta = \frac{\cos\gamma\ (1 - \frac{\phi_1-\phi_2}{\phi_3-\phi_2}) - \sin\gamma(\frac{\phi_1-\phi_2}{\phi_3-\phi_2})}{[2(\frac{\phi_1-\phi_2}{\phi_3-\phi_2})^2 - 2(\frac{\phi_1-\phi_2}{\phi_3-\phi_2}) + 1]^{\frac{1}{2}}} \qquad \text{(IX.3)}$$

ϕ_1 is the intermediate water level observed, ϕ_2 the minimum, and ϕ_3 the maximum observed water level.

APPENDIX X

ln T ESTIMATING EQUATION

The Stallman (1956) procedure for estimating transmissivity employs a finite difference form of the two-dimensional flow equation. Data requirements include water-level elevations from five observation wells distributed on a rectangular grid and the distance between wells.

The governing two-dimensional flow equation, assuming homogeneous transmissivity, is

$$\frac{\partial^2\phi}{\partial x^2} + \frac{\partial^2\phi}{\partial y^2} = \frac{S}{T}\frac{\partial\phi}{\partial t} - \frac{W}{T} \qquad (X.1)$$

where W is recharge. Approximating the second-order, spatial derivatives using the central difference technique gives

$$\frac{\partial^2\phi}{\partial x^2} \approx \frac{\phi_1 + \phi_3 - 2\phi_5}{L^2} + O(L^2) \qquad (X.2)$$

$$\frac{\partial^2\phi}{\partial y^2} \approx \frac{\phi_2 + \phi_4 - 2\phi_5}{L^2} + O(L^2)$$

where L is the spacing between observation wells, and the error term, $O(L^2)$, behaves as the network spacing squared. In the present analysis well separation is assumed to be constant throughout the observation network although such a restriction is not essential.

Substituting (X.2) into (X.1) produces an equation from which transmissivity can be estimated as a function of observed water levels

$$\hat{T} = \frac{L^2 S \frac{\partial \phi}{\partial t} - L^2 W}{\phi_1 + \phi_2 + \phi_3 + \phi_4 - 4\phi_5} \qquad (X.3)$$

For consistency, (X.3) is written in terms of the natural logarithm of transmissivity resulting in an equation for ln T

$$\ln \hat{T} = \ln(L^2 S \frac{\partial \phi}{\partial t} - L^2 W) - \ln(\phi_1 + \phi_2 + \phi_3 + \phi_4 - 4\phi_5) \qquad (4.14)$$

APPENDIX XI

FLOW PARAMETERS OF THE SAN ACACIA IRRIGATION AND DRAINAGE SYSTEM

Network-design results have been illustrated by analysis of parameters estimated for an irrigation and drainage system instrumented at San Acacia 15 miles north of Socorro, New Mexico (Wierenga, et al., 1979). This appendix tabulates the input data required to make these calculations.

The irrigation-return-flow water-quality study funded by the U. S. Environmental Protection Agency and the New Mexico Environmental Improvement Division, is jointly administered by Drs. L. W. Gelhar, New Mexico Institute of Mining and Technology, and P. J. Wierenga, New Mexico State University; Chris Duffy serves as field manager for the project.

The study area on the Herkenhoff Farm, bounded on the east by the Rio Grande, encompasses ancient river channel deposits and low-lying marsh areas which were inundated by high water prior to implementation of flood-control measures. Drilling on the farm indicates a sequence of mixed clay, sand, and gravel, 60 - 70 feet thick, underlain by a fairly continuous, dense clay, generally assumed to be the confining bed for the shallow near-surface flow system.

Extensive instrumentation and data collection by the EPA project has included 31 observation wells scattered around the farm, gage recorders on the irrigation and drainage canals, automatic sample collection for water-quality analysis, and a pan evaporation installation. Data collected in the study area includes weekly water-level and pan-evaporation measurements, extensive mapping of soil types, slug and bail

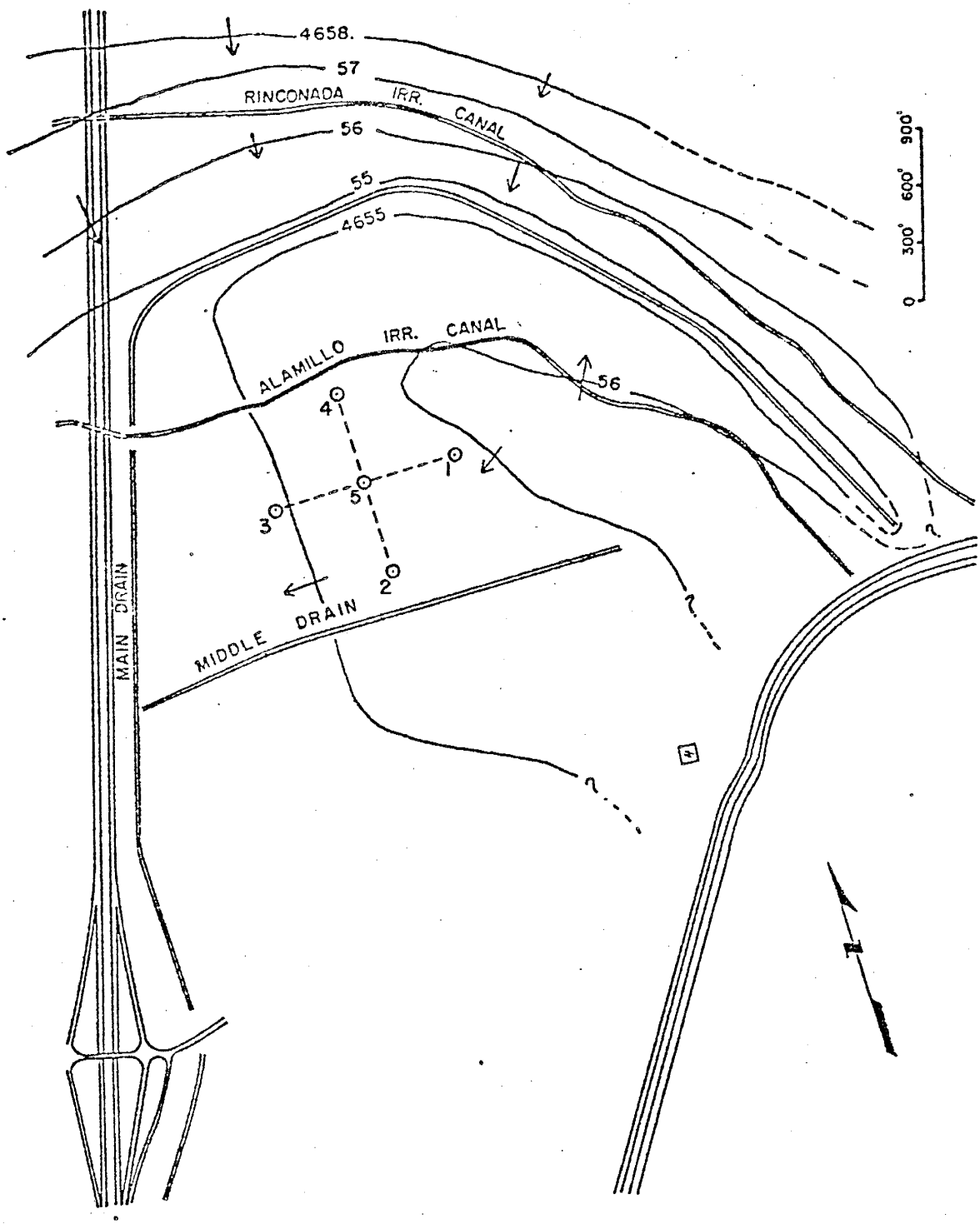

Figure XI.1: Map of the field study area at San Acacia, New Mexico showing the five-point well network and water-level contours during the Winter 1977-1978 (from Wierenga et al., 1979)

tests of soil permeability, and infiltrameter tests. Of particular interest in the network-design application to be considered is a five-point network of wells located between the Alamillo Irrigation Ditch and the Middle Drain (see Figure XI.1). Wells in this network are located on centers of 500 feet and the rotation angle appears to be about zero.

Table XI.1 lists water-level measurements in the network wells collected February 1977 to March 1978. The last 1977 irrigation occurred October 22 and water-level measurements for the winter season were begun November 10, week number 40 of the project. These winter-season measurements continued until March 23, week 58, and the first irrigation of 1978 occurred April 4. Various flow parameters required for the illustrative examples are discussed below. Results are presented in Tables XI.2 and XI.3.

The flow parameters of interest are S, T_ℓ, λ, J_1, $\frac{\partial \phi}{\partial t}$, σ_ε^2, σ_f^2, σ_h^2, Ω. Each of these is discussed below.

S: In the network design problems storage coefficient is assumed to be a deterministic constant. At the farm various attempts to determine S have yielded results ranging from 0.18 to 0.22; the median value, S = 0.2, is chosen for use in the illustrative problems.

T_ℓ: Estimation of mean transmissivity is carried out by rewriting (X.3) as

$$\Sigma\phi = \phi_1 + \phi_2 + \phi_3 + \phi_4 - 4\phi_5 = L^2\frac{S}{T}\frac{\partial \phi}{\partial t} - L^2\frac{W}{T} \qquad \text{(XI.1)}$$

The slope resulting from regression of $\Sigma\phi$ and $\frac{\partial \phi}{\partial t}$ indicates the value of aquifer transmissivity,

$$T = \frac{L^2 S}{m}$$

where m is the slope, if the storativity is known independently. Recharge, W, can be determined from the regression intercept.

Scatter of $\Sigma\varphi$ and $\frac{\partial \phi}{\partial t}$ resulting from water-level data collected during the 1977-1978 winter, when zero recharge is anticipated, does not exhibit a clear trend (Figure XI.2(A)). Alternatively, data obtained during periods of hydrograph recession, (see Figure XI.3) were plotted in Figure XI.2(B); a rough fit of these data has a slope of 12.5 days. The resulting transmissivity estimate, T = 4000 ft^2/day, is in reasonable agreement with the value of 2120 ft^2/day reported by Gelhar, et al., (1980, Table 4.2.1 (b)).

Note that the line fitted to the summer, recession-limb data does not pass through the plot origin, as would be expected if W = 0, but instead implies discharge of water from the instrumented aquifer.

λ: Average correlation distance of the ln T fluctuations is very difficult to evaluate accurately because of the extensive data requirements. A very simple procedure was used to estimate λ for these illustrations; characteristic dimensions of soil units were determined from detailed maps of the study area. The average dimension of these soil units is 500 feet; this value is assumed to represent a first-order attempt to estimate λ.

J_1: Of the five wells shown in Figure XI.1 those three forming the northwest corner are used to estimate the mean gradient magnitude. The estimating equation in terms of three water-level observations is

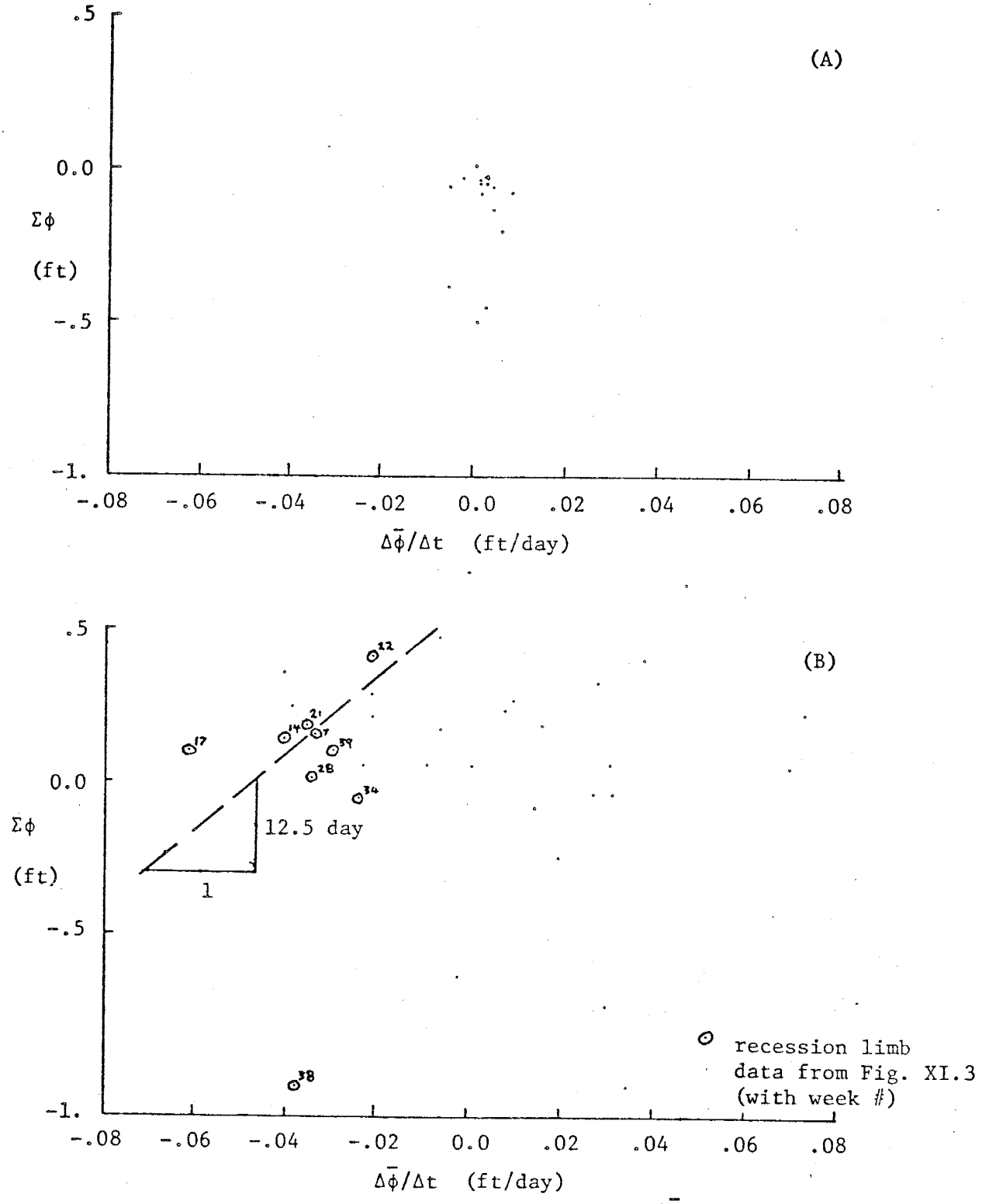

Figure XI.2: Plots of Stallman Data ($\Sigma\phi$ vs $\frac{\Delta\bar{\phi}}{\Delta t}$) for (A) Winter and (B) Summer Flow Regimes

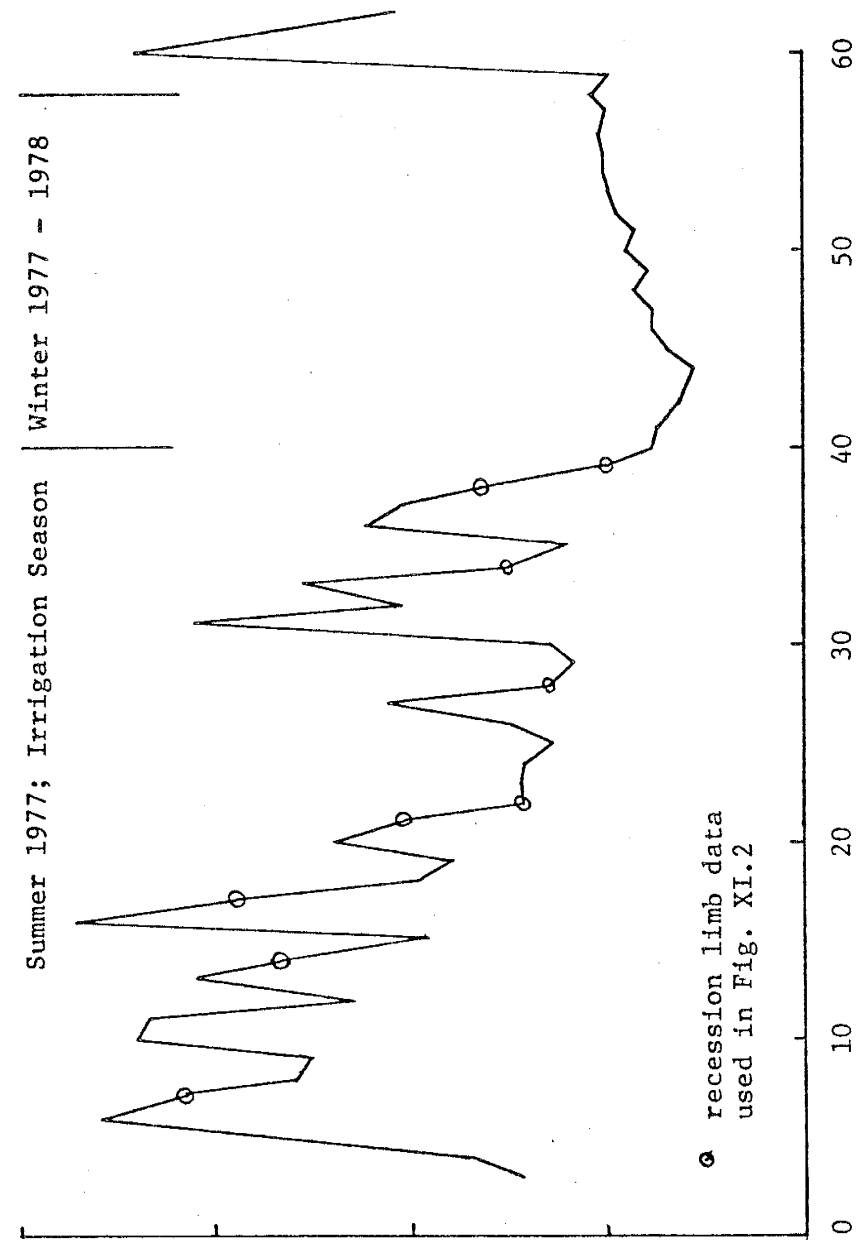

Figure XI.3: Average Water Level Hydrograph of the five-point network
San Acacia, New Mexico

$$E(J) = \left| \frac{(\sin\gamma - \cos\gamma)H_5 + \cos\gamma\ H_3 - \sin\gamma\ H_4}{L} \right| \qquad \text{(XI.2)}$$

Because $\gamma = 0$, (XI.3) is reduced to

$$E(J) = \left| \frac{-H_5 + H_3}{L} \right|$$

Values of E(J) were determined for each week of the winter season, 1977-1978, and are listed in Table XI.2. The value used in the network-design calculations is the average of weekly results

$$E(J) = 1.18 \times 10^{-3}$$

Using summer data this value is

$$E(J) = 1.42 \times 10^{-3}$$

$\frac{\partial \phi}{\partial t}$: Change in water level with respect to time is approximated according to the central difference technique applied to the average water-level of the five-well network. The equation for average water-level $\bar{\phi}$ is

$$\bar{\phi} = \frac{\phi_1 + \phi_2 + \phi_3 + \phi_4 + 2\phi_5}{6} \qquad \text{(XI.3)}$$

Values resulting from calculation with weekly data collected during the winter of 1977-1978 are presented in Table XI.1; averaging the absolute values of these data gives

$$\frac{\Delta\bar{\phi}}{\Delta t} = 0.003 \frac{ft}{day}$$

for the winter flow regime. The value assumed for the summer season was taken to be the central value of those calculated for weeks on recession limbs of the hydrograph (see Figure XI.2(B)).

$$\frac{\Delta\bar{\phi}}{\Delta t} = -0.04 \frac{ft}{day}$$

σ_ε^2: Water-level measurements are assumed to be accurate to 0.01 foot. Because measurement error is conceptually a zero-mean process the variance of measurement error is the accuracy squared

$\sigma_\varepsilon^2 = 0.0001$

σ_f^2: Variances of ln T for eight aquifers of differing lithology are reported by Delhomme (1979). He found the variance of the ln T process to range from 0.63 for a sandstone aquifer to 5.2 for a limestone aquifer. ln T variances for two alluvial aquifers are reported to be 1.007 and 1.431. The average of these two values

$\sigma_f^2 = 1.2$

is used in the illustrative network-design examples.

Parameters σ_h^2 and Ω evaluated by equations (3.10) and (3.12) as functions of the parameters indicated above have the values, using summer data

$\sigma_h^2 = 2.92 \text{ ft}^2$

$\Omega = 0.15$

using winter data

$\sigma_h^2 = 0.32 \text{ ft}^2$

$\Omega = 0.95$

Table XI.1

Weekly Water-Level Data Collected from the Five-Point Well Network, February 1977 - April 1978, with $\bar{\phi}$, $\Sigma\phi$, $\frac{\Delta\bar{\phi}}{\Delta t}$

WEEK #	ϕ_1	ϕ_2	ϕ_3	ϕ_4	ϕ_5	$\bar{\phi}$	$\Sigma\phi$	$\frac{\Delta\bar{\phi}}{\Delta t}$
Summer 1977:	irrigation season							
3	4656.35	4655.61	4654.84	4656.11	4655.69	4655.72	0.15	--
4	4656.39	4655.65	4654.85	4656.72	4655.74	4655.85	0.65	0.043
5	4656.79	4656.02	4655.44	4657.09	4656.28	4656.32	0.22	0.066
6	4657.19	4656.38	4656.02	4657.45	4656.82	4656.78	-0.24	0.019
7	4657.15	4656.18	4656.00	4657.02	4656.55	4656.58	0.15	-0.034
8	4656.92	4656.04	4655.57	4656.69	4656.29	4656.30	0.06	-0.023
9	4656.73	4656.08	4655.50	4656.48	4656.38	4656.26	-0.73	0.029
10	4657.55	4656.32	4655.73	4657.21	4656.69	4656.70	0.05	0.030
11	4657.28	4656.42	4655.92	4657.17	4656.64	4656.68	0.23	-0.039
12	4656.73	4655.89	4655.46	4656.54	4656.14	4656.15	0.06	-0.009
13	4657.18	4656.40	4655.59	4657.06	4656.58	4656.56	-0.09	0.014
14	4656.88	4656.05	4655.63	4656.83	4656.31	4656.34	0.15	-0.041
15	4656.59	4655.74	4655.30	4656.29	4655.97	4655.98	0.04	0.037
16	4657.84	4656.15	4655.46	4657.65	4657.02	4656.86	-0.98	0.034
17	4656.98	4656.18	4655.78	4656.93	4656.44	4656.46	0.11	-0.062
18	4656.75	4655.79	4655.30	4656.24	4655.93	4655.99	0.36	-0.041
19	4656.36	4655.78	4655.13	4656.36	4655.86	4655.89	0.19	0.015
20	4656.47	4655.73	4655.59	4657.08	4656.15	4656.20	0.27	0.009
21	4656.43	4655.58	4655.44	4656.70	4655.99	4656.02	0.19	-0.035
22	4656.19	4655.46	4655.25	4656.07	4655.64	4655.71	0.41	-0.021
23	4656.28	4655.62	4655.06	4655.93	4655.71	4655.72	0.05	0.0

Table XI.1 (cont.)

WEEK #	ϕ_1	ϕ_2	ϕ_3	ϕ_4	ϕ_5	$\bar{\phi}$	$\Sigma\phi$	$\frac{\Delta\bar{\phi}}{\Delta t}$
24	4656.28	4655.48	4656.99	4656.14	4655.68	4655.71	0.17	-0.006
25	4656.12	4655.40	4655.04	4655.81	4655.75	4655.64	-0.63	0.002
26	4656.26	4655.69	4655.10	4655.88	4655.74	4655.74	-0.03	0.031
27	4656.56	4655.74	4655.73	4656.40	4655.99	4656.07	0.47	-0.006
28	4656.24	4655.49	4655.01	4655.91	4655.66	4655.66	0.01	-0.034
29	4656.02	4655.52	4655.43	4655.62	4655.48	4655.59	0.67	-0.001
30	4656.17	4655.73	4655.03	4655.69	4655.64	4655.65	0.06	0.069
31	4657.00	4656.04	4655.94	4657.38	4656.51	4656.56	0.32	0.026
32	4656.59	4655.70	4655.35	4656.59	4655.98	4656.02	0.21	-0.021
33	4656.89	4656.03	4655.45	4656.37	4656.45	4656.27	-1.06	-0.019
34	4656.34	4655.61	4655.11	4655.97	4655.77	4655.76	-0.05	-0.024
35	4656.18	4655.44	4654.99	4655.76	4655.60	4655.60	-0.03	0.026
36	4656.18	4656.13	4655.60	4656.65	4656.08	4656.12	0.24	0.007
37	4656.44	4655.66	4655.41	4656.70	4655.98	4656.03	0.29	-0.021
38	4656.17	4655.46	4655.14	4656.16	4655.98	4655.82	-0.99	-0.038
39	4655.99	4655.31	4654.95	4655.77	4655.48	4655.50	0.10	-0.031
Winter 1977 - 1978								
40	4655.90	4655.25	4654.84	4655.58	4655.39	4655.39	0.01	-0.009
41	4655.86	4655.21	4654.77	4655.50	4655.43	4655.37	-0.38	-0.004
42	4655.87	4655.21	4654.74	4655.45	4655.33	4655.32	-0.05	-0.009
43	4655.82	4655.19	4654.72	4655.44	4655.30	4655.30	-0.03	-0.002
44	4655.65	4655.19	4654.76	4655.47	4655.30	4655.28	-0.13	0.004
45	4655.88	4655.25	4654.79	4655.45	4655.36	4655.35	-0.07	0.006
46	4655.89	4655.29	4654.84	4655.47	4655.38	4655.38	-0.03	0.002
47	4655.90	4655.30	4654.82	4655.48	4655.39	4655.38	-0.06	0.009

Table XI.1 (cont.)

WEEK #	ϕ_1	ϕ_2	ϕ_3	ϕ_4	ϕ_5	$\bar{\phi}$	$\Sigma\phi$	$\frac{\Delta\bar{\phi}}{\Delta t}$
48	4655.91	4655.31	4654.83	4655.49	4655.51	4655.43	-0.50	0.001
49	4655.91	4655.30	4654.84	4655.48	4655.40	4655.39	-0.07	0.001
50	4655.95	4655.32	4654.86	4655.50	4655.52	4655.45	-0.45	0.003
51	4655.96	4655.35	4654.89	4655.52	4655.44	4655.43	-0.04	-0.001
52	4655.99	4655.37	4654.90	4655.54	4655.50	4655.47	-0.20	0.004
53	4656.05	4655.41	4654.94	4655.58	4655.50	4655.50	-0.02	0.001
54	4656.07	4655.42	4654.94	4655.60	4655.52	4655.51	-0.05	0.001
55	4656.07	4655.44	4654.94	4655.59	4655.52	4655.51	-0.04	0.0
56	4656.09	4655.46	4654.93	4655.61	4655.52	4655.52	0.01	-0.001
57	4656.09	4655.43	4654.90	4655.60	4655.51	4655.51	-0.02	0.001
58	4656.12	4655.45	4654.93	4655.67	4655.54	4655.54	-0.01	-0.001
59	4656.11	4655.42	4654.85	4655.64	4655.48	4655.50	0.06	--
Summer 1978:	irrigation season							
60	4657.43	4656.27	4655.87	4657.33	4656.70	4656.72	--	--
61	4657.01	4656.06	4655.65	4656.96	4656.35	4656.40	--	--
62	4656.62	4655.78	4655.34	4656.46	4656.04	4656.05	--	--

[1] ϕ_i and $\bar{\phi}$ in feet above sea level

[2] $\Sigma\phi$ is in feet

[3] $\frac{\Delta\bar{\phi}}{\Delta t}$ is in feet/day

Table XI.2

Mean Gradient Magnitude and Direction
as estimated from weekly Water-Level Data
of the 1977 - 1978 Winter Season

WEEK #	$E(J) \times 10^{-3}$	θ (degrees)
40	1.1	-19.06
41	1.3	- 6.05
42	1.2	-11.50
43	1.2	-13.57
44	1.1	-17.47
45	1.1	- 8.97
46	1.1	- 9.46
47	1.1	- 8.97
48	1.4	1.68
49	1.1	- 8.13
50	1.3	1.74
51	1.1	- 8.28
52	1.2	- 3.81
53	1.1	- 8.13
54	1.2	- 7.85
55	1.2	- 6.88
56	1.2	- 8.67
57	1.2	- 8.39
58	1.2	-12.03
average	1.18	- 8.62

Table XI.3

Summary of Parameter Values Used in the

Illustrative Network-Design Calculations

SEASONAL PARAMETERS

SUMMER		WINTER	
PARAMETER	VALUE	PARAMETER	VALUE
J_1	1.4×10^{-3}	J_1	1.2×10^{-3}
$\frac{\Delta\bar{\phi}}{\Delta t}$	$-0.04 \frac{ft}{day}$	$\frac{\Delta\bar{\phi}}{\Delta t}$	$0.003 \frac{ft}{day}$
σ_h^2	$2.92\ ft^2$	σ_h^2	$0.32\ ft^2$
Ω	0.15	Ω	0.95

NON-SEASONAL PARAMETERS

PARAMETER	VALUE
L	500 ft
λ	500 ft
γ	0 degrees
θ	-8.62 degrees
S	0.2
T_ℓ	$4000 \frac{ft^2}{day}$
σ_f^2	1.2
σ_ϵ^2	$0.0001\ ft^2$

This dissertation is accepted on behalf of the faculty of the Institute by the following committee:

Lynn W. Gelhar
Adviser

Allan Hatjdu

John R. MacMillan

10/31/80
Date